# CHARACTERIZATION OF THE BEHAVIOR OF PALNICRO BRAZING ALLOY FOR STAINLESS STEEL JOINTS

by

**Fabian Edelmann**

*Department of Mining, Metals and Materials Engineering*

**McGill University, Montreal**

A Thesis Submitted to the
Faculty of Graduate Studies and Research
in partial fulfillment of the requirements for the degree of
**Master of Engineering**


**August, 2005**

*Your file Votre référence*
*ISBN: 978-0-494-22643-8*
*Our file Notre référence*
*ISBN: 978-0-494-22643-8*

*To the love of my life, Mona,*
*for all her patience, support,*
*understanding and everlasting love...*

# *ABSTRACT*

Brazing is a low-cost process used extensively in manufacturing and repair of component assemblies in the aerospace industry. For stainless steel joints requiring an airtight seal, the brazing metal Pd-Ni-Cr-Si-B (PalNiCro) is commonly applied. However the underlying mechanisms of the brazing process are not well understood, which has precluded optimization of the brazing parameters and reduced the cost-effectiveness of the production process. To address these issues, the role of processing conditions on the wetting characteristics of austenitic AISI 347 and martensitic AISI 410 stainless steel was studied in this work using PalNiCro as the brazing alloy. Sessile drop tests were conducted to assess the effect of time, temperature and surface roughness on the wettability conditions between the stainless steel substrate and brazement. The effect of time and clearance on the microstructure and hardness of the brazement was then examined.

A brazing temperature of 980°C and a surface roughness from 600 grit SiC grinding paper were determined as the optimal wetting conditions. Under such conditions, the value of the equilibrium contact angle for the AISI 347 and AISI 410 stainless steels was determined to be approximately 10° after 100 seconds of melting. Examination of the brazements produced using optimized wetting conditions revealed the formation of borocarbide ($M_x(C,B)_y$) and boride ($M_xB_y$) precipitates primarily confined to the grain boundaries and some locations within the interior of the grains, which resulted from the diffusion of boron from the brazing metal. The microstructure of the joint seam consisted of the three distinct regions: (1) a soft ductile nickel solid solution with dissolved palladium and chromium (hardness ~ 220 HV) and (2) palladium silicide (over 600 HV) surrounding (3) very hard Ni-rich islands (over 1000 HV) with the presence of nickel borides. An increase in brazing time showed a slight increase in the maximum brazing clearance (MBC) with also an increase in the diffusion layer for both AISI 347 and AISI 410. The volume fraction of the secondary phases within the joint seam exhibited marked increases up to a clearance of 150 μm with a decrease thereafter and an estimated value of 300 μm as the maximum attainable clearance.

# *RÉSUMÉ*

Le brasage est un procédé peu coûteux qui est très utilisé lors de la fabrication et de la réparation d'assemblages dans le domaine de l'industrie aérospatiale. Dans le but d'obtenir des joints en acier inoxydable étanches, le métal d'apport Pd-Ni-Cr-Si-B (PalNiCro) est généralement utilisé. Cependant, les mécanismes définissant le procédé de brasage ne sont pas encore maîtrisés, ce qui ouvre la voie à de nombreuses possibilités d'optimiser les procédés de brasage et de réduire le rapport coût/efficacité de la production. Afin de mieux comprendre ces incertitudes, la mouillabilité de l'alliage de brasage PalNiCro sur un acier inoxydable austénitique AISI 347 de même qu'un acier inoxydable martensitique AISI 410 fut étudiée en fonction des paramètres du procédé. De plus, l'essai de goutte statique a été réalisé afin de déterminer l'effet du temps, de la température et de la rugosité de surface sur les conditions de mouillabilité entre les substrats d'acier inoxydable et le métal d'apport. L'effet du temps et de l'écartement sur la microstructure et la dureté de la brasure a également été examiné.

Les conditions de mouillabilité optimales furent obtenues pour une température de brasage de 980°C et une rugosité de surface provenant d'un papier abrasif de carbure de silicium 600 grit. Ces conditions ont mené à la mesure d'angle de contact d'équilibre de 10° après 100 secondes pour les substrats d'acier inoxidable AISI 347 et AISI 410. L'évaluation des joints brasés sous ces conditions a révelé la formation de précipités de borocarbures ($M_x(C,B)_y$) et de borures ($M_xB_y$) retrouvés principalement aux joints de grains et dans quelques régions à l'intérieur des grains, prevenant de la diffusion de bore à partir du métal d'apport. La microstructure des joints était composée de trois régions distinctes (1) une zone ductile composée d'une solution solide de nickel contenant du palladium et du chrome (dureté ~220 HV) et (2) des siliciures de palladium (dureté supérieure à 600 HV) autour (3) d'îlots très durs, riches en Ni (dureté > 1000 HV) et de borures de nickel. L'augmentation du temps de brasage montrait une légère augmentation de l'écartement maximale de brasage et une augmentation de l'épaisseur de la couche de diffusion pour les deux aciers inoxydables AISI 347 et AISI 410. La fraction volumique des phases secondaires dans les joints augmentait jusqu'à un écartement de 150 μm suivit d'une réduction et une valeur estimée à 300 μm pour un écartement maximal.

# *ACKNOWLEDGEMENTS*

First and foremost I would like to express my sincere gratitude to my supervisor, Professor Robin A. L. Drew, for all his moral, technical, and financial support as a thesis supervisor. He provided me with numerous opportunities to explore and broaden my knowledge by attending and participating in conferences related to material science. I am grateful for all his continuous encouragement and I will treasure this experience throughout my entire professional career.

The success of my experiments would not be possible without the aid and support of numerous laboratory technicians. A special thanks to Florence, Monique, Helen, Line and Lang. I am also grateful to Ray, Edwin, Pierre, Alain, Csaba and Frank for all your laboratory assistance.

I would like to thank those who have aided with the administrative aspect of my research. Thanks to Norma, Nikki, Genny, Carol, Barbara and Linda for all those helpful email reminders and creating a really friendly atmosphere.

Thanks to Mamoun, Claudia, David, Neivi, Chun Hui, Juan, Kaled, Greg, Rocco, Faramarz, Ahmad, Abdel, Guillermo, Naser and Laura for all their good company and assistance in the laboratory. A special thanks goes out to Mathieu, who convinced me in the first place to pursue graduate studies and who provided me with guidance and support. I cannot forget my wonderful office mates, Farzad, Ozzy and Ramona for providing me with all your help, which was crucial to my experiments. Thank you for all the good and bad times we shared together. I am grateful to Priti for all your insight and help with writing my thesis, I could not have done it without you. Lastly, I would like to thank Pratt and Whitney Canada for the financial support provided for the project. A special *merci* to Daniel Turner, Alain Bouthillier, David Holford, Denis Blanchet and my work colleagues Claude, Renald, Christian, Orlando and Emmanuelle.

A very special thanks goes out to my mom, dad, aunt, and my brother for all your patience and understanding. I would like to thank everyone else in the family for all their encouragement and support. Finally, thank you to my love, Mona, for all the sacrifices you have made, and all the patience you showed waiting for me to finish. You have given me the strength to persevere through all the difficult times.

# *TABLE OF CONTENTS*

# *LIST OF FIGURES*

# *LIST OF TABLES*

# *CHAPTER 1*

## *INTRODUCTION*

As performance advancements continuously increase in the aerospace industry, there is an ever-increasing demand for stronger, lighter and more efficient structures that are capable of operating at elevated temperatures[1]. In an effort to adapt aerospace components to meet the stringent physical and mechanical property requirements, a growing trend has been to combine different material and geometrical configurations, which has considerably increased the complexity of each individual part. Although, in the past, fusion welding was predominantly used as a joining method where adhesion was required, the use of brazing is increasingly providing a more efficient means of joining the complex components in the aerospace industry[2,3]. In particular, the use of much lower temperatures during brazing can preserve the original tailored microstructure of the base materials and avoid the presence of the relatively large heat-affected zones as found in the case of fusion welding[4]. Furthermore, brazing can be performed on components with limited geometric accessibility where tight tolerances are required.

Of the various brazing techniques, vacuum furnace brazing is extensively used in the aerospace industry for manufacturing and repair of aircraft gas turbine engines on account of the ability to join dissimilar base materials as well as multiple components within a single brazing cycle. In particular, aerospace assemblies often require leak-free joints in which brazing can be implemented as a sealant, as for example stator assemblies

(Figure 1.1) located within the compressor stage of the engine that experience relatively low temperatures. The materials of frequent interest for such low temperature applications are typically austenitic and martensitic stainless steels, which are known for their superior corrosion resistance and high strength up to 800°C.

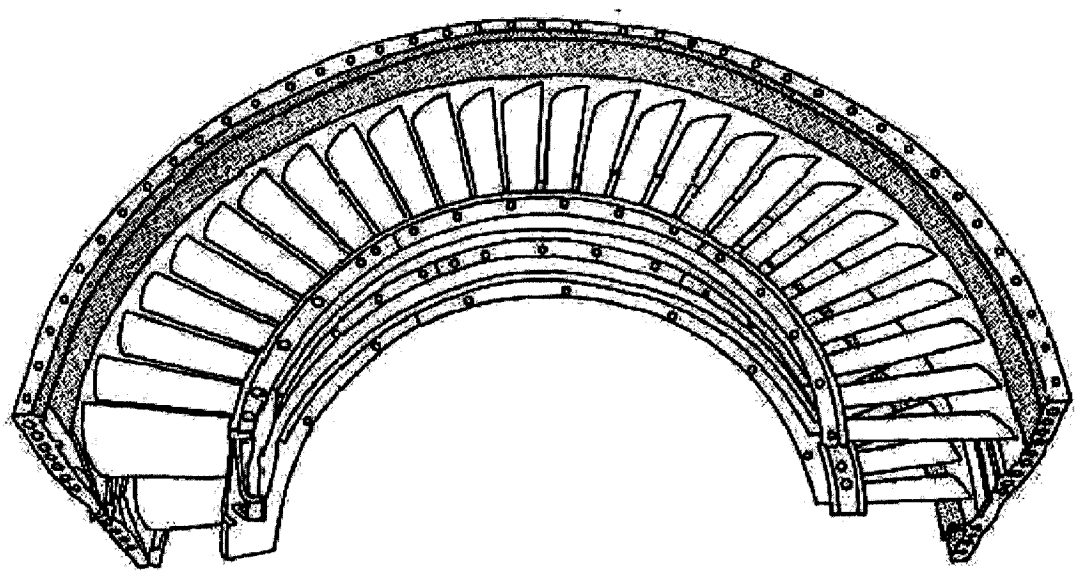

**Figure 1.1** Typical compressor stator assembly located within the compressor stage of a gas turbine engine[5].

Although, the brazing operation in the aerospace industry has remained unchanged for many years, there has been a constant strive for manufacturers to reduce production costs and increase productivity. Hence, optimizing brazing conditions for specific metallurgical requirements would contribute towards increasing the energy savings, reducing the length of brazing cycles and thereby, reducing both the operating costs and inefficiencies. Moreover, small tolerances commonly required of aerospace assemblies translate into high machining costs, that can be accounted for during brazing by adjusting the gap between the components in order to minimize material removal and related costs. Another consideration involves the common practice of surface preparation of the faying surface of the joint assembly, which manifests as an additional cost to the final product. Through, knowledge of surface roughness, in relation to the wetting behavior of the material, such surface preparation requirements can be minimized.

In this work, the role of processing conditions on the wetting characteristics of austenitic AISI 347 and martensitic AISI 410 stainless steel was studied by considering the effect of time, temperature and surface roughness. The effect of time and clearance on the microstructure and hardness of the brazement was also examined. This analysis then permitted the definition of the optimal brazing conditions for the processing of AISI 347/410 stainless steel joint configurations.

# *CHAPTER 2*

# *LITERATURE REVIEW*

## *2.1 Brazing Process*

Brazing can be defined as a physical joining method that entails processing at temperatures below the melting or plastic-state of the base metal. Specifically, during the brazing process coalescence between the joint interface is generated by heating to temperatures (usually above 450°C) that exceed the liquidus temperature of the brazing metal, but remain below the solidus temperature of the base metal. Upon heating, the filler metal comes in contact with the faying surfaces and then distributes itself across the joint by capillary action under the vacuum environment of the furnace[6]. The formation of a metallurgical bond can either occur by simple wetting of the mating surfaces or by a reaction between filler metal and base metal (alloying). According to Humpston and Jacobson, this alloying that occurs during brazing generally leads to the formation of solid solutions[7].

To heat the joint, a variety of methods exists such as torch brazing, induction brazing and furnace brazing, of which the latter is the principal technique applied for aerospace components, and thus the subject and focus of the present work.

### 2.1.1 Furnace Vacuum Brazing

Brazing is often performed in a furnace due to its ability to process within each heat cycle multiple joints and/or assemblies at large production rates with a uniform temperature distribution[8]. The application of vacuum furnace brazing is usually considered for joining aerospace components as embrittlement of the weldment from surrounding environmental contaminants is of particular concern. Specifically, vacuum brazing is used for a range of materials including stainless steels, superalloys, aluminum alloys, titanium alloys and metals containing refractory or precious metals. The components to be joined by brazing are usually processed by placing mating surfaces in a retort furnace, such as that illustrated in Figure 2.1, which is maintained under a vacuum environment. There exist various different degrees of vacuum levels and corresponding pressures as tabulated in Table 2.1[8]. Although the degree of vacuum varies depending on the type of vacuum brazing vessel, maintaining a relatively high vacuum seal (pressure less than $10^{-4}$ torr) is essential for preventing oxidation of the mating surfaces for most applications. Moreover, as flux reagents are not required during vacuum brazing, good surface cleanliness prior to joining is critical for good wetting and filler metal flow[9].

**Table 2.1** Various degrees of vacuum and their corresponding pressure ranges[8].

| Condition | Pressure Range (torr) |
|---|---|
| Low Vacuum | 760 to 25 |
| Medium Vacuum | 25 to 1.0 |
| Fine Vacuum | 1.0 to $1.0 \times 10^{-3}$ |
| High Vacuum | $1.0 \times 10^{-3}$ to $1.0 \times 10^{-6}$ |
| Very High Vacuum | $1.0 \times 10^{-6}$ to $1.0 \times 10^{-9}$ |
| Ultra High Vacuum | $1.0 \times 10^{-9}$ and below |

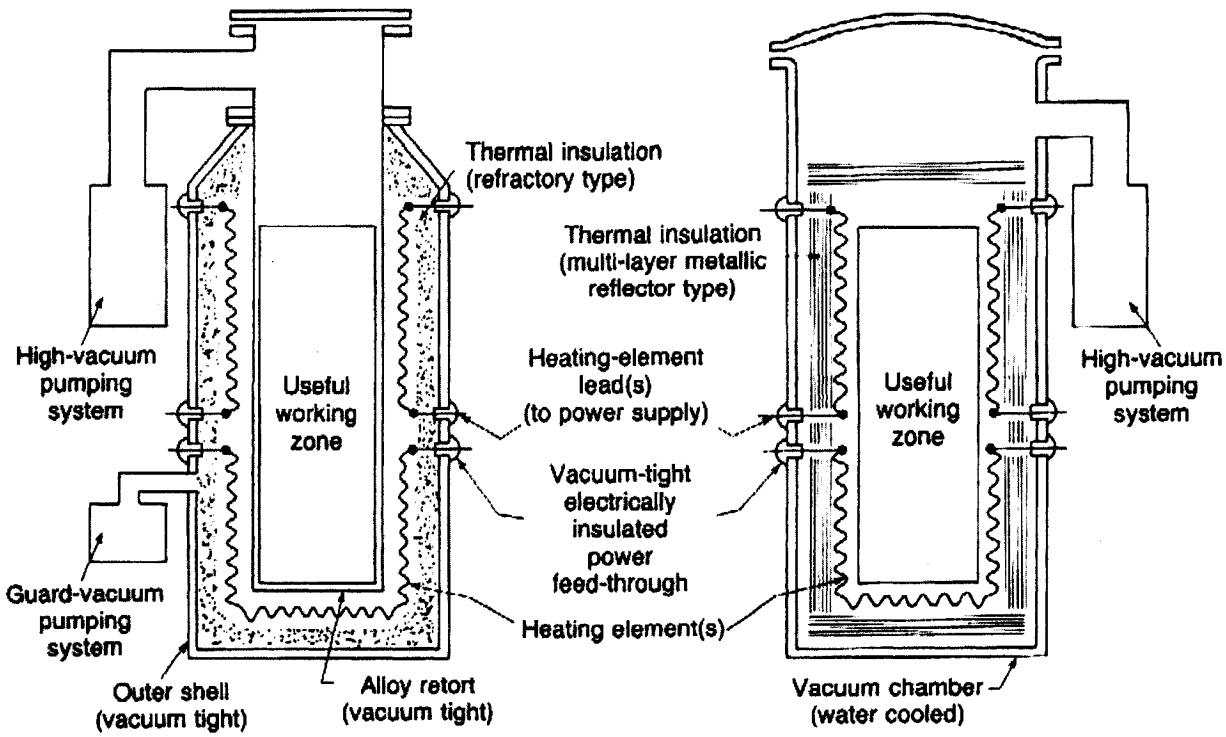


**Figure 2.1** Retort furnace for vacuum brazing process[9].

## *2.2 Brazing Parameters*

Brazing is governed by many factors, which often act simultaneously and directly influence the interactions that occur during brazing. The following are key aspects that must be considered to ensure a metallurgically sound brazement[7]:

- Surface energy and surface tension
- Wetting and contact angle
- Brazing filler metal spreading characteristics
- Surface roughness
- Dissolution effects
- Joint clearances

## 2.2.1 Surface Energy and Surface Tension

The concept of surface energy and surface tension can be illustrated by the use of a simplified diagram showing a vapor-solid system as given in Figure 2.2. In the solid phase there are an array of neighboring atoms around atom A within the bulk material, whereas atom B (at the surface) that is lacking neighbors has unsaturated bonds. The lack of neighbors for atom B leads to a potential energy that is higher than in atom A, such that the difference between the two atoms is defined as the surface energy $\gamma_{SV}$[7]. Moreover, according to Humpston and Jacobson[7], the surface of a liquid acts like an elastic skin covering liquid metal, which acts in tension. This tensile force is known as the surface tension and under isothermal conditions the surface tension is equivalent to surface energy.

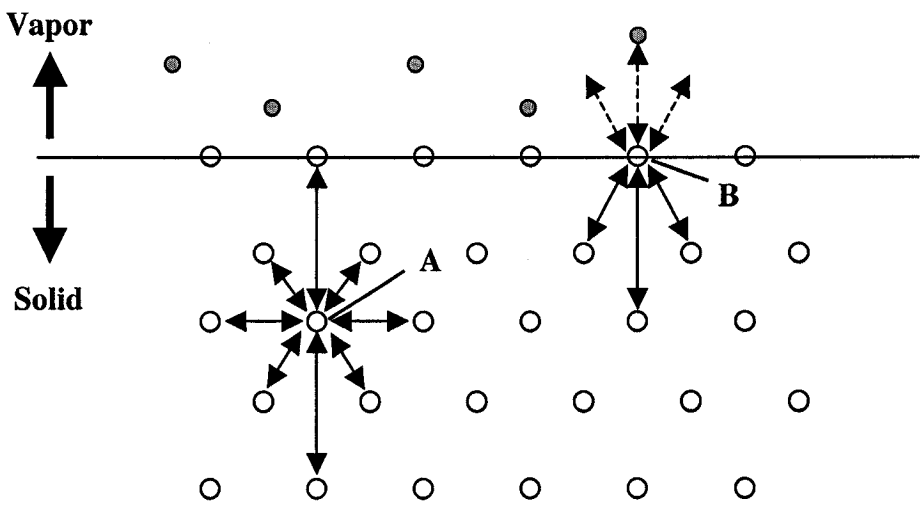


**Figure 2.2** Molecular diagram of surface energies. Atom B has unsaturated bonds, leading to a higher potential energy than atom A. This difference constitutes the origin of the surface energy between the solid and vapor phases, $\gamma_{SV}$[7].

## 2.2.2 Wetting

Brazing depends greatly on the ability of the filler metal to wet the base metal and consideration of wetting phenomena is necessary to ensure the production of sound brazed joints. In particular, both thermodynamic and kinetic phenomena play an

important role related to wetting and must be considered when evaluating a given system. According to Nikitinskii[10], wetting is referred to as the first stage of a physico-chemical interaction between a liquid and the surface of the solid leading to the spreading of the liquid in a thin layer. During brazing, wetting is the interaction between the liquid brazing alloy atoms and the solid base metal atoms such that the adhesive forces are greater than the cohesive forces of the liquid brazing alloy[10].

### *2.2.2.1 Contact Angle*

The classical model of wetting dictates that a liquid metal will spread over a solid substrate until the three surface tensions, shown in Figure 2.3, are in equilibrium.

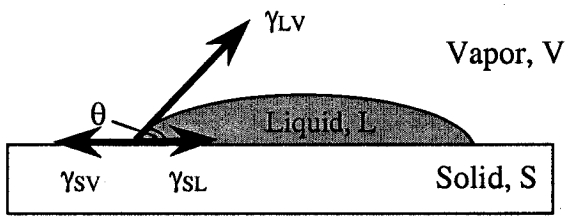


**Figure 2.3** Classical wetting model of the surface tension forces acting on a liquid that wets a solid[7,11, 12].

In particular, a balance of forces can be derived from the above model, which is known as Young's equation[7,11,12]:

$$\gamma_{SL} = \gamma_{SV} - \gamma_{LV} \cos \theta \qquad \text{(Eq. 2.1)}$$

The angle that is subtended by the liquid surface and the solid-liquid interface is known as the contact angle, which is related to the surface tensions between the solid and liquid ($\gamma_{SL}$), the liquid and vapor ($\gamma_{LV}$), and the solid and vapor ($\gamma_{SV}$). A contact angle greater than 90° is defined as non-wetting, while for a wetting system the angle is less than 90°. Complete wetting only occurs when the contact angle is zero[7,11,12].

Considering that wettability is improved by decreasing the contact angle, it then follows from Eq. 2.1 that an increase in $\gamma_{SV}$, a decrease in $\gamma_{SL}$, or a decrease in $\gamma_{LV}$ will also tend to increase wetting. The quantity $\gamma_{SV}$ can be maximized by ensuring that the

solid substrate is extremely clean. In general, $\gamma_{SL}$ is highly dependant on temperature such that an increase in temperature will result in a decrease $\gamma_{SL}$. The value of $\gamma_{LV}$ can be altered by changing the atmospheric pressure, whereby the application of a vacuum provides a reduction in the partial pressure and minimizes $\gamma_{LV}$[7].

### *2.2.2.2 Interfacial Reactions*

During brazing, reactions tend to occur at the interface that will act to modify the surface tensions, on account of the formation of a reaction layer between the base metal and the brazing metal, as demonstrated in Figure 2.4. This layer modifies the wetting and spreading behavior of the liquid filler metal in contact with the base metal[13].

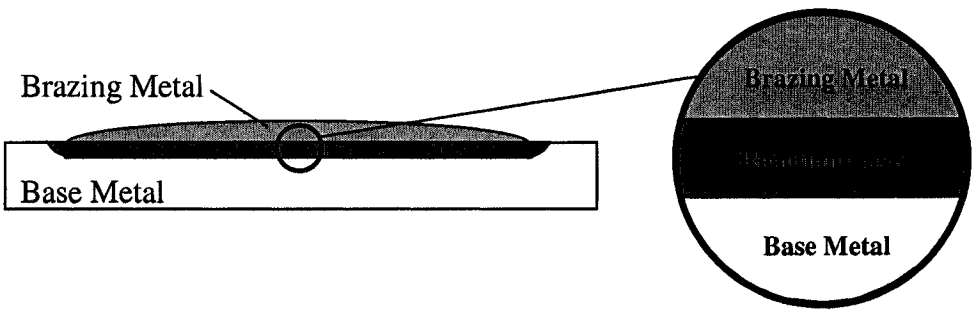


**Figure 2.4** Interfacial reaction layer that occurs during wetting of a brazing filler metal on a base metal[13].

To consider the interactions between the brazing filler metal and the base metal, it is necessary to adopt a modified version of Young's equation including the free energy of the reaction, $\Delta G_r$, to describe the change in the solid-liquid interface:

$$\gamma_{SV} - (\gamma'_{SL} - \Delta G_r) = \gamma_{LV} \cos \theta \qquad \text{(Eq. 2.2)}$$

where $\Delta G_r$ is the free energy of reaction per unit area and time, and $\gamma'_{SL}$ is the modified surface energy due to the reaction at the interface. Both $\gamma'_{SL}$ and $\Delta G_r$ tend to increase the driving force for wetting, such that for a driving force greater than $\gamma_{LV} \cos \theta$ spreading will occur until the liquid has reacted completely with the solid[13].

It is noteworthy that although the evaluation of wetting on the basis of the contact angle does not truly reflect the physical nature of the wetting process, it has been accepted due to the fact no other simple quantitative method for estimating wetting exists. Hence, although the evaluation of the contact angle through indirect measurements is often a rough estimate, it nonetheless provides practical use in technical literature for characterizing wetting.

### *2.2.2.3 Cohesion, Adhesion and Spreading*

For the condition of wetting, the change in free energy, $\Delta G$, which dictates whether or not a process occurs spontaneously, can be related to the work of cohesion, adhesion and spreading. Given that the force of cohesion is defined as the attraction force between similar liquid molecules, the work needed to separate the liquid molecules per unit area is then the work of cohesion, $W_{LL}$. The separation process involves the production of two new interfaces, as shown in Figure 2.5a, from which the following expression has been derived[14]:

$$\Delta G = 2\gamma_L = W_{LL} \qquad \text{(Eq. 2.3)}$$

The surface tension of the liquid, $\gamma_L$, is an indication of the $\Delta G$ associated with the removal of molecules from the bulk to the surface and is thus related to the work of cohesion. Similarly, since the force of adhesion is defined as the attraction force between a liquid and a solid, the work performed to separate these forces between the liquid and solid phases, is known as the work of adhesion, $W_{SL}$, which is defined by[14,6]:

$$W_{SL} = \gamma_{SL}\,(1 + \cos\theta) \qquad \text{(Eq. 2.4)}$$

For a low contact angle, or $\theta = 0°$, $W_{SL} = 2\gamma_{SL} = W_{LL}$ and the work of adhesion and cohesion are equivalent. Therefore, in order to have spreading, or sufficient flow during brazing, $W_{SL}$ must be greater than $W_{LL}$. The work of spreading, as shown in Figure 2.5c, means that a positive spreading coefficient $S_{SL}$ will lead to the liquid spreading across the solid and, thereby leading to wetting[14].

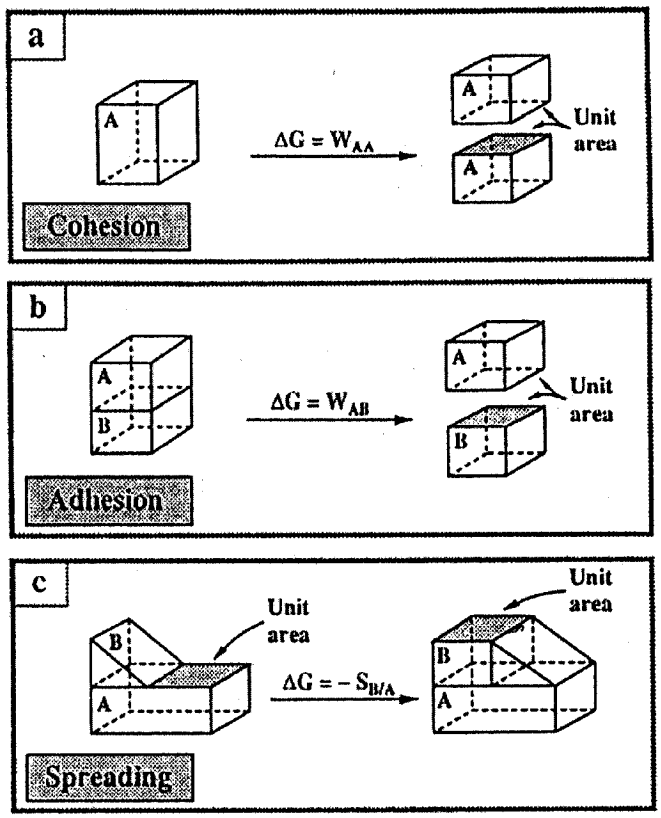


**Figure 2.5** Schematic representation of the processes for which ΔG equals (a) the work of cohesion, (b) the work of adhesion, and (c) the work of spreading[14].

## 2.2.3 Capillarity

The wetting of two mating surfaces presents another physical phenomena called capillarity, which is defined by Schwartz[9] as the physical force that governs the action of a liquid against solid surfaces in small, confined areas. The capillary force is depicted schematically in Figure 2.6, where a liquid is allowed to rise between two parallel plates of a given distance, D. A contact angle of less than 90° will exhibit a positive capillary force, which in turn will act to fill the joint. A balance of the capillary force and its own hydrostatic head determines the extent to which the liquid can rise, where the capillary force per length is equivalent to $2\gamma_{LV}\cos\theta$[7].

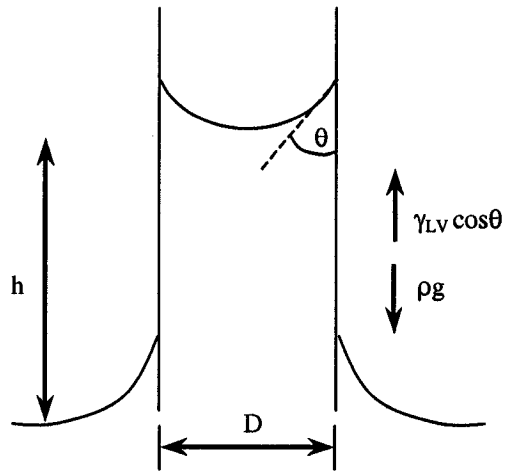


**Figure 2.6** Rise of a liquid between two parallel plates by capillary force and the associated acting forces[7].

The amount of spread and capillary penetration may vary according to specific values of the contact angle as shown in Figure 2.7. In particular, a decrease in the contact angle will result in an increase in the area of spread, with values less than 20° giving a significant increase. Conversely, the capillary rise increases continuously for contact angles of 90° and less, but below 20° relatively low changes are observed[11]. Hence, critical values can be extrapolated, in which maximum capillarity and spread area can be determined.

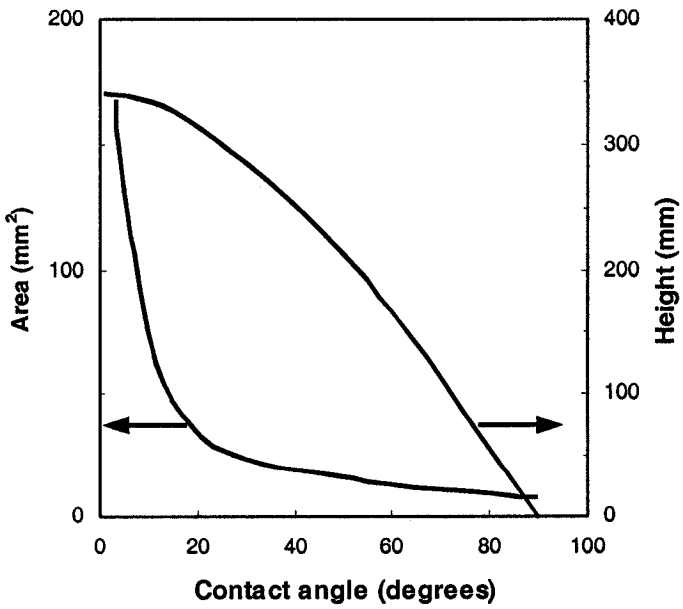


**Figure 2.7** The effect of contact angle on the area of spread and capillary rise of a 0.01mL drop of Cu for a capillary gap of 0.1mm[11].

The expression for the capillary forces acting on two parallel horizontal plates is given by:

$$F = \frac{2l\,\gamma_{LV}\cos\theta}{l} \qquad \text{(Eq. 2.5)}$$

where F is the force needed to wet a plate of length, l. Given that the pressure, P, is the force divided by the area, the relationship for the pressure of liquid between the two parallel plates can be considered as the driving force of the joint filling, and is given by:

$$P = \frac{2\gamma_{LV}\cos\theta}{D} \qquad \text{(Eq. 2.6)}$$

where D is the plate gap spacing. Hence, as the gap is increased, the decrease in pressure will cause the liquid to cease. Thus, the flow velocity into the spacing is given by:

$$\frac{dl}{dt} = \frac{\gamma_{LV} D\cos\theta}{6\eta l} \qquad \text{(Eq. 2.7)}$$

where $\eta$ is the viscosity of the liquid[7]. Equation 2.7 represents the rate of filling of a joint, in which the gap spacing becomes proportional to the rate. Conversely, the gap spacing is inversely proportional to the driving force of filling. Therefore, a balance must be realized between the driving force and the rate of filling of a joint as the two quantities act in opposition.

### 2.2.4 Brazing Metal Spreading Characteristics

Although the type of brazing filler metal is selected according to the chemistry of the base metal, certain general characteristics are necessary to ensure the occurrence of spreading on the substrate with increasing temperature and an atmosphere that is more reducing[7]. In order to ensure good flow characteristics of brazing filler metals it is desirable to have a good liquid surface tension, a low viscosity, as well as a low brazing temperature. Moreover, the time and cooling rate should be kept to a minimum to prevent cracking or distortion of the assembly. In general, eutectic compositions of brazing filler metals are usually used for their ability to melt at a specific temperature. Alloys with

## 2.2.5 Base and Brazing Metal Interactions

The interactions that occur during brazing depend on a number of factors including, base and filler metal compositions, joint geometry, temperature, and time[9]. In order to characterize these interactions, the underlying mechanisms that are usually considered include diffusion, erosion, and dissolution or alloying.

### *2.2.5.1 Diffusion*

The method of diffusion is a solid-state process that is highly dependent on temperature, and during brazing, the occurrence of this mechanism is relatively slow. Hence the main diffusion mechanism is interstitial with elements such as carbon and boron (as well as Si to a lesser extent) contained in the filler metal diffusing into the base metal interstitially due to their relatively small atomic radii. In most austenitic alloys, interstitial atoms have a tendency to diffuse along grain boundaries and migrate into the lattice positions of the base metal to form intermetallics, carbides, borides or borocarbides, which form during superheating and aging. Larger atoms migrate substitutionally in the base metal and typically include Ni, Cr, and Si from the brazing filler metal that produce at the interface, complex solid solutions of Fe-Cr-Ni-Si in austenitic alloys. The solid solutions are usually unstable when cooled after brazing, and decompose to form an eutectoid mixture of solid solution and intermetallic compounds[9].

### *2.2.5.2 Erosion and Dissolution*

As molten filler metal wets the base metal, there is normally intersolubility between the alloys, which is manifested as dissolution of the surfaces of the base metal in the joint region and the formation of new phases at either interface upon solidification[7]. Hence the dilution phenomena observed during brazing can be viewed as alloying between the base metal and filler metal. Fletcher[12] explains that alloying on a limited scale at the interface can be beneficial for increasing the joint strength. However, excessive alloying that causes detrimental effects to the joint integrity is known as aggression or erosion, due to which the effective thickness of a component can be reduced, as shown in Figure 2.8[12]. The effectiveness of the erosion mechanism depends

on the rate of erosion, which is influenced by the joining technique used, the joint design, the contact area and the amount of filler metal, with the value of the latter parameter kept to a minimum to achieve adequate joint filling[12].

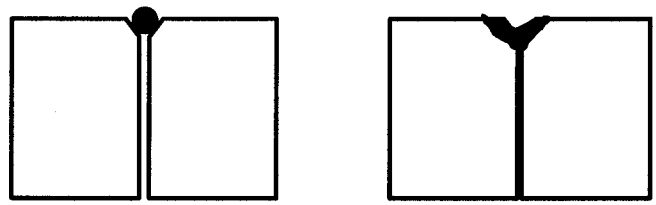


**Figure 2.8** Schematic diagram of the effect of aggression between a brazing metal and a base metal during brazing. (a) Before brazing (b) After brazing[12]

For interactions that involve the production of a reaction layer (Figure 2.4) that consists of a continuous layer of an intermetallic compound over the joint interface, the erosion rate decreases because it is governed by the relatively slow diffusion rate of the base metal atoms through the solid intermetallic compound[7].

Dissolution of the base metal and resulting growth of the reaction layer of intermetallic compounds both follow an Arrhenius-type behavior represented by the following generic relationship:

$$\text{rate} \propto \exp [ - Q / kT ] \qquad \text{(Eq. 2.8)}$$

where Q is an activation energy that characterizes the reaction taking place at a temperature T (in Kelvin) and k is the Boltzmann constant.

## 2.2.6 Surface Roughness

The models and predictions considered in the previous sections have been formulated on the assumption that the mating surfaces during brazing are truly flat. In practice, the surface roughness of the component has a significant impact on the wetting behavior which must be incorporated into the surface energy relationships given in Eq. (2.1). Fletcher[12] has postulated that in the general case, a liquid that wets readily on a

smooth surface will wet to a greater extent when rough. However, Humpston and Jacobson[7] have stated that there is an optimal roughness for maximizing the spreading of a brazing filler metal. Thus, the presence of a roughened surface has introduced the idea of an effective contact angle, $\theta^*$, where $\theta^*$is related to $\theta$, the contact angle of a truly flat surface, by the following relationship[7]:

$$\cos \theta^* = r \cos \theta \qquad \text{(Eq. 2.9)}$$

where,

$$r = \frac{\text{actual area of rough surface}}{\text{plan area}} \qquad \text{(Eq. 2.9a)}$$

According to equation 2.9, an increase in the surface roughness by a roughness ratio, r, will decrease the effective contact angle. Bailey and Watkins[15] have argued that the relationship stated in Eq. 2.9 is only valid for a specific topographic orientation by considering an idealized rough surface shown in Figure 2.9, which increases spreading of a liquid by the enhanced capillary action of the grooves.

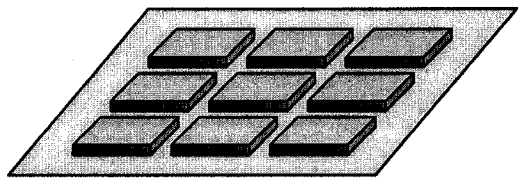

**Figure 2.9** Idealized rough surface conceived by Bailey and Watkins[15].

Conversely, the spreading behavior of the negative of the surface depicted in Figure 2.9, which yields exactly the same roughness ratio, would show a retarded capillary action on account of the array of pits[15]. Moreover, roughening can be directional, as shown in Figure 2.9, or non-directional. In the case of directional roughening, fine channels are produced, and texturing of the component can increase the capillary force between the filler metal and the base metal, such that the flow will tend to be parallel to the channeling. A surface texture that is jagged has been suggested to produce a maximum wetting effect that is associated with the sharp angles in the jagged texture, which modify the crystallographic orientation. In particular, the poor adhesion of oxides along jagged

wetting effect that is associated with the sharp angles in the jagged texture, which modify the crystallographic orientation. In particular, the poor adhesion of oxides along jagged edges provide sites at which the oxide layer can be easily penetrated, which produces an additional contribution to wetting[7].

### 2.2.7 Joint Clearances

The joint clearance is the gap between two faying surfaces to be brazed. For cases where the dimensional or machining (cost) conditions necessitate adherences to strict tolerances for components to be brazed, joint clearances are not always optimal, and thus a compromise can lead to defects such as shrinkage and voids that can be found in large gaps due to the wetting behavior deviating from capillary to non-capillary[12]. Specifically, as the gap increases, the capillary rise decreases as illustrated in Figure 2.6[7].

## *2.3 Vacuum Brazing of Stainless Steels*

Although stainless steels can be brazed similar to other low alloy steels, the high chromium content can cause the formation of chromium oxide ($Cr_2O_3$), which tends to interfere with wetting on account of its stable and strongly adherent characteristics[16]. In order to alleviate this difficulty, vacuum brazing is applied because the vacuum atmosphere guarantees, to a certain extent, the removal of residual oxygen. Furthermore, the use of a vacuum environment allows oxide films to be either reduced into pure metals or partially reduced to form surface active oxides, which are dissolved or wetted by the molten filler metal[17]. To determine the oxygen partial pressure needed to reduce a metal oxide as a function of temperature, reference to the Ellingham diagram (Figure 2.10) gives an indication of the stability of a metal oxide. Specifically, the line segment A-A in Figure 2.10 denotes that the critical oxygen partial pressure needed to reduce $Cr_2O_3$ at a typical brazing temperature of 1000°C is about $10^{-22}$ atm, which seems unrealistic for commercial use. Fletcher[12] has suggested that there is another driving force which exists to enhance the removal of surface oxide films during brazing; the presence of discontinuities in the oxide film that form by solid solution with the base metal allow the liquid filler metal to penetrate the surface oxide. Upon passing through the oxide film, the

filler metal interacts with the base metal to form a reaction layer between the oxide and the base metal that eventually causes the oxide to float out of the joint as dross[12,19,20], as depicted in Figure 2.11.

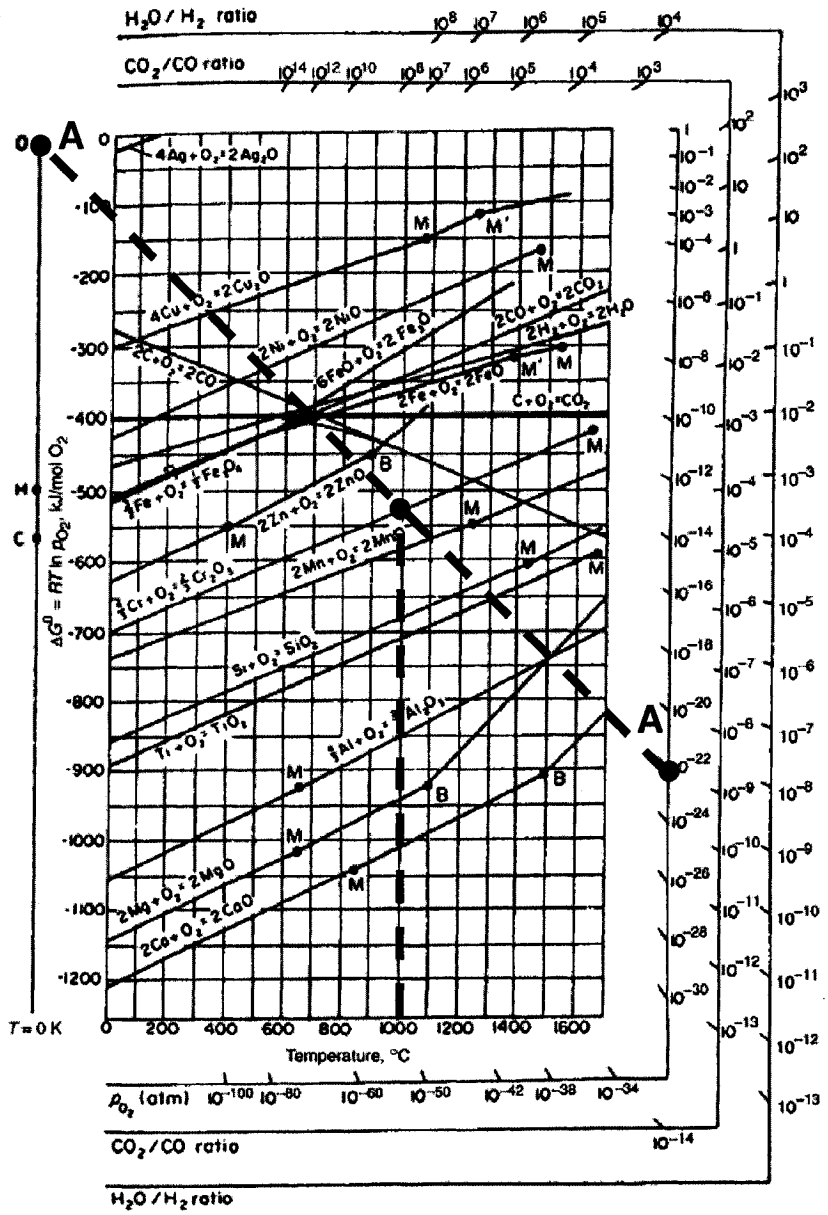


**Figure 2.10** Ellingham diagram for various oxides. Segment A-A denotes a typical brazing temperature of 1000°C and the corresponding oxygen partial pressure[18].

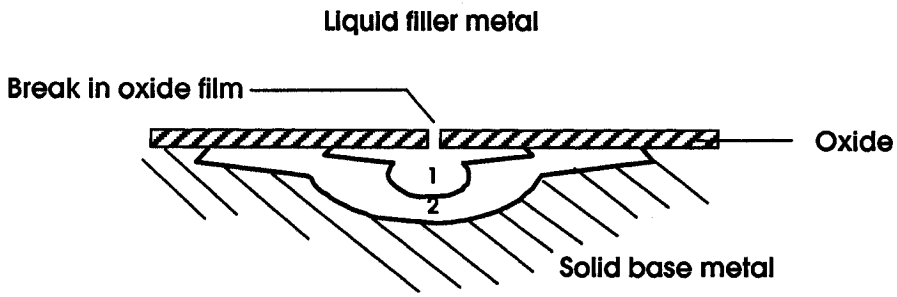


**Figure 2.11** The principles of brazing metal penetration of an oxide film and flow beneath the film. Stages 1 and 2 are progressive positions of the advancing phase[12].

Alternatively, Arata *et al.*[21] have proposed that for the removal of the Cr oxide from a stainless steel (304L, 304 2B, 321) surface requires decarburizing to reduce the $Cr_2O_3$ by carbon as follows:

$$Cr_2O_3 + 3C \rightleftharpoons 2Cr + 3CO \qquad \text{(Eq. 2.10)}$$

Experimental results have shown that the $Cr_2O_3$ present during vacuum heating at 750 °C, could be reduced by the carbon in steel when heated to 860 °C under a vacuum of $2 \times 10^{-5}$ Torr. Arata *et al.* have stated that the reduction occurs at the locations where grain boundaries intersect with the surface, because diffusion of carbon is greatest in these regions[21].

## 2.3.1 Brazing of Austenitic Stainless Steels

Austenitic stainless steels are nonhardenable and nonmagnetic due to nickel and manganese additions which stabilize the austenite phase to room temperature. They are susceptible to a phenomenon known as sensitization during reheating between 425 to 815 °C or slow cooling through this range. In particular, excess carbon combines with chromium at the grain boundaries of the austenite to form chromium carbide ($Cr_{23}C_6$) and the region then becomes chromium depleted and susceptible to corrosion[9,13,22]. Sensitization can be prevented by the addition of austenite stabilizers, or by redissolving the precipitated carbides through the use of heat treatment after brazing[9].

### 2.3.2 Brazing of Martensitic Stainless Steels

As the martensitic stainless steels have low chromium and carbon contents and the heat treatment temperatures are comparable to that of the brazing cycle, there is the possibility of cost savings by performing the two operations simultaneously using an appropriate filler metal with a brazing temperature that is sufficient for austenization of the base metal. However after brazing, rapid cooling is necessary for the transformation of austenite to martensite to occur and the cooling rate must be uniform to prevent dimensional changes in the component[9,13].

### 2.3.3 Nickel-Based Family of Filler Metals

Brazing fillers can be supplied in a variety of forms such as, foil, tape, powders, pastes, and sintered preforms[13]. Although brazes for stainless steels are mostly silver or gold-based filler metals for high-temperature service applications, the nickel-based filler metals (BNi) are frequently needed for corrosion resistance and high-temperature strength. According to Lugscheider and Kruger[23], high temperature brazing with nickel-based filler metals is being successfully used as a modern joining technique in the aircraft, space, turbine and nuclear industries, as illustrated by the brazed joint depicted in Figure 2.12 where a boron-containing nickel-based filler brazing alloy was used on a Cr-Ni-Nb steel. Specifically, the addition of boron in the filler metal acts as a melting point depressant to lower the melting temperature of the filler metal. The brazement shows evidence of a nickel solid solution and the presence of hard phases, while both inter- and transcrystalline precipitations are within the base metal, suggesting that sufficient time for diffusion during brazing has occurred to allow interstitial atoms to diffuse out of the brazement.

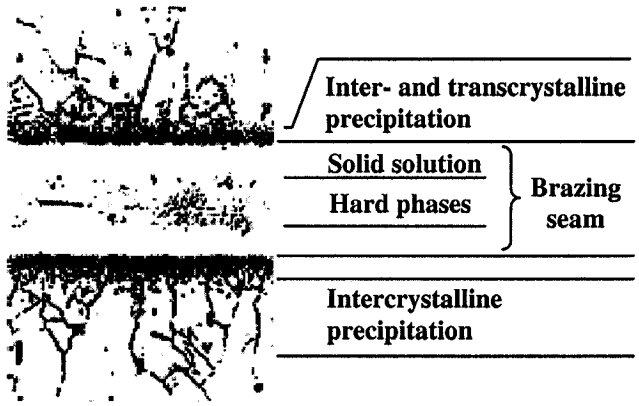


**Figure 2.12** Metallographic characterization of a high temperature brazed joint. Filler metal is BNi-2, Base: X8 Cr Ni Nb 16 13 (347 H). Brazing temperature: 1120 °C - for 60 min[23].

Although boron-containing nickel-based filler metals have the ability to sufficiently penetrate into the base metal, the diffusion of carbon and boron at the grain boundaries, can render the joint brittle[23,24]. This has led to the recent development of boron-free, nickel-based filler metals with small amounts of phosphorus for the nuclear industries. Lugscheider *et al.*[25] have shown that hard phases can also result from brazing 321 stainless steel with a phosphorus-containing nickel-based filler metal which forms brittle nickel-phosphides and nickel-silicides. However, the amount of these is dependent on the brazing temperature, time and in particular, the rate of silicon diffusion into the base metal. Specifically, Lugscheider *et al.*[25] have shown that for shorter brazing times, the percentage of hard phases is higher than for longer brazing times, which allow the dissolution of the precipitates through diffusion of the silicon and phosphorus into solid solution with nickel.

### *2.3.3.1 Nickel-Palladium Brazing Alloys*

The need for the development of nickel-palladium based brazing alloys for joining high-strength components has recently escalated due to the high cost associated with gold bearing alloys[23,26]. These filler metals produce high strength joints at lower brazing temperatures (1000°C) due to the excellent wettability and good flow characteristics, which enable, overall, large cost savings[23,27,28]. Presently, a range of Ni-Pd-Cr-B-Si filler

metals (Table 2.2) are being selected for various applications in the aircraft, space, turbine and nuclear industries. Although, some preliminary brazing research with Pd-based nickel filler alloys has indicated the precipitation of hard phases such as silicides and borides[29], systematic studies to optimize the processing conditions for maximized properties with microstructural control has yet to be examined.

### 2.3.4 Wetting Behavior

As the wetting behavior for the combination of stainless steel and nickel palladium base alloys is not well documented in the literature, a variety of combinations will be discussed in the following section including different stainless steel substrates and nickel-based or silver-based filler metals. In particular, previous wetting behavior studies by McGurran and Nicholas[30] have shown that the contact angle assumed by a Ni-Pd-Si alloy on a 321 stainless steel substrate is approximately 15° at its liquidus temperature of 861°C. The relatively low contact angle and rapid wetting characteristics of the Ni-Pd-Si alloy are attributed to the palladium being capable of dissolving iron into solution and enabling the liquid filler metal to pass under the metal-oxide interface more extensively.

**Table 2.2** Chemical compositions and melting ranges of various nickel-palladium based brazing alloys[29].

| Alloy | Chemical Composition (wt. %) | | | | | Melting range* (°C) |
|---|---|---|---|---|---|---|
| | Pd | Cr | Si | B | Ni | |
| Pd36 | 36.8 | 11.0 | 2.2 | 2.4 | 47.6 | 818 – 992 |
| Pd 36M | 36.0 | 10.0 | 1.0 | 3.0 | 50 | 825 – 955 |
| NiPd1 | 24.7 | 10.4 | 7.8 | 2.2 | 54.9 | 832 – 914 |
| NiPd2 | 24.1 | 10.2 | 7.6 | 2.5 | 55.6 | 846 – 895 |
| NiPd3 | 19.6 | 8.8 | 6.9 | 2.5 | 62.2 | 838 – 966 |

* Melting characteristics above were determined by differential thermal analysis

Moreover, the wetting experiments of Pelster and Lugscheider[29] with various low-precious-metal nickel-based brazing alloys on austenitic X 10 CrNiNb 18 9 (AISI 347) substrates, using a brazing cycle of 1000 °C for 60 minutes, indicated that above 950 °C in a vacuum of $10^{-4}$ to $10^{-5}$ mbar, the chromium oxides were completely removed from

the surface of the base metal, and good wettability was achieved, as summarized in Table 2.3 for numerous brazing alloys.

**Table 2.3** Wetting angle between low-precious –metal; nickel-based brazing alloys and austenitic steel X 10 CrNiNb 18 9[29].

| Alloy | Wetting angle (degrees) |
|---|---|
| Pd36 | 1 |
| Pd36M | 4 |
| NiPd1 | 3 |
| NiPd2 | 10 |
| NiPd3 | 5 |

In a similar study carried out by D'Silva[31], a 36Pd-48.7Ni-11Cr-2.2Si-2.1B filler metal (#36) was used to wet an Inconel 718 substrate in comparison with BNi-2. The spreading behavior of the nickel-palladium based filler metal was determined to be better than that of BNi-2 as indicated in Figure 2.13 by the uniformity of the melt drop in all directions due to the presence of the palladium.

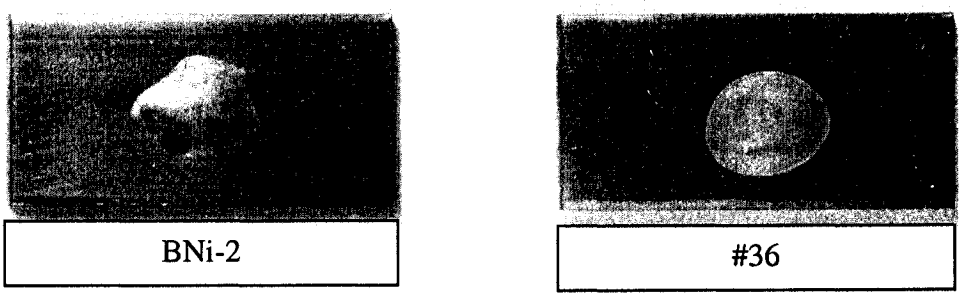


**Figure 2.13** Spreading of BNi-2 and Pd based nickel alloy # 36 on Inconel 718 substrate [31].

Although the addition of alloying elements to the brazing alloy composition can have a profound effect on the properties, the combination of various elements may produce an opposite result. The role of various alloying elements for nickel-based brazing alloys is summarized in Table 2.4, considering steel and superalloy base metals.

**Table 2.4** The role of alloying elements used in nickel-based brazing alloys for steel and superalloy base metals[4,8,23,25,26,28,31].

| Alloying Element | Melting Point Depressant | Corrosion Resistance | Improved Strength | Solid Solution Former | Improved Ductility | Wettability | Compatibility | Comments |
|---|---|---|---|---|---|---|---|---|
| Ni | | ✓ | ✓ | | | | ✓ | • Used for high temperature applications replacing gold-based alloys.<br>• Frequently used for brazing stainless steels and nickel-based superalloys. |
| Pd | | ✓ | | ✓ | ✓ | ✓ | | • Typically used as a replacement for highly priced gold.<br>• Readily forms solid solutions with most metals and has excellent flow characteristics. |
| Cr | | ✓ | | | | | | • Provides excellent corrosion resistance.<br>• Contents above 13% are undesirable due to an increase in brazing alloy liquidus temperature. |
| B | ✓ | | | | | | | • Contents below 1% will have little effect as a melting point depressant.<br>• Greater than 4% will promote brittleness of the brazing alloy.<br>• Act as a diffusing species attributed by its small atomic radius.<br>• Provides a self-deoxidizing action during brazing. |
| P | ✓ | | | | | | | • Similar effect as B, but larger atomic radius results in slightly less mobility.<br>• Large depth of penetration of base metals and results in brittle joints. Used exclusively for nuclear applications. |
| Si | ✓ | | | | | | | • Melting point depressant that is not as effective as B or P.<br>• Combination with other elements can reduce ductility.<br>• Less than 2% will have little temperature depressant effect.<br>• Greater than 5% will result in a reduction of the structural integrity of the joint.<br>• Provides a self-deoxidizing action during brazing. |
| Co | | | | | | | ✓ | • Compatible with most steels, nickel-based superalloys, and Co-based alloys.<br>• Used to reduce concentration gradient of co-based alloys, preventing unidirectional diffusion into the base metal, which reduces strength. |
| Fe | | | | | | | ✓ | • Compatible with steels, however tends to increase the liquidus temperature. |
| Mo | | ✓ | | | | | | • Preserves the low liquidus temperature of brazing alloy, while decreasing overall mass transfer of high mobility species. |

### *2.3.4.1 Effect of Time and Temperature on Wetting*

The effect of time and temperature on the wetting angle has been considered in the work by Chen and Shiue[32] on a Ag-Cu eutectic filler metal, with 4.5 wt% Ti (Ticusil) on a 304 stainless steel substrate, as shown in Figure 2.14(a). Although, the wetting angle was found to decrease with increasing temperature and time, at a higher temperature the decrease in wetting angle was more pronounced, while increases in the time produced a gradual decrease in the wetting angle. Liu *et al.*[33] performed a similar study with Braze 580 (57Ag-33Cu-7Sn-3Mn) on 304 stainless steel that showed a similar trend as illustrated in Figure 2.14b. Considering that the melting ranges reported for the Braze 580

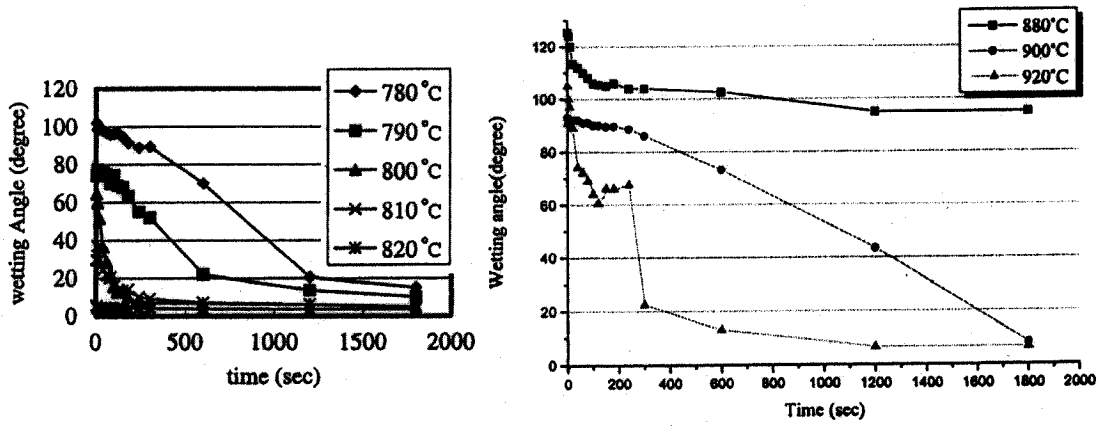


**Figure 2.14** The dynamic wetting of braze alloy (a) Ticusil® and (b) Braze 580[32,33].

and Ticusil alloy were 605-730 °C and 830-850 °C, respectively[33], the results in Figure 2.14 indicate that a minimum superheat of 50°C is required to improve wettability. Specifically, the wetting angle of the Ticusil and Braze 580 at temperatures near (or below) 880 °C and 780°C, respectively, show little improvement in the wetting behavior with time and can be considered non-wetting on 304 stainless steel for such processing conditions. Besides the effect of temperature and time, the experiments of Ambrose *et al.*[34] with a Ni-11%P braze on a Fe-20%Cr alloy substrate, have indicated an effect of chromium content in the substrate on the area of braze spread as illustrated in Figure 2.15.

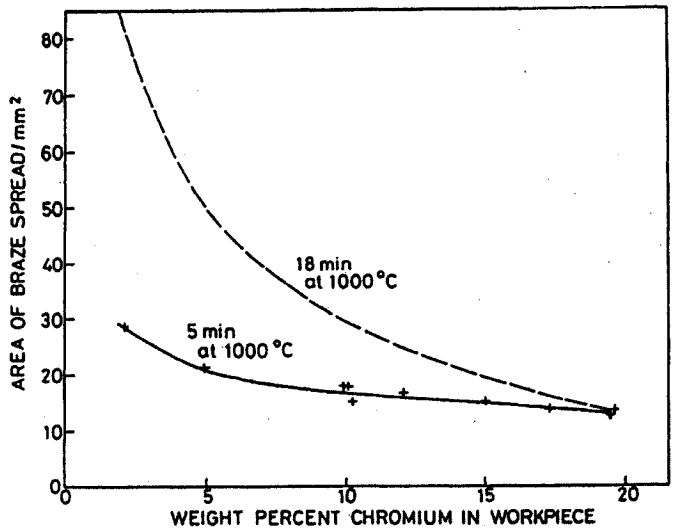


**Figure 2.15** Effect of time on the spreading of Ni-11%P braze on Fe-20%Cr alloy substrate[34].

For a specific temperature of 1000°C, the spreading of the braze was determined to increase with increasing brazing time and decrease with increasing chromium content. A critical chromium content of 10 wt.% was defined by Ambrose *et al.*[34] by considering wetting as a surface phenomenon; the composition of the surface oxide present on the iron chromium alloy would change from pure FeO for low chromium levels to a spinel solid solution containing increasing amounts of $Cr_2O_3$ with increasing chromium concentration. Alternatively, Gale and Wallach[20] have proposed that the detrimental effect of chromium addition on wetting and flow for Ni-Cr-P, Ni-Cr-Si-B, Ni-Pd-Si, and Cu filler metals on Ni-Cr substrates is related to the filler-metal oxide, filler metal viscosity and liquid-vapor interfacial energy. In boron-containing filler metals, peaks in the spreading were observed for Ni-10%Cr and 20% Cr as result of alloying reactions between the filler metal and the substrate, rather than from the composition of the substrate oxide. Furthermore, since the results indicated that isothermal solidification terminates the spreading of the Ni-Si-B brazes, it was hypothesized that once the Ni-Si-B and Ni-Pd-Si solidify at the brazing temperature, subsequent remelting is not possible even with a 200°C increase in temperature. Specifically, the melting point depressants B/Si and Pd/Si, readily diffused into the substrate during brazing to form the intermetallic phases and the resultant isothermal solidification due to boron diffusion from the braze

seam into the substrate is dependent on the time, as well as temperature due to the fact that the rate determining mechanism is solid-state diffusion of boron. Also, for palladium-bearing filler metals, Izui and Suezawa[35] have shown an increase in the spreading behavior as a function of time, using a SUS 316L type stainless steel substrate (Figure 2.16) and the brazing conditions listed in Table 2.4. Hence overall, the general effect of thermal input conditions for various filler metal and base metal combinations is an increase in the wetting behavior with increasing temperature or time.

**Table 2.4** Brazing conditions for various brazing filler metals[35].

| Alloy | Brazing Temperature (°C) | Brazing Time (min.) | Pressure (Pa) |
|---|---|---|---|
| 33Pd-64Ag-3Mn | 1290 | 5 | $2.6 \times 10^{-3}$ - $6.7 \times 10^{-3}$ |
| 40Pd-50Ni-10Co | 1300 | | |
| 30Pd-50Ni-10Cu-10Co | 1230 | | |
| Ni-Co-Cr-Mo-Fe-B | 1200 | | |

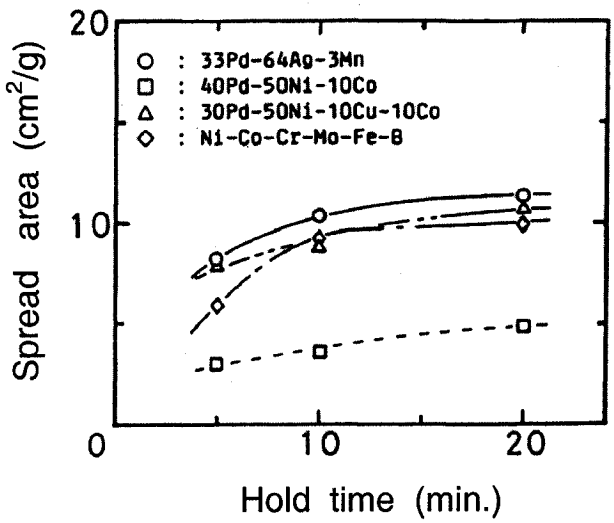


**Figure 2.16** Relations between spread area and hold time for various brazing filler metals[35].

### *2.3.4.2 Effect of Surface Roughness on Wetting*

Previous studies on the effect of surface roughening on braze spreading, conducted by Ambrose *et al.*[34], have used two different roughening methods, namely, isotropic and anisotropic. Isotropic roughening corresponds to a random roughening pattern produced by grit or shot blasting while anisotropic roughening entails directional channels produced from surface grinding or milling. The surface roughness, $R_a$, produced by either method is then measured by quantifying the average amplitude of the peaks and valleys of the surface. In the case of grinding and milling, exhibited in Figure 2.17, the area of spread has a tendency to increase as the surface roughness increases. In contrast for grit and shot blasting, the area of spread is inclined to decrease with a rougher surface finish as demonstrated in Figure 2.18. The difference in the spreading behavior has been attributed to a preferred orientation of the roughened surface during grinding and milling that results in the formation of parallel channels that facilitate spreading by a tunneling effect. Hence, Rymar *et al.*[36] have indicated that spreading will increase with increasing surface roughness and is associated with capillary effects.

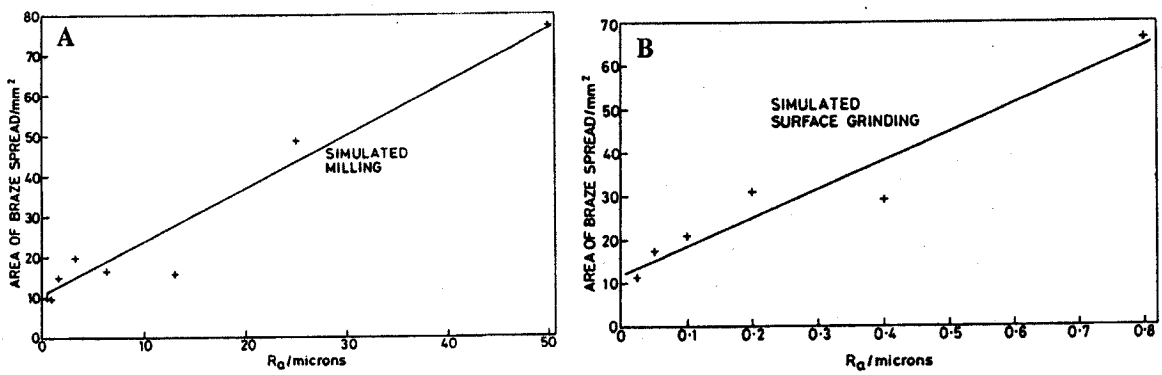


**Figure 2.17** The effect of surface roughness, $R_a$ on spread of Ni-11%P braze on simulated surface (a) ground and (b) milled nickel[34].

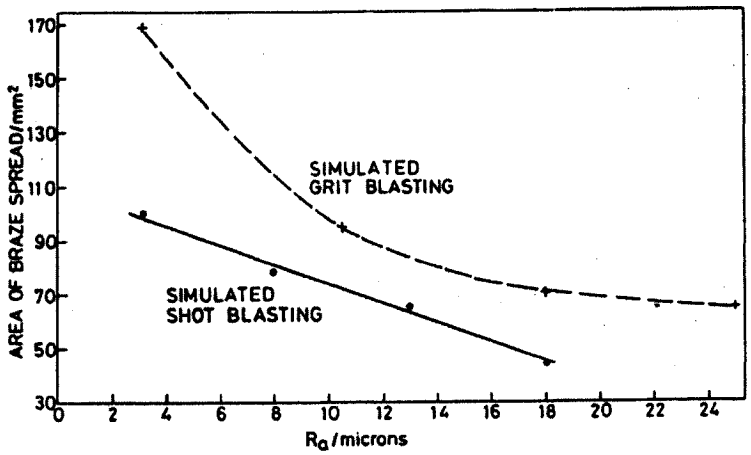


**Figure 2.18** The effect of surface roughness, $R_a$ on spread of Ni-11%P braze on simulated shot blasted and grit blasted nickel[34].

Wetting experiments using a Ag-Cu braze on a 321 stainless steel substrate, conducted by McGurran and Nicholas[29] involved the evaluation of two surface treatments for wettability: a surface finish that was (1) ground using a 400 grit SiC paper and (2) polished using 1 μm diamond. It was determined that there was a small difference in the minimum contact angle using the specified brazing temperature range for the ground and polished samples of approximately 58 and 42°, respectively. These studies signify that analysis of the wetting behavior as a function of surface roughness requires careful consideration of the material and processing conditions such that almost every system needs to be examined individually to understand the synergistic effect of the various parameters including at least the chemical composition of the filler and base metal, the interfacial reactions, the surface roughness and the processing cycle.

## 2.3.5 Effect of Time, Temperature and Clearance on Brazement

In developing the relationship between time and temperature on the wetting characteristics, it was observed that with a number of nickel-based filler metals the presence of melting point depressants resulted in the formation of hard phases within the brazement[37]. Lugscheider *et al.*[22,24,38,39] showed with the beginning of hard phase formation, there exists a maximum brazing clearance (MBC), which has been defined as a new brazing parameter. In their work, various nickel-based filler metal brazements were

examined by brazing wedged samples of 316 stainless steel with a clearance varying from 0 to 100 μm. The dependence of MBC on brazing temperature and time was investigated for silicide-boride stabilizing (BNi-2), boron and phosphorus-free (BNi-5), and phosphide stabilizing (BNi-7) filler metals, as shown in Figures 2.19-2.21[38], respectively. For all three filler metals, the brazing temperature and time were observed to have an impact on the MBC. In the case of the BNi-2, the increase in MBC was the greatest with increasing temperature at a brazing time of 60 minutes. This behavior can be attributed to the presence of boron (2.9 %), which diffuses from the seam faster than either phosphorus or silicon at higher temperatures and longer times, thereby giving the progressive increase in the MBC.

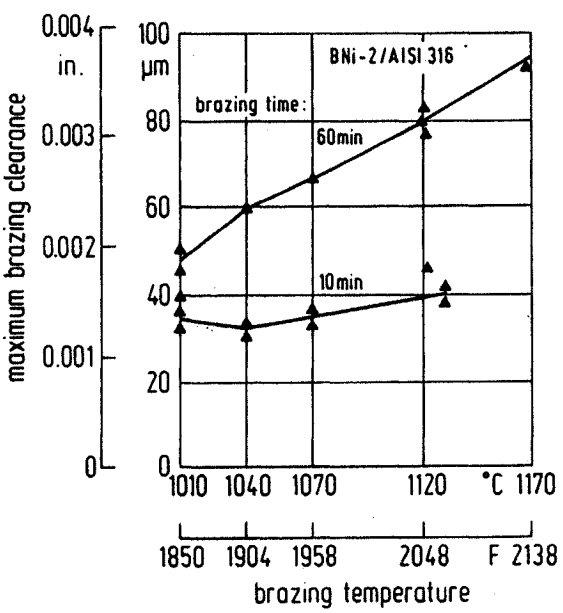


**Figure 2.19** Dependence of MBC on time and temperature for BNi-2[38].

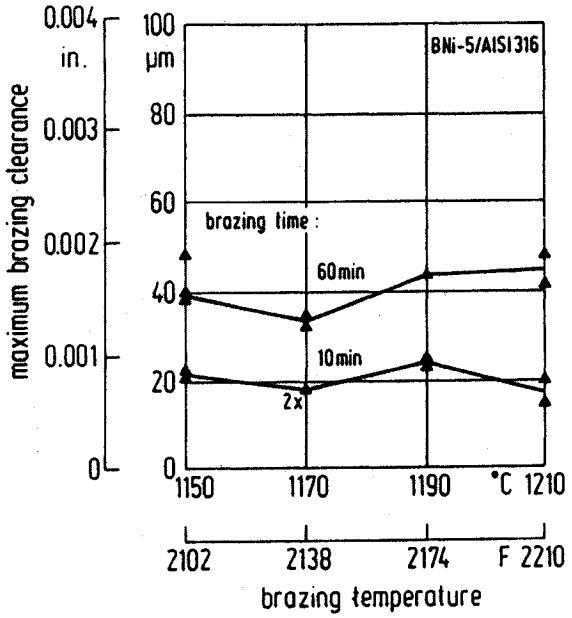


**Figure 2.20** Dependence of MBC on time and temperature for BNi-5[38].

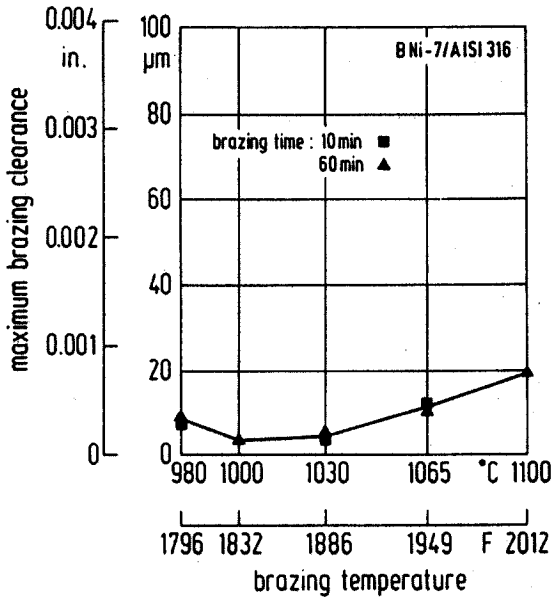


**Figure 2.21** Dependence of MBC on time and temperature for BNi-7[38].

BNi-5 showed a similar dependence of the MBC on the brazing conditions, and a higher brazing time is favored to achieve boron diffusion. In contrast, joints brazed with the BNi-7 demonstrated a low MBC value that was not as dependent on the brazing conditions most probably due to the high phosphorus content, which makes it is difficult to eliminate brittle phosphides by diffusion, even at a long brazing time of 60 minutes[38].

In a similar study using a wedge specimen to vary clearance, Lugscheider and Cosack[39], investigated joints of AISI 321 stainless steel with boron-free, nickel-based filler metals to examine the evolution of the microstructural characteristics as a function of the MBC. At a clearance less than the MBC, the microstructure of the brazement consisted of a Ni-solid solution. In the base metal, the solid solution structure containing dissolved silicon and phosphorus was observed to grow along concentric circles towards the brazing filler metal, so as to combine at the center of the brazement[39]. Hence, at a clearance value less than the MBC the brazement is free of hard phases, as shown in Figure 2.22a. However, at a joint clearance greater than the MBC, the large diffusion distance prevents complete dissolution of the hard phases into the solid solution.

Consequently, hard phases are present at the center of the brazement rendering the joint brittle, as illustrated in Figure 2.22b.

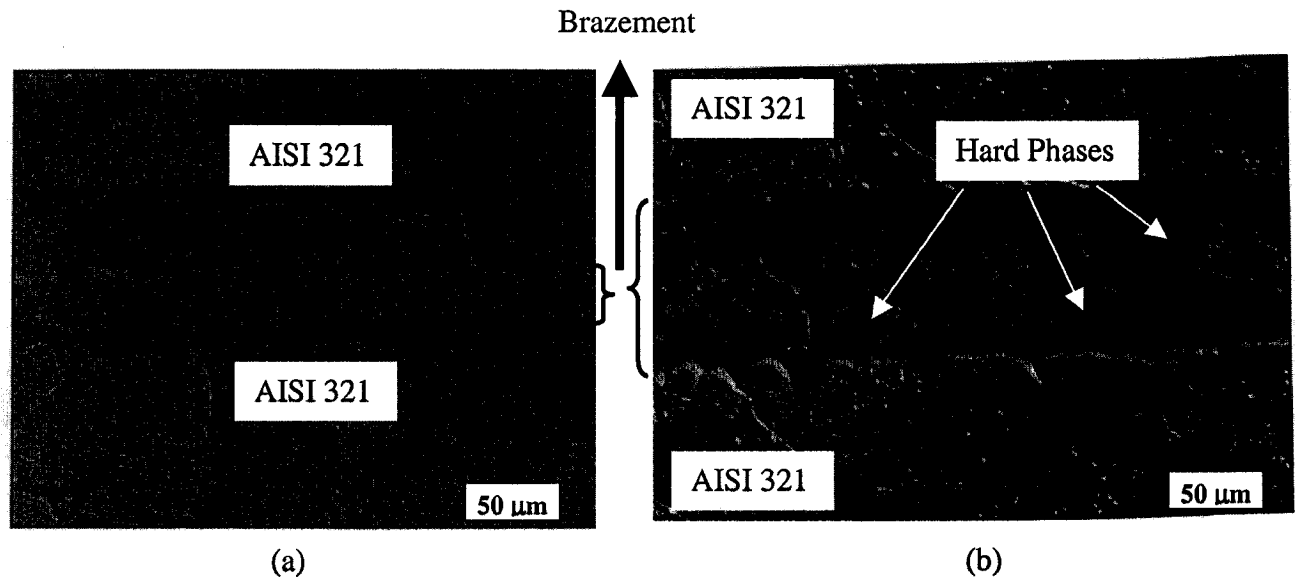


**Figure 2.22** Microstructure of joint brazed with 20.3Cr-11.5Si-0.5P-bal Ni on AISI 321. Brazed at a cycle of 1150 °C / 10 min. with a joint clearance of (a) 20 µm and (b) 93 µm[39].

In addition, AISI 321 stainless steel joints brazed with 14.8Cr-8.0Si-3.0P-3.0Fe-Bal Ni filler metal using a 40 µm clearance showed evidence of an intermediate region of hard phases consisting of solid solution bridges throughout the brazement. However, reducing the joint clearance to a value between 20 and 30 µm enabled brazements without hard phases.

By examining the role of phosphorus content on the microstructural evolution of nickel-based filler metal brazements on AISI 321 stainless steel, it was determined that hard phases such a silicides and phosphides are present within the brazement, but as the brazing time is increased, both the amount of hard phases and the nickel solid solution microhardness decreases[24]. In particular, since the filler metals contain silicon and varying contents of phosphorus, a shorter brazing time results in less diffusion of silicon/phosphorus out of the seam, which gives a higher microhardness. At a longer

brazing time, the decomposition of silicides and phosphides by the parallel diffusion of silicon and phosphorus from the seam reduces the microhardness. The brazing temperature has a similar influence on the microhardness with higher temperatures achieving more effectively silicon and phosphorus diffusion and resulting in brazements with a lower microhardness, which is dependent on the solubility of the silicon and phosphorus within the nickel solid solution.

## 2.3.6 Effect of Surface Roughness on Brazement

Since the surface roughness was previously reported to affect the flow of liquid filler metal, and in turn, influence the wetting characteristics of the brazing surface, it is then not surprising that additional bond strength can be achieved by abrading mating surfaces slightly[40,41]. Lugscheider *et al.*[41] have shown that an average peak-to-valley surface roughness value of ≤ 4 μm by grinding in the flowing direction yields strong joints when brazing AISI 316 Ti with BNi-5 using a temperature of 1195 °C (2183 °F) for 10 minutes. Conversely, when the mating surfaces were milled across the flowing direction, the prediction of the strength was not possible due to large variations of the results. Other surface roughness work by Suezawa and Izui[42] on brazed joints of SUS 410 with 5Pd-95Ag and 18Pd-82Cu filler metals indicated that the residual stress and tensile stress of the brazement with rough brazing surfaces ($R_{max}$ = 11.2 μm) were higher than those of brazed joints with smooth surfaces ($R_{max}$ = 0.4 μm). Under a tensile applied load, the filler metal in the brazed joint contracts along the width resulting in a compressive stress, which is reduced by the tensile residual stress in the width that causes a higher tensile strength.

## 2.3.7 Nickel-Palladium-Chromium-Silicon-Boron Brazing Alloys

### *2.3.7.1 Brazement Characteristics*

Although many nickel-based brazing filler alloys, containing boron and silicon as temperature depressants and chromium for corrosion resistance, have been successfully used in recent years for high temperature vacuum brazing, these alloys contain brittle intermetallic borides and silicides, which degrade the ductility and quality of a joint.

Moreover, the high brazing temperature requirements of some nickel-based filler alloys necessitate post braze reaustenitising for martensitic stainless steels and solution heat treatment for precipitation hardenable nickel-based alloys. These microstructural issues have lead to the recent development and use of Ni-Pd based filler metals, such as Alloy 36 and 36M[26]. In the work of Pattanaik and Mizuhara[26] non-continuous brittle (Cr, Ni, Fe) boride phases approximately 9B-24Ni-3Fe-64Cr by wt% were observed along the centreline of a AISI 410 stainless steel brazement using alloy 36 with a joint clearance of 100 μm (0.004") and a brazing time of 10 minutes, as illustrated in Figure 2.23a. An increase in the brazing time to 120 minutes for a clearance between 50 to 100 μm or a reduction in the clearance to <50 μm (0.002") with a brazing time of 10 minutes was observed to eliminate the presence of the brittle phases in the AISI 410 joints brazed with the Ni-Pd-based filler metals (Figures 2.23b and 2.24), due to the sufficient ability to diffuse boron in the seam to the base metal.

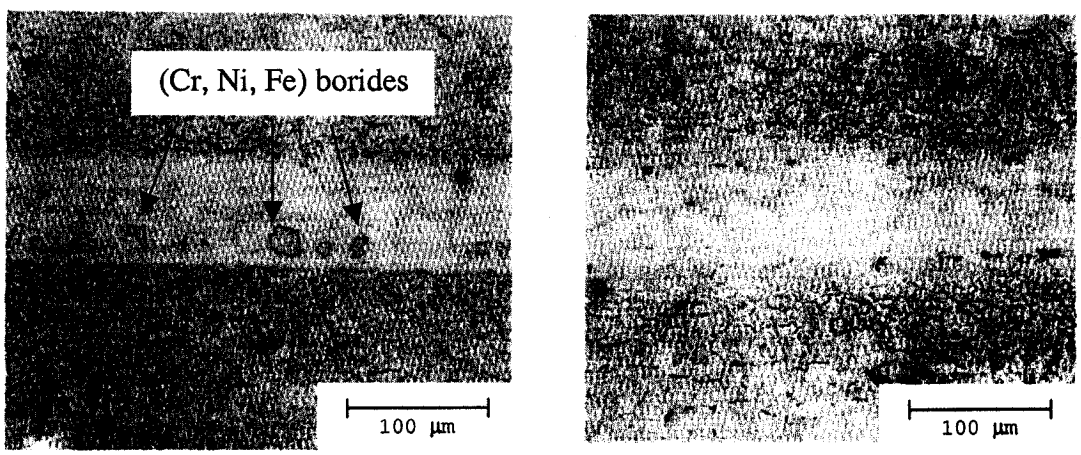


**Figure 2.23** Brazement of an AISI 410 with Alloy 36 using a clearance 100 μm. Brazing time of (a) 10 minutes at 1000 °C (1832 °F) (b) 120 minutes at 1000 °C (1832 °F)[26].

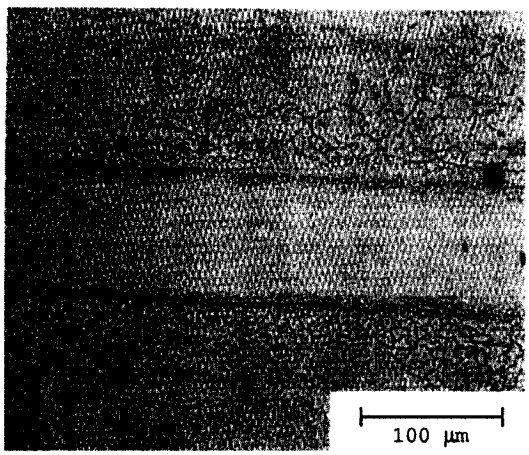


**Figure 2.24** Brazement of an AISI 410 with Alloy 36M using a clearance 100 μm and 120 minutes brazing time at 1000 °C (1832 °F)[26].

In other work, Lugscheider and Pelster[43] investigated brazing of 347 stainless steel with Pd-36, Pd-36M, NiPd-1, and NiPd-2 (Table 2.2) all of which have a melting range less than 1000°C due to the formation of low melting eutectics with palladium. These alloys permit low temperature brazing and allow minimal thermal stresses on the brazing components which result in energy savings during processing[44]. Moreover, the palladium content provided increased ductility and improved filling capabilities of wider joint clearances without the stabilization of hard phases[45,46]. Specifically, wedge samples with clearances of <50 μm could be brazed without having brittle phases in the brazement, and for larger clearances the brittle phases that were present did not decrease the strength of the brazed joints noticeably[43].

Hence, during brazing of stainless steels, the diffusion of boron into the base metal is critical and according to Kotek and Lugscheider[47] the migration of boron occurs by volume diffusion without diffusion along grain boundaries. The formation of borides parallel to the brazing interface and the location of the precipitates from the interface depends on the heat treatment and the composition of the filler metal, as illustrated by Figure 2.25, in which layers of $Fe_2B$ and FeB were observed[47]. Specifically, in 316 stainless steel Kotek and Lugscheider have suggested that carbon reduces the diffusion activity of boron, and due to the gradient present within the interface and base metal, the diffusion rate of boron is initially high, and then decreases rapidly to enter an activation

energy valley[47]. According to D'Silva[48], the depth of penetration of boron and silicon were 22 and 34 μm into a nickel-base superalloy using a nickel-palladium based brazing alloy.

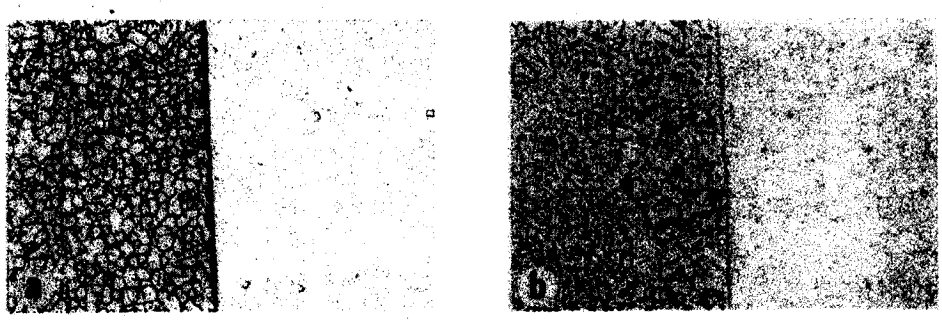

**Figure 2.25** Boron diffusion test of the brazing filler metal composition (wt%: 2B-5.3Cr-2.6Si-2.9Fe-Bal. Ni) at the joint interface with stainless steel 316. (a) Brazed sample, (b) Brazed and heat treated[47].

Therefore, although the use of Ni-Pd based filler alloys for both AISI 410 and 347 stainless steels joints has been considered in previous studies, a systematic examination of brazing dissimilar substrate combinations has yet to be carried out. Moreover, for brazing studies on either the AISI 347 and 410 stainless steel substrates, an examination of the influence of the brazing time, temperature and clearance has effectively shown that for specific conditions the microstructural characteristics can be optimized for these alloys. However, the role of wetting characteristics through the incorporation of the surface roughness conditions has not yet been considered in developing optimized processing cycles for obtaining a sound joint, which will be addressed in this work.

# *CHAPTER 3*

## *EXPERIMENTAL PROCEDURE*

The experimental procedure comprised of three main phases as demonstrated in the flow chart depicted in Figure 3.1. The first phase of the experimental plan was to evaluate the wetting behavior. Phase two involved vacuum brazing of dissimilar materials to produce sound joints, which were characterized in phase three.

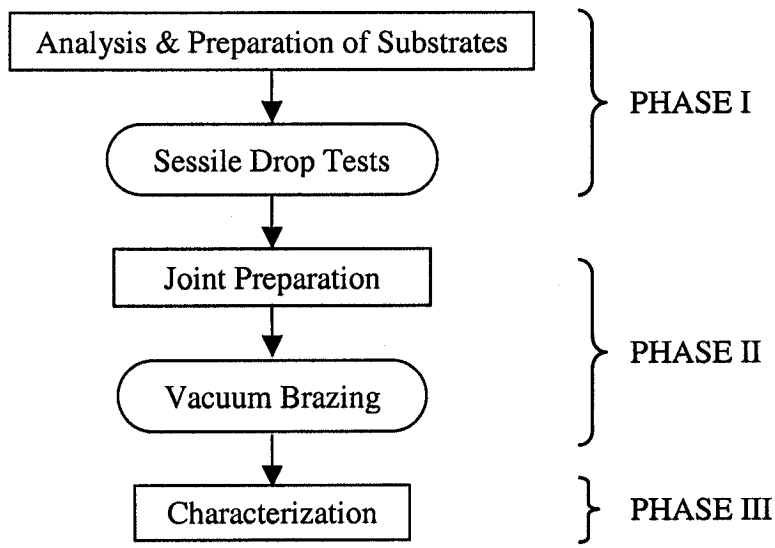


**Figure 3.1** Flow chart of the experimental plan.

## *3.1 Raw Materials*

Two types of stainless steels were investigated in this work for phases one and two of the experimental plan: a commercial grade martensitic AISI 410, and an austenitic AISI 347, which were supplied by Allegheny Ludlum (Washington, Pennsylvania) and Avesta Sheffield Plate Inc. (New Castle, Indiana), respectively. Both types of stainless steels were hot rolled, oiled and pickled slit strips from a 0.48 cm x 122 cm x 254 cm master sheet. The final strips of AISI 347 and 410 measured 0.48 cm x 5.1 cm x 91.4 cm and 0.48 cm x 5.1 cm x 122 cm, respectively. The chemical compositions of the stainless steels used are given in Table 3.1 according to the Mill certificate of analysis and laboratory testing at McGill University using atomic emission spectroscopy.

**Table 3.1** Chemical compositions of AISI 347 and 410 base metal.

| Base Metal | Composition, wt. % | | | | | | | | |
|---|---|---|---|---|---|---|---|---|---|
| | C | Cr | Ni | Si | Mn | P | S | Nb | Fe |
| AISI 347 | 0.05 | 17.12 | 9.12 | 0.40 | 1.23 | 0.023 | 0.01 | 0.79 | Balance |
| AISI 410 | 0.12 | 12.27 | 0.31 | 0.39 | 0.35 | 0.023 | 0.005 | -- | Balance |

The brazing alloy PalNiCro™ used for the vacuum brazing tests was a commercial grade paste (PWA 36099-140) having a particle size of -140 mesh supplied by Aimtek Inc. (Auburn, Massachusetts). The chemical composition of the PalNiCro™ brazing alloy is given in Table 3.2 according to the certificate of analysis. The melting range, given in Table 3.2, for the PalNiCro™ alloy is defined by the solidus and liquidus temperatures, which are 821°C and 960°C, respectively. The paste contained an organic binder that was 12% by weight and had a boiling temperature of approximately 650°C.

**Table 3.2** Chemical composition of PalNiCro™ brazing alloy paste.

| Filler Metal | Chemical Composition (wt.%) | | | | | Melting Range (°C) | |
|---|---|---|---|---|---|---|---|
| | Pd | Cr | Si | B | Ni | Solidus | Liquidus |
| PalNiCro™ | 35.9 | 10.6 | 0.6 | 2.9 | Balance | 821 | 960 |

## *3.2 Wettability Tests*

### 3.2.1 Preparation of Substrates

Samples of AISI 347 and 410 were sectioned into square coupons of 15 mm x 15 mm from a 4.8 mm thick strip. The oxide layer on all the exposed surfaces was removed by rough grinding. Each specimen was then cold mounted using an epoxy resin having a low curing temperature and overnight sitting. The surface was then prepared for the various experiments using standard metallographic techniques. Specifically, to investigate the influence of brazing temperature for determining the optimal value by sessile drop testing, the specimen surface preparation involved grinding with successively finer SiC grit paper from 120 grit to 600 grit followed by polishing, on nylon cloths with 6, 3, and 1 μm diamond suspension and an alcohol-based lubricant. Once the surface was prepared, the substrate was carefully removed from the cold mounting media. The substrates were then cleaned with soap and water and placed in an ultrasonic bath of acetone for 20 minutes. Subsequent handling of the substrates was performed using tongs to minimize contamination from dirt, dust and fingerprints.

Alternatively, to investigate the effect of surface roughness on the brazing characteristics the surface of the specimens was ground after cold mounting with SiC paper from grit sizes of (1) 120 to 240, (2) 120 to 600 and (3) 120 to 1200 grit. The samples were then removed from the cold mount and cleaned as previously mentioned. Prior to brazing, the surface characteristics of the 240, 600, and 1200 finish specimens were examined using atomic force microscopy as related in section 3.2.2.

### 3.2.2 Topographical Analysis of Substrates (Atomic Force Microscopy)

The surface topography of the substrates used in the sessile drop tests was evaluated using the atomic force microscopy (AFM) technique. The atomic force microscope can be used to measure local features such a length, width, and height over a small region by utilizing a probe tip that is placed very close to the sample. In particular, the raster scan moves the tip across the surface to acquire an image similar to a scanning electron microscope. The tip of the probe is connected to a cantilever, which measures the vertical deflection for determining a local height. The end tip radius typically measures about 30 nm, which allows for excellent resolution. The resulting 3-D image consists of rows of lines one above another.

The substrates were analyzed using the Digital Instruments Dimension 3100 Series AFM with image analysis software. All scans were executed using the contact mode of the AFM for which the tip remains in constant contact with the surface. The scanned area was a square measuring 50 x 50 μm and the image resolution was 512 lines including a trace and a retrace. The probe tip was positioned perpendicular to the grinding markings in order to measure the height and depth of the peaks and valleys. Three separate representative regions were chosen for each sample to obtain a normalized average value for the roughness parameter of three different substrates (240, 600, and 1200 grit finish). Also, three dimensional surface topography images were obtained, by sectioning the surface to enable direct measurements of the minimum and maximum heights. A minimum of three sections was taken for each topographic surface.

### 3.2.3 Sessile Drop Tests

The sessile drop test, which was performed to evaluate the wettability of the substrates through measurement of the contact angle, involved the use of an experimental set-up as depicted in Figure 3.1. In particular, a Lindberg 54233 furnace with a quartz tube of 47 mm inner diameter and 91 cm in length was used for the heating cycle that was programmed with a Eurotherm 2416 controller. The tube was sealed at one end with a transparent viewport, and the other end was connected to a vacuum/gas line to allow a vacuum atmosphere for purging of the tube with ultra high purity (UHP) argon gas. The

vacuum system consisted of a diffusion pump and rotary backing pump. A high-resolution digital camera was positioned on a tripod at the viewport to capture in-situ photographs during melting, by ensuring that the vertical position of the center of the camera was aligned with the surface of the substrate. A drop of brazing metal was centrally placed onto a prepared substrate, which was then positioned onto a boron nitride tray located within the tube furnace. As the boron nitride tray was attached to a metal wire-tube assembly, the substrate could be moved into different zones of the furnace using a magnet without having to break the vacuum. After placing the substrate into the boron nitride tray in the cold zone of the furnace, the tube was evacuated until a vacuum better than $10^{-5}$ Torr was reached. The temperature inside the tube was then increased above the liquidus temperature (960°C) of the brazing metal and held constant for a period of time (~10 minutes). Using the magnet from the exterior, the substrate was then introduced into the hot zone of the furnace, and upon incipient melting of the brazing filler metal drop, photographs were taken in-situ as a function of time. During heating, the tube was periodically purged with UHP argon gas. To investigate the influence of temperature on the wettability and determine the optimal brazing temperature, substrates having a 1 μm finish were examined using the sessile drop technique with the furnace temperature set at 970, 980, 990, 1000, and 1015°C. The optimal temperature was then selected on the basis of superior wetting characteristics. To investigate the influence of surface roughness, substrates with finishes of 240, 600, and 1200 grit were examined using sessile drop testing at the optimal temperature. From these experiments, the optimal surface roughness was determined. Due to the dynamic nature of the experiments, it was only possible to obtain one still image per unit of time, thus to ensure repeatability, a sessile drop test was carried three times for a given substrate, temperature and surface finish.

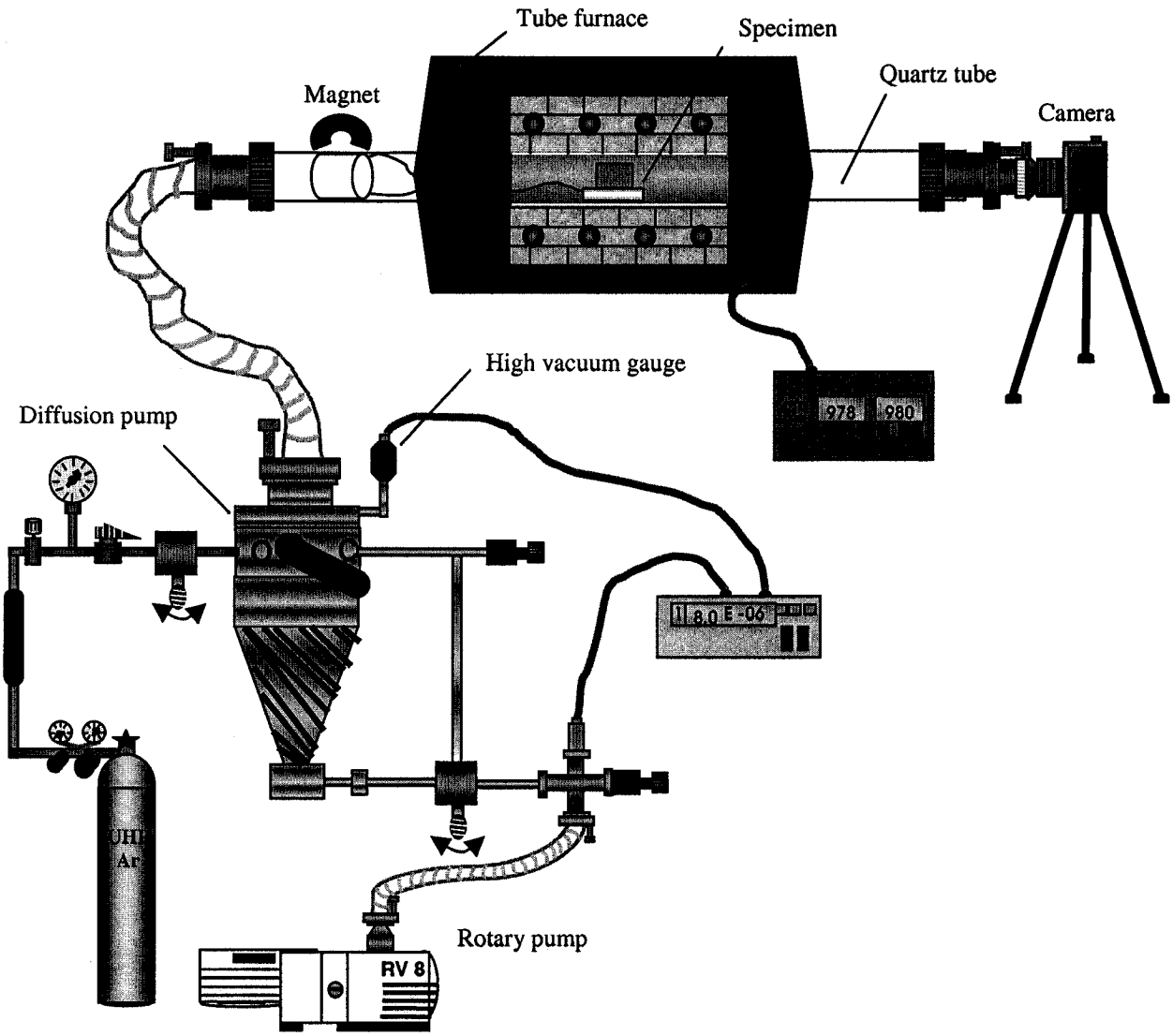


**Figure 3.2** Schematic diagram of the experimental set-up for the sessile drop tests.

### *3.2.3.1 Contact Angle Measurements*

From the digital photographs taken during the sessile drop testing, the contact angle between the molten brazing metal and the substrate sample was analyzed using a photo editing software. The contact angle was obtained by magnifying the digital image and delineating two intersecting line segments: one line segment parallel to the substrate

surface and the other tangential to the liquid drop as depicted in Figure 2.3. The angle subtended by the two line segments defined the contact angle.

## *3.3 Preparation of Joints*

Prior to vacuum brazing, the joints to be brazed were prepared according to the joint design developed by Lugscheider *et al.*[41], in which a wedge configuration was used with a clearance or gap varying from 0 to 250 μm, as illustrated in Figure 3.2. The faying surfaces were prepared with the optimized finish for wettability (i.e. 240, 600 or 1200 grit) as given in *Section 3.2.1*. A 304 stainless steel foil spacer was inserted between the two base metals to produce a V-wedge, which was then tack welded together to produce a solid assembly. Notches were machined at a 45° angle on opposite sides of the joint to encapsulate the brazing metal once molten.

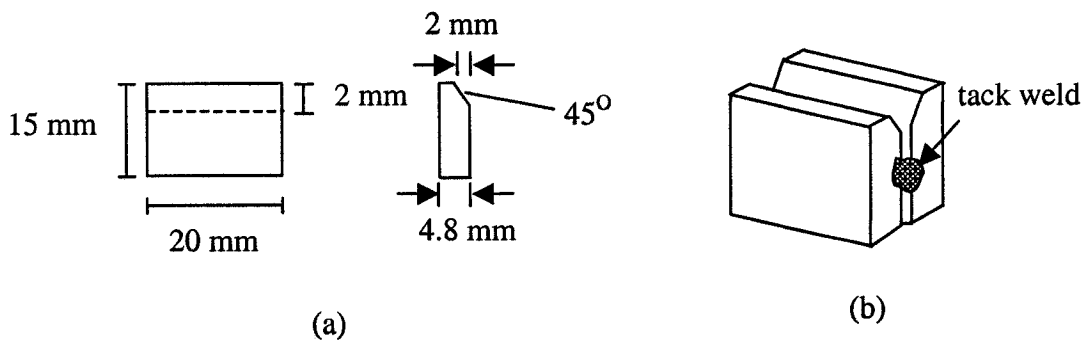


**Figure 3.2** Schematic diagram of (a) the front and side view of wedge joint including the dimensions and (b) the 3-D view.

## *3.4 Vacuum Brazing*

The wedge samples were vacuum brazed using the tube furnace shown in Figure 3.1 that was modified by replacing the viewport on the closed end (for the sessile drop tests) with a 60 cm long K-type thermocouple, which was connected to a vacuum fitting and used to monitor the thermal cycle. Prior to brazing, a thick bead of the brazing metal paste was applied by means of a syringe into the notch of the wedge specimen depicted in

Figure 3.2. The assembly was then placed into the center or hot zone of the furnace, and the tube was sealed.

The thermal schedule that was used for all the brazing cycles is outlined in Figure 3.3. For the optimized conditions of the brazing temperature and surface finish (as determined from the sessile drop tests), the effect of brazing time on the joint characteristics was studied for a holding time of 15, 30, and 60 minutes. After holding for the duration of the brazing time, the furnace power was turned off and the specimen was furnace cooled to room temperature.

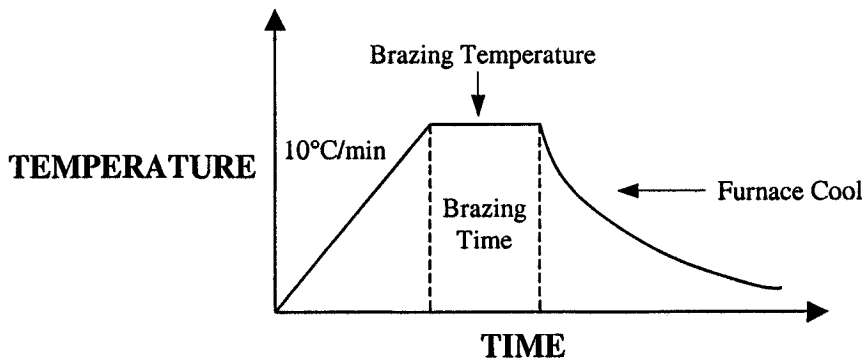


**Figure 3.3** The thermal schedule for vacuum brazing cycles.

## *3.5 Joint Characterization*

The joint was characterized using several different techniques to identify the different phases present, quantify the volume fraction of phases, and identify the composition of different constituents.

### 3.5.1 Metallographic Preparation

After brazing, the specimens were sectioned in various locations as illustrated in Figure 3.4a. The Sections A-B and B-C were mounted in cross section, to enable metallographic preparation of the surface in the vicinity of B and C as described in Figure 3.4a. The sectioned view demonstrated in Figure 3.4b shows the clearance variation.

Metallographic preparation of the specimens involved grinding with successively finer SiC paper from a grit size of 240 to 600 grit with water as a coolant. The specimens were then polished using 6, 3, and 1 μm diamond suspension and an alcohol-based lubricant on nylon cloths for 2 minutes with a pressure of 5 lbs/sample and a rotation speed of 150 rpm. The microstructure of the brazement was revealed using Vilella's reagent for the AISI 410, and Kalling's reagent for AISI 347[49].

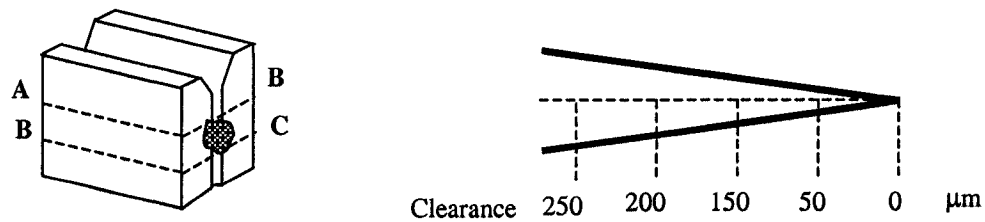


(a)

**Figure 3.5** (a) Location of sections A-B and B-C (b) Clearance variation of wedge specimen taken from prepared sections.

### 3.5.2 Optical Microscopy

The brazement was examined using an optical microscope (Nikon Epiphot 200) coupled with a Clemex Vision PE image analysis software for quantitative analysis of the phase constituents including the relative fraction, size and distribution. Specifically, the brazement microstructure image was digitized to generate a histogram of grey levels that were then associated to particular phases to determine the relative fraction based on an area percent calculation, which was the quotient of the phase area and the area occupied by the joint.

### 3.5.3 Electron Microscopy

To resolve the fine precipitates in the boron-containing brazement, a Hitachi S-4700 field emission gun scanning electron microscope (FEGSEM) was used, which was equipped with energy dispersive spectroscopy (EDS) for qualitative chemical analysis of the brazement and interface of the joint. Also, a JEOL 840A SEM was also utilized to

obtain both secondary electron (SE) and backscattered electron (BSE) images to identify and differentiate the different constituents present in the brazement.

### 3.5.4 Micro Indentation Hardness Measurements

The hardness of the various regions and different phases of the brazed joints was measured using of a load of 25 g for 15 seconds on a Buehler Micromet 2101 Vickers Microhardness Tester to support the microstructural identification of the various phases performed using the electron microscope. These hardness values can also provide an indication of the strength of the joint through the general relation H = TS / 3.45, where TS is the tensile strength in MPa and H is the Brinell hardness[50]. All indentations were performed on mounted, polished and etched specimens and measurements were made manually using a 400x objective lens. The hardness values for the various phases or regions obtained during processing were a normalized average of at least five measurements for statistically representative results.

# *CHAPTER 4*

# *RESULTS AND DISCUSSION*

## *4.1 Optimization of Wetting Conditions*

### 4.1.1 Effect of Time and Temperature

The wetting behavior was studied using the sessile drop tests over a range of processing conditions to determine the optimum temperature and time for brazing. In particular, at a normalized initial value for the contact angle of 20°, measurements of the contact angle as a function of both time and temperature were obtained. Figure 4.1 illustrates the initial condition of a contact angle of 20° for a sessile drop with the geometrical configuration of spherical or curved cap situated on a completely horizontal substrate (Figure 4.1b). As indicated by the circular morphology of the sessile drop on the smooth surface of the substrate (i.e. mirror finish by polishing) that is illustrated in Figure 4.1b, uniform spreading of the molten brazing metal was observed. It is noteworthy that a substrate with a smooth surface was used in order to circumvent or reduce any topographic effects so as to study the relationship between experimental and theoretical models that predict wetting behavior using the assumption of an ideal smooth surface.

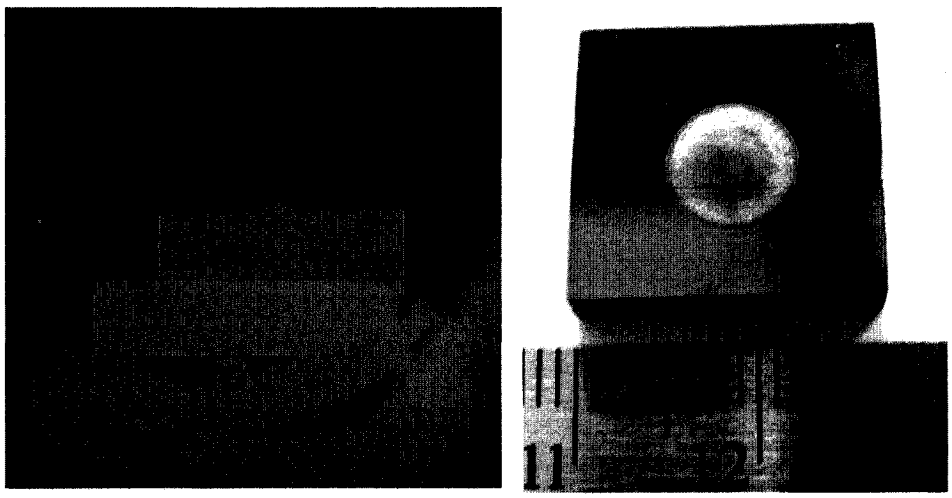

(a) (b)

**Figure 4.1** Sessile drop test representing a contact angle of 20° shown from (a) the side-view within the brazing furnace and (b) the top-view after cooling.

Figures 4.2 and 4.3 illustrate the wetting behavior for AISI 347 and AISI 410 substrate materials as a function of time for five different temperatures in the range of 970 to 1015°C. The graphs represent a family of curves, which can be divided into three separate stages denoted as regimes I, II, and III. Regime I is characterized by the initial stage of wetting in which the slope of the curve is relatively steep on account of the rapid decrease in contact angle with time. The occurrence of spreading (or decrease in the contact angle) can be related to incipient melting and binder vaporization that enables the brazing metal to assume a liquid spherical cap. However, to initiate spreading the tenacious surface oxide that is usually present on the substrate must be removed. A number of mechanisms have been proposed to account for the removal of the surface oxide and subsequent spreading of the brazing metal. Specifically for vacuum brazing, the discontinuities within the surface oxide have been reported by Fletcher[12] to act as a pathway for the liquid brazing metal to interact with the substrate material. Alternatively, Gale and Wallach[20] have documented that the boron within the brazing metal possesses the ability to reduce the surface oxide on the substrate, which then permits spreading of the molten brazing metal. Specifically, the diffusion of boron from the liquid brazing metal to the substrate causes an increase in melting temperature of the brazing metal, such that the

liquid front advances and produces isothermal solidification. Gale and Wallach[20] have reported that the occurrence of isothermal solidification is succeeded by a significant reduction in the contact angle, due to the formation of a reaction layer from the interaction of the liquid brazing metal and the substrate. This phenomenon then represents the transition condition between Regime I and II. For noble metal palladium containing brazing metals, McGurran and Nicholas[30] have reported that the brazing metal is incapable of reducing the surface oxide of stainless steels ($Cr_2O_3$). Instead the palladium containing brazing metal has the ability to dissolve elements such as iron into solution, due to d-band vacancies and intermediate atomic diameter[28], which enables the brazing metal to undermine the surface oxide widely and cause wetting to progress rapidly. The enhanced wettability of palladium containing brazing metals is also supported by the work of Bennett *et al.*[51] that reported improved wettability of AISI 304 stainless steel with increasing palladium concentration in silver-copper-palladium alloys. Regardless of the brazing metal/substrate combination, the progression into Regime II is typified by further decreases in the contact angle, albeit at a decreasing rate. The beginning of Regime III denotes the termination of the surface reactions, and a state of equilibrium is reached as suggested by the asymptotic nature of the curves resulting from a stabilization in the contact angle, and cessation of further spreading.

Figure 4.2 illustrates the wetting behavior for AISI 347 stainless steel at temperatures between 970°C and 1015°C and holding times until the state of equilibrium. From the various curves, the equilibrium contact angles for the five temperatures ranged between 5 and 10°, which suggests overall very good wettability between the AISI 347 stainless steel and the PalNiCro brazing metal. At the highest brazing temperature of 1015°C, a minimum value for the equilibrium contact angle was achieved. However, for process optimization selection of a lower brazing temperature with a small compromise in the wettability would be cost effective for industrial practice. However, it was observed that for the lowest brazing temperature examined in this work of 970°C, the wettability kinetics for reaching an equilibrium value for the contact angle of approximately 10° was particularly sluggish (> 200 seconds). Hence, the application of a slightly higher brazing temperature of 980°C was determined to be the most effective for attaining relatively

good wetting between the AISI 347 stainless steel and the PalNiCro brazing metal within a reasonable brazing time.

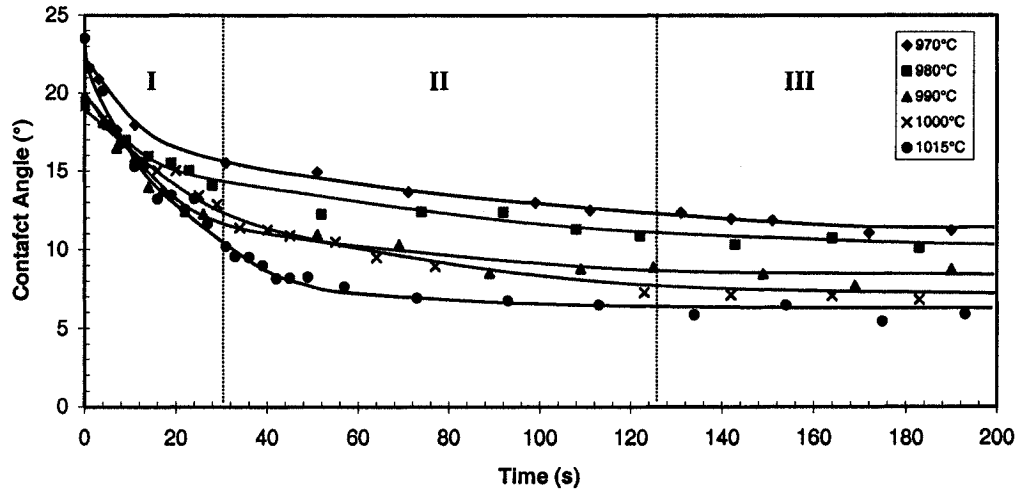


**Figure 4.2** The effect of time and temperature on contact angle for a smooth AISI 347 substrate.

The family of curves depicted in Figure 4.3 shows the wetting behavior for AISI 410 stainless steel, using PalNiCro brazing metal at brazing temperatures between 970°C and 1015°C. Although the five curves given in Figure 4.3 indicated that the AISI 410 stainless steel exhibited a similar wetting behavior to AISI 347, the spreading kinetics were determined to be almost twice as rapid for the former compared to the latter. In particular, the time to reach an equilibrium contact angle value for the AISI 410 stainless steel with PalNiCro was approximately 80 seconds, while that for AISI 347 stainless steel was roughly 140 seconds, for brazing temperatures in the range of 970°C to 1015°C. Nonetheless, the value of the equilibrium contact angle for the AISI 410 stainless steel which ranged between 13 and 7° was similar to that observed for the AISI 347 stainless steel. Also, similar to AISI 347 stainless steel, the optimum condition for using AISI 410 stainless steel was determined to be 980°C since the wetting kinetics were sluggish for 970°C. Hence, at the optimum brazing temperature of 980°C, both AISI 347 and AISI 410 stainless steel exhibited an equilibrium contact angle of roughly 10°, which indicates relatively good wettability for both substrates using PalNiCro brazing metal. Previous

work by Feduska[52] using a Ni-Cr-Si-B-C brazing metal at 1115°C on AISI 347 and AISI 410 stainless steel substrates has indicated equilibrium contact angles of 3° and 2°, respectively. Albeit the difference in equilibrium contact angle which can be attributed to the higher brazing temperature, the results reported by Feduska[52] indicated good overall wettability of AISI 347 and AISI 410 stainless steels and supports the findings in this work.

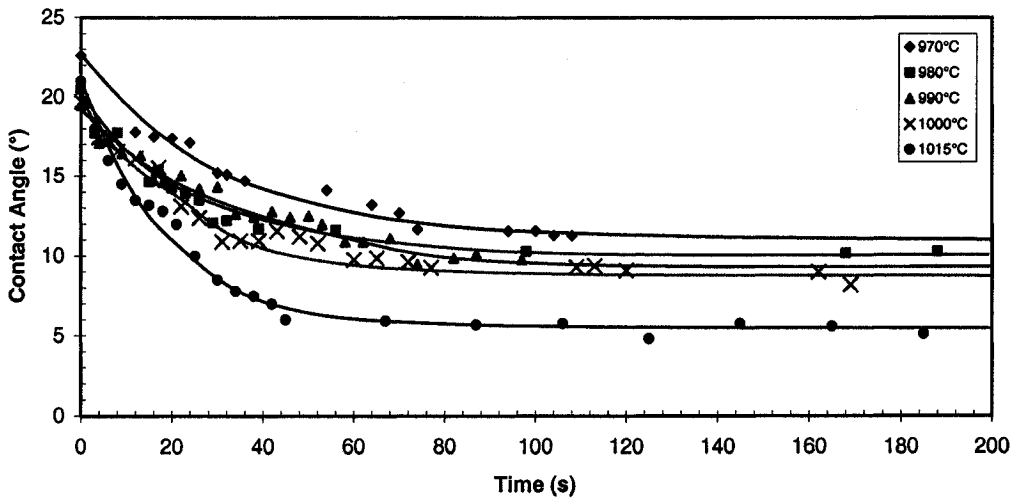


**Figure 4.3** The effect of time and temperature on contact angle for smooth a AISI 410 substrate.

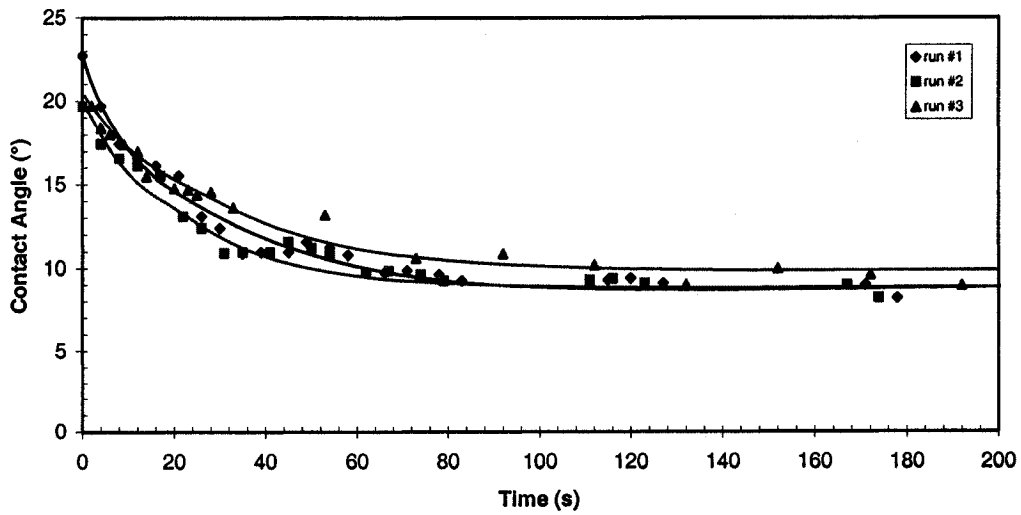


**Figure 4.4** Repeatability analysis for sessile drop tests using a smooth AISI 410 substrate at a brazing temperature of 980°C.

Due to the accelerated wetting kinetics for the AISI 410 stainless steel, the relative error in determining the wettability behavior was observed to be greater than that of the AISI 347 stainless steel. As such, it was realized that a repeatability analysis for the sessile drop test performed on the AISI 410 polished substrate at the optimized brazing temperature of 980°C would be representative of the maximum possible variability for the contact angle value. Figure 4.4 represents three independent sessile drop tests, which exhibit good repeatability. The values of the equilibrium contact angles were all within approximately 1°. The time to reach equilibrium was approximately 80 seconds for all three trials, which exemplifies identical wetting kinetics.

### 4.1.2 Atomic Force Microscopy (AFM) Analysis

In general, the wettability of a roughened substrate is dependent on the surface and interfacial energy changes of the actual area, as opposed to the apparent area given by *equation 2.9*. Also, the influence of the topographic changes of the surface can cause the flow to become turbulent instead of laminar, hence increasing the resistance to flow. Therefore, the energy changes require a knowledge of the roughness ratio, r, while the type of flow is governed by the shape and height of the local asperities[53].

For the two different stainless steel materials, the effect of surface roughness was studied by preparation of the substrates to a roughness of 120, 600 and 1200 grit. Examination of the substrate surface after roughening indicated that a slightly preferred orientation with a network of parallel channels, resulted from the grooving of the SiC particles into the substrate, as shown in Figure 4.5. Measurements of the maximum peak to valley height between 240 to 600 grit and 600 to 1200 grit indicated roughly an order of magnitude difference. Specifically, the maximum peak to valley height values ranged between 3.6, 0.3, and 0.1 μm for the 240, 600 and 1200 grit surface finishes on the stainless steel substrates, respectively. Furthermore, it was observed that for a smoother surface finish, the horizontal spacing increased and values of approximately 5, 2.5, and less than 1 μm were determined for the 240, 600 and 1200 grit surface finishes, respectively.

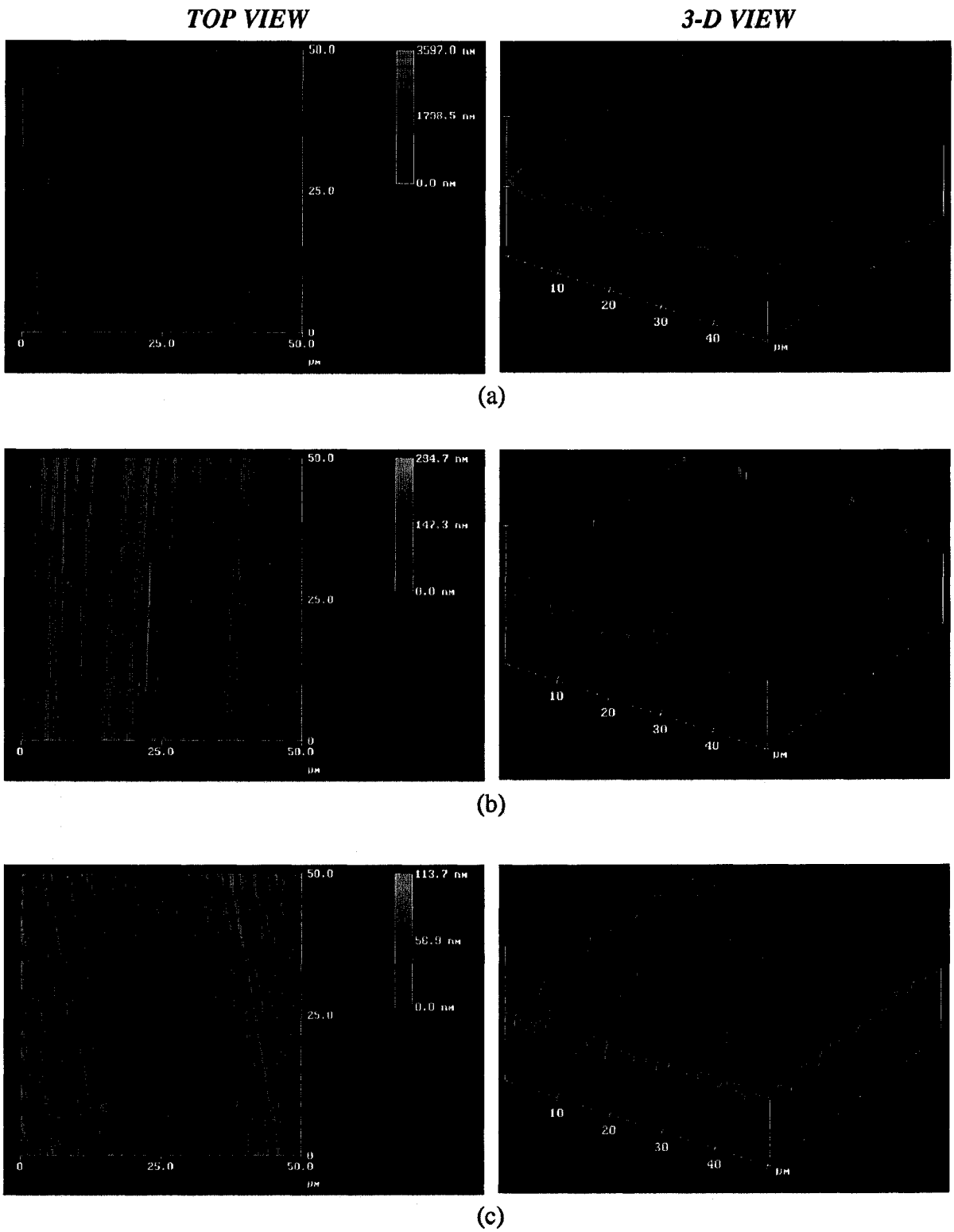


**Figure 4.5** Top view and 3-D view of the substrates profiles prepared with (a) 240 grit, (b) 600 grit and (c) 1200 grit SiC grinding paper.

Analysis of the three-dimensional profiles for the 240, 600 and 1200 grit surfaces are given in Figure 4.5, was also performed to quantify the surface roughness in terms of a mean value ($R_a$), for the surface relative to the center plane and the standard deviation ($R_q$ or RMS) of the z-values within a given area. The definitions of both $R_a$ and RMS are given by the following expressions:

$$R_a = \frac{1}{L_x L_y} \int_0^{L_x} \int_0^{L_y} \left| f(x,y) \right| dydx \qquad \text{(Eq. 4.1)}$$

where $L_x$ and $L_y$ are the lengths in the x and y-direction, respectively.

$$RMS = \sqrt{\frac{\Sigma(Z_i - Z_{ave})^2}{N}} \qquad \text{(Eq. 4.2)}$$

where $Z_i$ is the height in the z-direction and $Z_{ave}$ is the average height[54].

The three-dimensional topographic profiles for the 240, 600 and 1200 finishes on the stainless steel substrates, as illustrated in Figure 4.5 enabled the observation of waveform characteristics of the surface. Specifically, for the 240 grit finish, a smoothened sinusoidal waveform was observed that featured regions resembling walls that would act in a similar fashion to capillary tubes. In contrast, for the 600 SiC grit finish, a large array of sharper valleys were observed with spikes associated with the peaks that can be attributed to background noise and residual dust particles. The profile generated for the 1200 grit SiC finish on the stainless steel substrate comprised of a mixed regime of finely distributed peaks and valleys, and a large region of minor relief.

The histogram presented in Figure 4.6 shows the results of this quantitative analysis for the various 3-D profiles for the 240, 600, and 1200 grit finishes on stainless steel substrates in terms of the RMS and $R_a$ values. On average, each value was the mean of at least nine measurements. From the plot of RMS or $R_a$ as a function of the SiC grit size, it was determined that the surface roughness was greatest for the coarsest grinding paper size of 240 grit. Between 240 grit and 600 grit, the surface roughness was observed

to decrease rapidly as indicated by the considerably lower values for the RMS (32.3 μm) and $R_a$ (24.1 μm). Further decreases in the surface roughness were realized for the 1200 grit finish on the stainless steel substrate, albeit the change in the RMS (7.5 μm) and $R_a$ (5.8 μm) values was relatively low compared to the 600 grit.

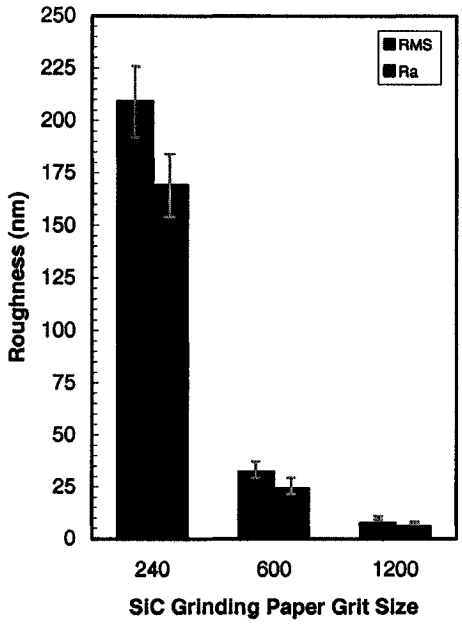


**Figure 4.6** Histogram of the RMS and $R_a$ values for SiC grinding paper grit sizes 240, 600 and 1200.

Their dependence of the RMS and $R_a$ on the SiC grit size can be rationalized based on the findings of Zipperian[55] that indicated a correlation between the mean diameter of the SiC particles and the grit size of the grinding paper, as depicted in Figure 4.7 for a steel substrate roughened randomly with SiC paper of varying grit sizes from 60 to 1200. In particular, Zipperian determined that the mean diameter of the SiC particles decreased with increasing grit size and the most significant changes occurred between 60 and 400 grit, which support the dependence observed for the $R_a$ and RMS values on the SiC grit size. Specifically, as the SiC grit size increases, the average diameter of SiC particles decreases and results in finer capillary walls as demonstrated by the decrease in the size of the troughs (Fig. 4.5) and the values of the RMS and $R_a$ (Fig. 4.6).

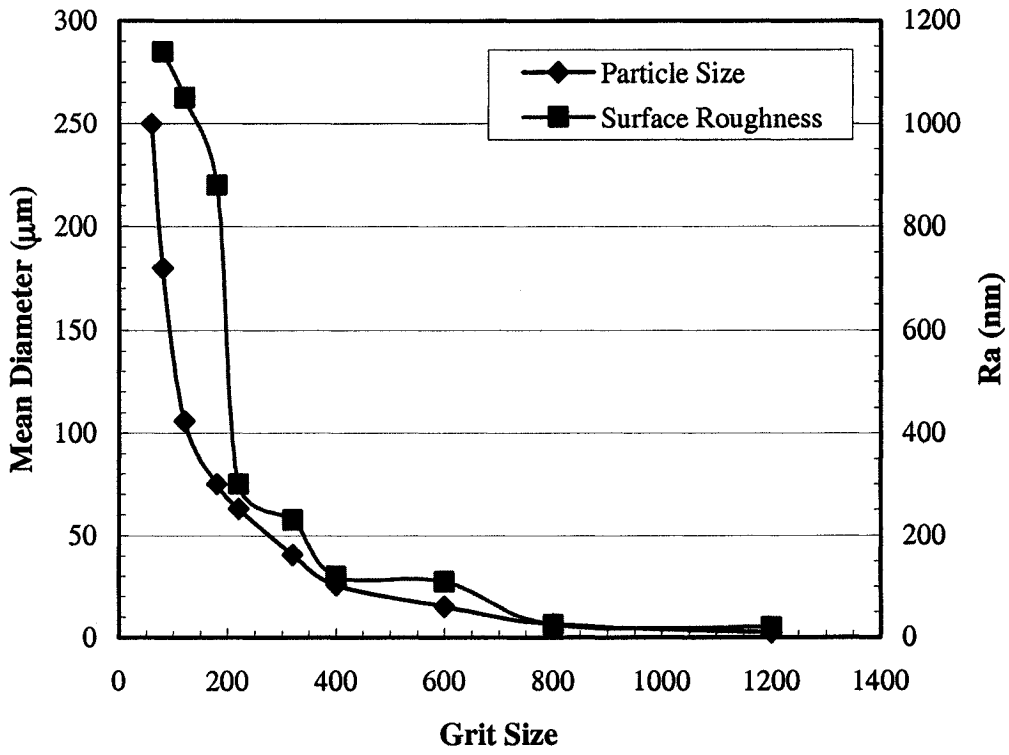


**Figure 4.7** Mean diameter and typical surface roughness ($R_a$ value) for abrasive grinding using SiC grit paper[55].

### 4.1.3 Effect of Surface Roughness

At the optimal temperature of 980°C, as determined from the sessile drop tests, the effect of surface roughness was determined for surface finishes of 240, 600 and 1200 grit SiC on stainless steel substrates. Specifically, sessile drop tests were performed for each surface at a temperature of 980°C to observed the change in the contact angle with time as indicated in Figure 4.8 and 4.9 for the AISI 347 and AISI 410 stainless steel substrates, respectively. The relationship between the contact angle and time for the different surface roughness was similar to that observed previously for the different temperatures (Figure 4.2 and 4.3). Moreover, the equilibrium contact angle values also ranged between 5 and 10° and steady state was reached within 100 seconds. The wettability results for the surface analysis indicated that for the AISI 347 stainless steel the roughness produced using 600 grit SiC paper enabled a lower equilibrium contact

angle than the polished surface and the 1200 grit or 240 grit finishes. The enhanced wettability observed for the 600 grit surface finish may be related to efficient flow of the liquid brazing metal against the capillary walls generated by the roughening process. With the 240 grit finish, the increased spacing between the two adjacent peaks was observed to reduce the driving force for wetting, while grinding to a finer finish (1200 grit) appeared also to decrease the wettability probably due to the constrictive passages restricting the viscous drag of the liquid phase.

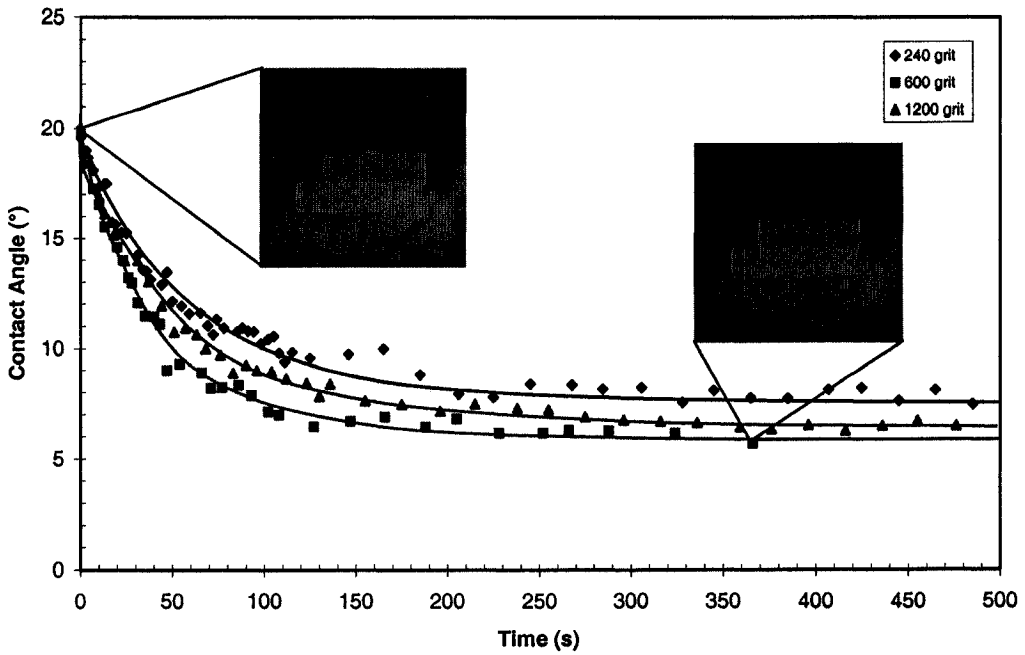


**Figure 4.8** The effect of time and surface roughness on contact angle for an optimal temperature of 980°C using an AISI 347 substrate.

Similar wettability results were observed for the AISI 410 stainless steel substrate, except for the 1200 grit finish , the equilibrium contact angle value was similar to that of the 600 grit roughened surface. This suggests that AISI 410 is slightly less sensitive to roughening effects, which may be related to the more adherent nature of the surface oxide from the lack of nickel and lower chromium content. In addition, the free energy associated with the interaction between the substrate and brazing metal is likely to be lower for the AISI 410 due to the difference in chemical composition of the brazing metal and stainless steel materials, while for AISI 347 the similarity in composition to the brazing metal would have a tendency to increase the driving force of wetting.

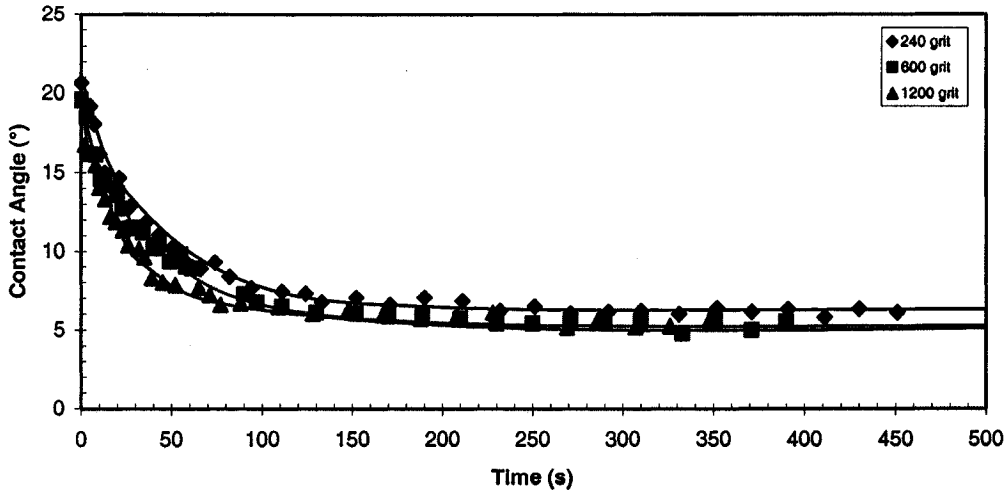


**Figure 4.9** The effect of time and surface roughness on contact angle for an optimal temperature of 980°C using an AISI 410 substrate.

In summary, optimized wettability for the AISI 347 and AISI 410 stainless steel substrates was observed at a temperature of 980°C and with a surface finish of 600 grit. Humpston and Jacobson[7] have proposed that a low contact angle ($\gamma_{LV}$) results through the addition of palladium in the brazing alloy due to a decrease in the surface tension of the liquid in contact with the vapor phase which is a consequence of a decrease in the surface energy of nickel from 1.615 x $10^{-4}$ to 1.570 x $10^{-4}$ J/cm$^2$[27]. This supports the findings in this work of good overall wettability between the PalNiCro brazing metal and the stainless steel materials that was optimized further by considering the brazing temperature and surface preparation to be cost efficient.

## *4.2 Effect of Brazing Conditions on the Joint Characteristics*

Optical microscopy, SEM, and microhardness were used to characterize the brazements. The following section is devoted to determining the effect of time and clearance with respect to the microstructural evolution. Upon optimization of the surface condition of the substrates and the brazing temperature, the vacuum brazed joints were examined in cross section as illustrated in Figure 4.10. The micrograph represents a typical brazement identifying the different regions that exist for a clearance of approximately 100 μm, namely the diffusion layer, the reaction layer, the brazing metal,

and the base metal. The brazing metal consisted of a two-phase region: a solid solution and a secondary phase. The effect of time and clearance on the liquid phase and the diffusion layer will be explored in the following sections. The effect of clearance on the MBC will also be examined. A qualitative microanalysis was carried out to determine the chemical composition of the different components mentioned in Figure 4.10.

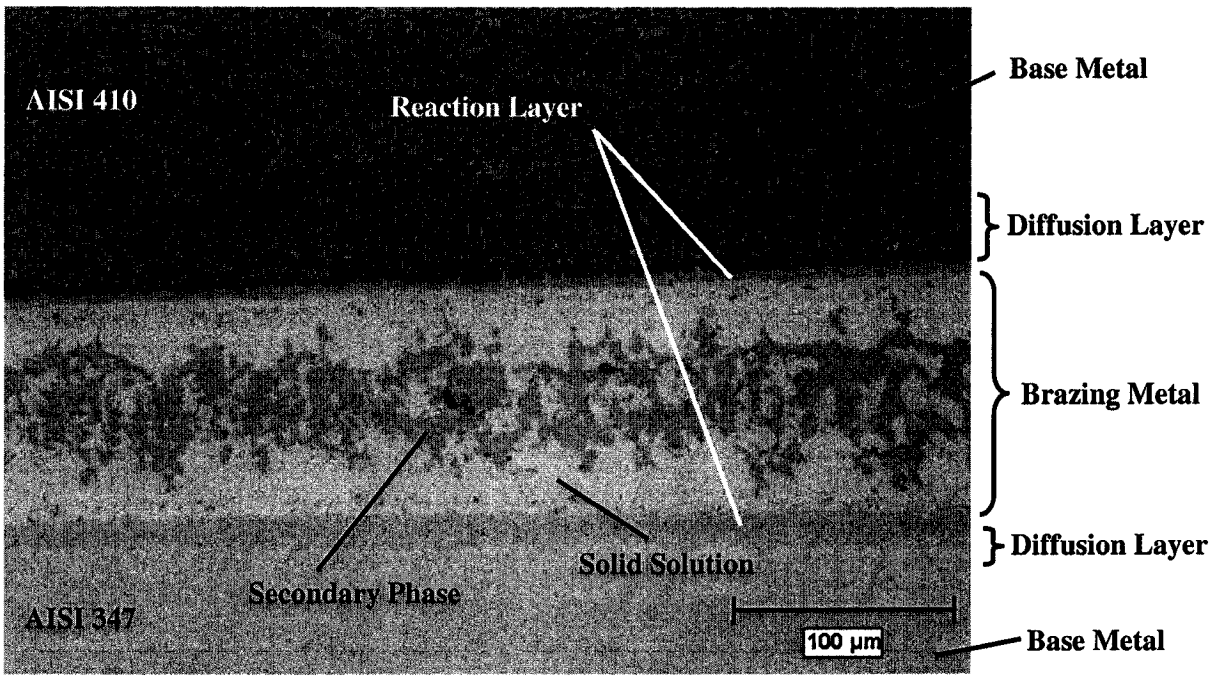


**Figure 4.10** Optical micrograph of a typical AISI 347/410 brazed joint.

During the brazing heating cycle, the two base metals are influenced, in addition to the physical and chemical changes occurring at the interface with the brazing metal. AISI 410 is a martensitic stainless steel that is hardenable within the range of 925-1010°C therefore a brazing temperature of 980°C would have a tendency to increase the hardness into the range of 450 HV[56]. The AISI 347 is austenitic stainless that is only hardenable through cold working, however the cooling cycle becomes critical when heated in the critical range between 800 and 850°C with regards to carbide precipitation and the possibility of inducing sensitization[57]. However, the typical AISI 347 composition will have niobium as an alloying element used as a carbide former. Niobium is a strong carbide former, even more so than chromium, hence niobium carbides will form instead

of chromium carbides, which would result in detrimental corrosion resistance such as sensitization. Nonetheless, the avoidance of carbide precipitation at the grain boundaries is desired to ensure optimal mechanical properties of the brazed joint. The carbide precipitation curves are presented in Figure 4.11 for 316 and 316L stainless steels. The carbon content of AISI 347 (0.05%C) corresponds to a curve that lies roughly in the center of the two curves in Figure 4.11, where it would take about 6 minutes until precipitation will commence (0.1 hours). The cooling curve presented in APPENDIX A, demonstrates that the residence time within the range between 800 and 850°C is well below 6 minutes. In terms of grain growth, no significant change was observed in both base metals due to the fact that the brazing temperature of 980°C is well below the limit for grain growth to occur. The brazing time has little effect compared to the temperature, therefore the brazing time was negligible with respect to grain growth[57].

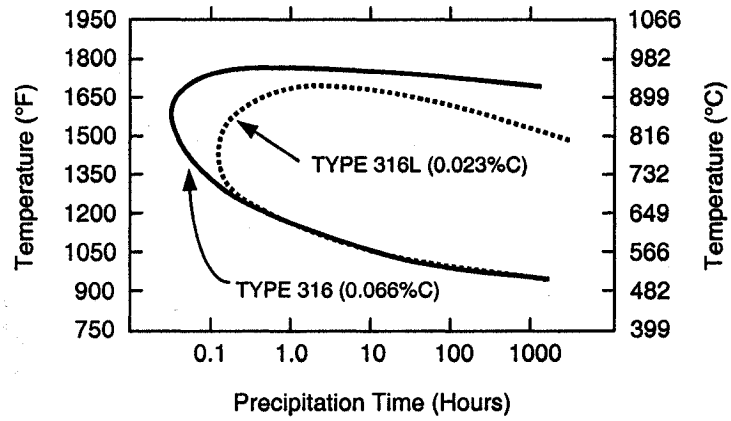


**Figure 4.11** Carbide precipitation curves as a function of time for AISI 316 and 316L stainless steels[57].

A hardness profile across the brazed joint is illustrated in Figure 4.12, where the average values of the AISI 347 and 410 were 166 and 338 HV, respectively. The hardness value of AISI 347 in the as received condition was approximately 160 HV, therefore no significant change in hardness was observed and the cooling cycle did not promote any measurable hard carbides to form. However, the martensitic stainless steel AISI 410 had a marked increase in hardness, as compared to the as received value of about 155 HV. Although the hardening range lies within the brazing cycle, and furthermore, a tempering cycle of 740°C is typically employed, the integrity of the joint and its mechanical

properties are unlikely to be compromised[56]. An evaluation of the joint strength would be necessary to evaluate the effect of base metal hardening. The strength of the joint is dependent on its weakest link, and due to the nature of the brazing metal, which contains dispersed regions of high hardness, it would tend to promote failure of the joint within the seam and not in the base metal. The variation in hardness values across the joint seam in Figure 4.12 appear to be a combination of soft and hard regions which may support the presence of the different phases depicted by the microstructure in Figure 4.10.

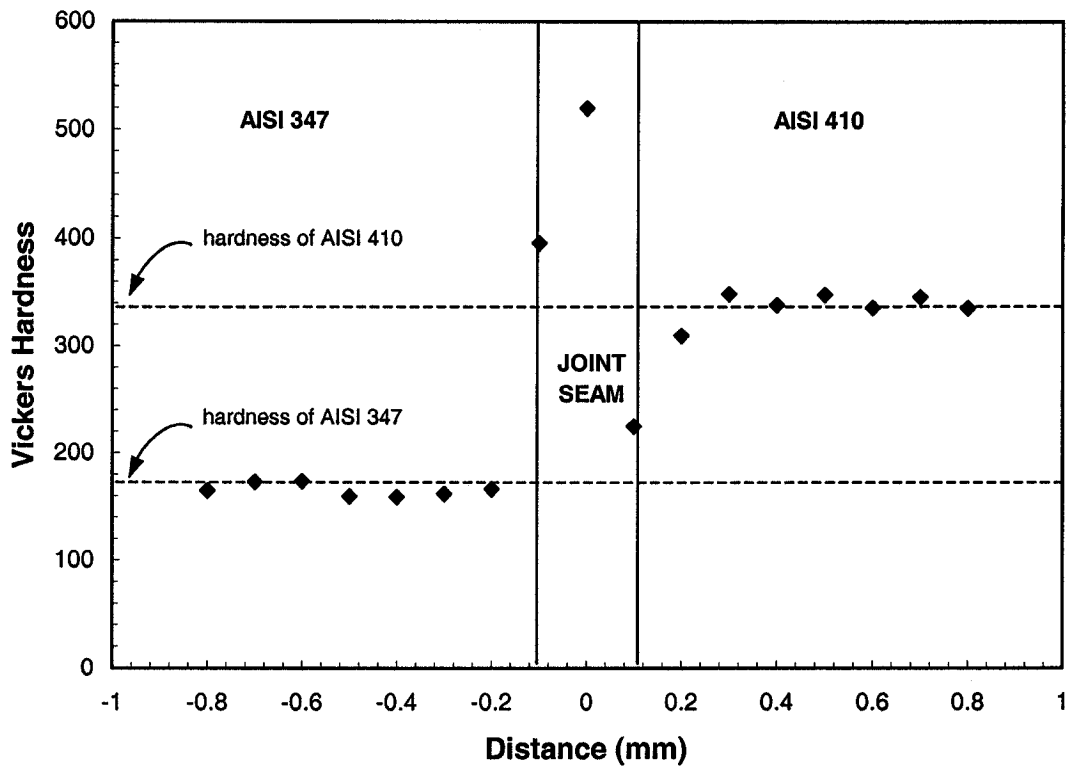


**Figure 4.12** Typical hardness profile of a brazed joint for a holding time of 15 minutes.

During brazing, a number of interfacial reactions take place as illustrated schematically in Figure 4.13. Initially, the brazing paste is added between the two faying surfaces at room temperature shown in Figure 4.13a, and the joint assembly is heated. During heating, solid state diffusion begins at the interfaces between the brazing alloy and the base metal (Figure 4.13b). Volume and grain boundary diffusion takes place, and upon further heating dissolution and interdiffusion of the brazing alloy and base metal

occur at the interface (Figure 4.13c). A liquid zone is produced during brazing and the elements of the base metal and the brazing alloy dissolve forming a reaction layer at the interface. Once the diffusing species (i.e. boron and silicon) have reached an equilibrium concentration in the brazing alloy, dissolution of the base metal ceases. Following dissolution, diffusion of silicon and boron from the brazing alloy into the base metal commences, which signifies the beginning of isothermal solidification. The result is the formation of a solid solution that produces coalescence[27,58].

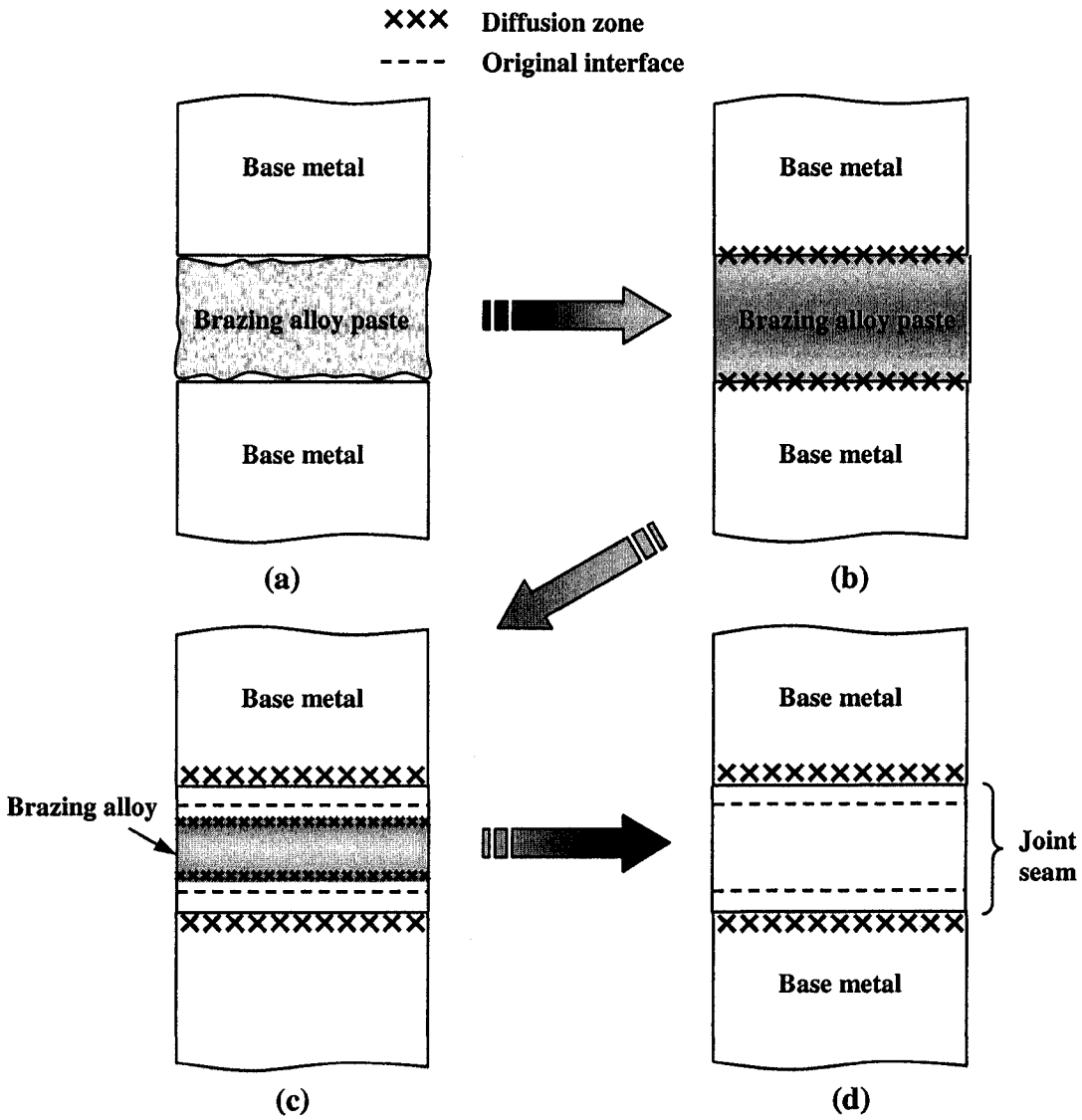


**Figure 4.13** Schematic diagram of interfacial reactions during brazing for ideal conditions[27].

Given sufficient time, the brazed seam is allowed to produce a solid solution free of secondary phases (Figure 4.13d). Figure 4.13 illustrates a brazed joint using ideal conditions such as a clearance below the MBC, sufficient time, and high enough temperatures to produce a seam free of secondary phases, however this may not always be the case (i.e. Figure 4.10).

A microanalysis of the joint seam confirmed the presence of two phases within the brazing metal. Figure 4.14 illustrates a back-scattered electron (BSE) image of the joint seam, which highlights differences in chemical compositions by gray scale contrast. The lighter phases correspond to constituents of higher atomic number whereas the darker phases contain elements of low atomic number. A light gray matrix, a dark gray phase and a white phase was observed, in which elemental mapping was carried out to characterize the composition of the individual phases.

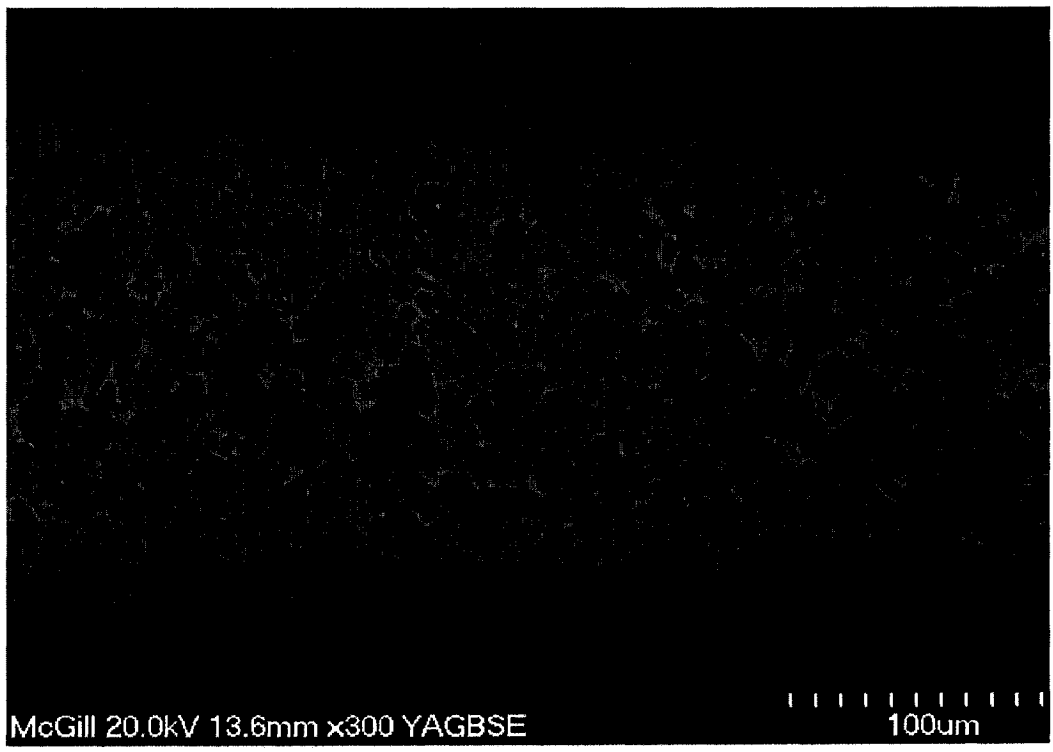


**Figure 4.14** BSE image of the brazement at a clearance of approximately 200 μm, and a holding time of 15 minutes.

Figure 4.15 illustrates a magnified view of the center of the brazement and an elemental mapping of palladium, silicon, chromium and nickel. The three regions previously mentioned are labeled from 1 to 3. The elemental mapping for the matrix (region 1) reveals elevated concentrations of palladium and nickel with traces of chromium, which suggests that a Ni solid solution formed containing some dissolved palladium, and chromium. Upon cooling, the solid solution is typically the first phase to form[2,4]. Figure 4.16 illustrates the fact that nickel and palladium are mutually soluble in one another and form a complete solid solutions at room temperature, however the brazing alloy contains a greater amount of nickel therefore a nickel solid solution was acknowledged[43]. The work of Nikiforova *et al.*[59] also demonstrated that the palladium concentration in the brazing seam always remains high due to the nonexistence of grain boundary penetration into the base metal. The hardness of the matrix was approximately 220 HV which is consistent with the study performed by D'Silva[31] having reported the microhardness of a T-joint using filler metal #36 as 260 and 280 HV for a brazing temperature of 955 and 1010°C, respectively. Similarly, Johnson *et al.*[60] and Lugscheider and Pelster[43] determined the microhardness of the typical α-nickel solid solution was 180-300 and 230-250 HV, respectively.

Region 2 corresponds to the white phase, formed as a dendritic network between the dark gray islands that was primarily rich in palladium (dark orange) and silicon (dark magenta) suggesting a silicide may have formed. After the formation of the nickel solid solution, the remaining liquid becomes enriched with silicon and boron, until a critical concentration is reached. According to the Pd-Si phase diagram illustrated in Figure 4.17, palladium and silicon are virtually insoluble in one another. There are a number of silicide compounds that may form; however given the low silicon content of the brazing alloy, the silicide most likely to form would be the type $Pd_5Si$[27]. Therefore region two, is assumed to be primarily composed of a palladium (solid solution) + $Pd_5Si$ phase, which is located at approximately 5 wt.% silicon as shown by the highlighted region in Figure 4.17. Microhardness measurements were taken to confirm the presence of the silicides by establishing their relative hardness values. The Vickers hardness values were in excess of 600 indicating a brittle nature characteristic of a silicide. A study conducted by Johnson *et al.*[60] showed that the microhardness of silicides formed within the seam of a ferritic steel

brazement using BNi-4 as a brazing alloy measured between 600-1000 Vickers, which is in agreement with the reported findings.

The dark gray islands corresponding to location 3 show no evidence of palladium, silicon or chromium, however a high concentration of nickel was evident. The nickel had segregated as islands within the joint microstructure as a distinct dispersed phase. The microhardness of these islands was as high as 1100 HV, which is not characteristic of pure nickel, suggesting that another compound forming with nickel must be contributing to the elevated hardness value. Although boron is known to diffuse into the base metal[23,24,47,48], if the diffusion distance is too large, any remaining solidifying liquid would tend to concentrate boron. The Ni-B phase diagram illustrated in Figure 4.18, demonstrates that boron is essentially insoluble in nickel. Various nickel borides may form upon the addition of boron, therefore the reported hardness values are consistent with the presence of nickel borides. Furthermore, Johnson[2] stated that nickel borides form in a brazement seam using a Ni-B-Si-Fe brazing alloy (BNi-4). The addition of boron as a melting point depressant in the PalNiCro brazing metal, shows a significant drop in the melting point of nickel-based alloys, as illustrated by the phase diagram in Figure 4.18. Therefore isothermal solidification via diffusion of boron into the base metal has an effect of increasing the remelt temperature of the brazement. Hence, upon the diffusion of boron, the melting point within the seam of the joint will be inclined to increase, resulting in a joint capable of withstanding higher service temperatures.

Detection of boron by conventional EDS analysis was difficult due to the relative low concentration and poor signal-to-noise ratio. In addition, the EDS detector of a conventional beryllium window contributes to absorption effects for light elements such as boron. However, when using the FEGSEM for microanalysis, an ultra thin window is employed to minimize absorption effects. Consequently, the presence of boron/borides was not detected within the brazing metal most probably due to low concentrations, which result in a weak signal.

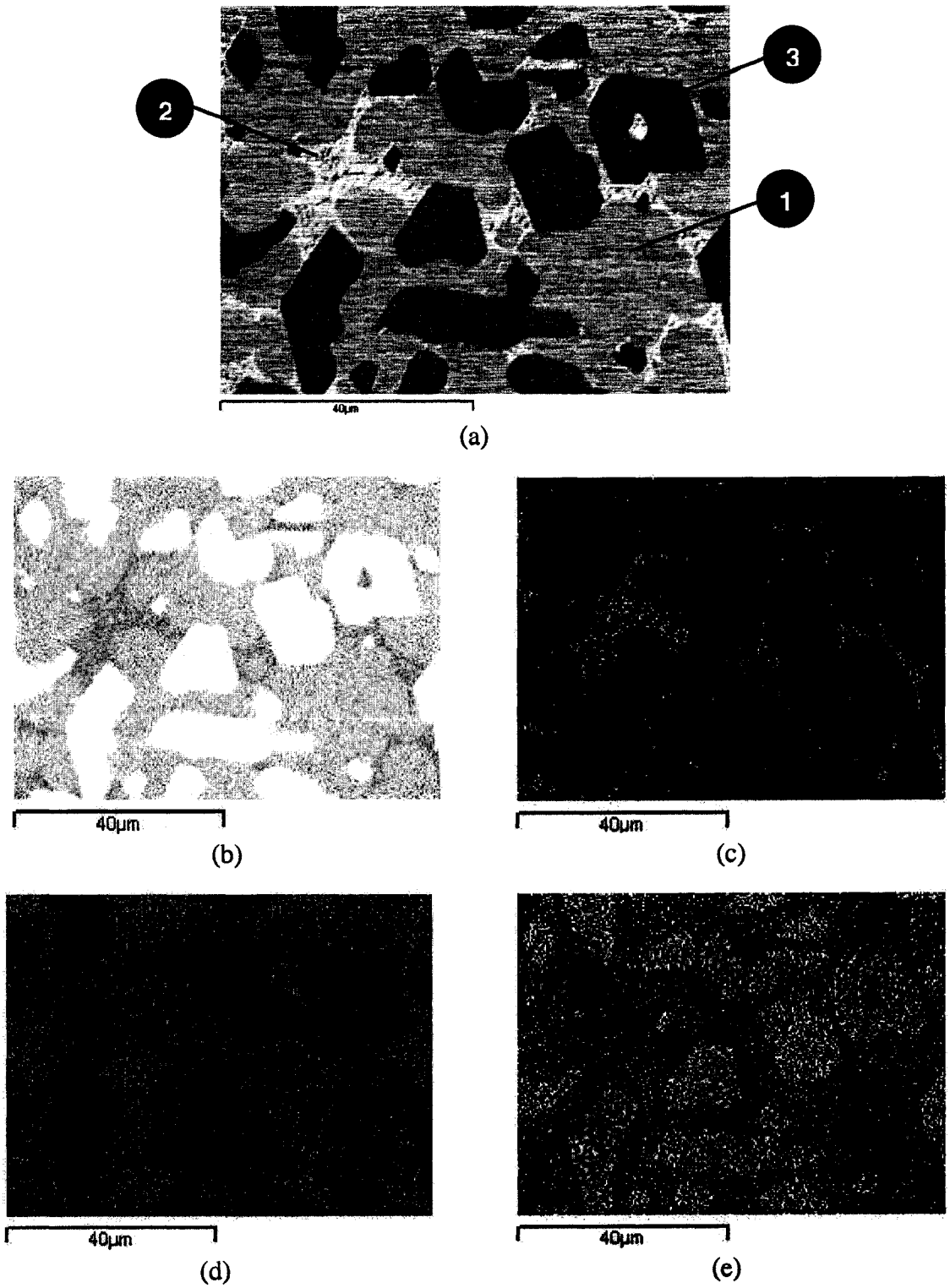


**Figure 4.15** Elemental mapping of (a) the constituents of the joint seam microstructure (regions 1, 2 and 3), (b) palladium concentration (orange), (c) silicon concentration (magenta), (d) chromium concentration (green), (e) nickel concentration (multicolor).

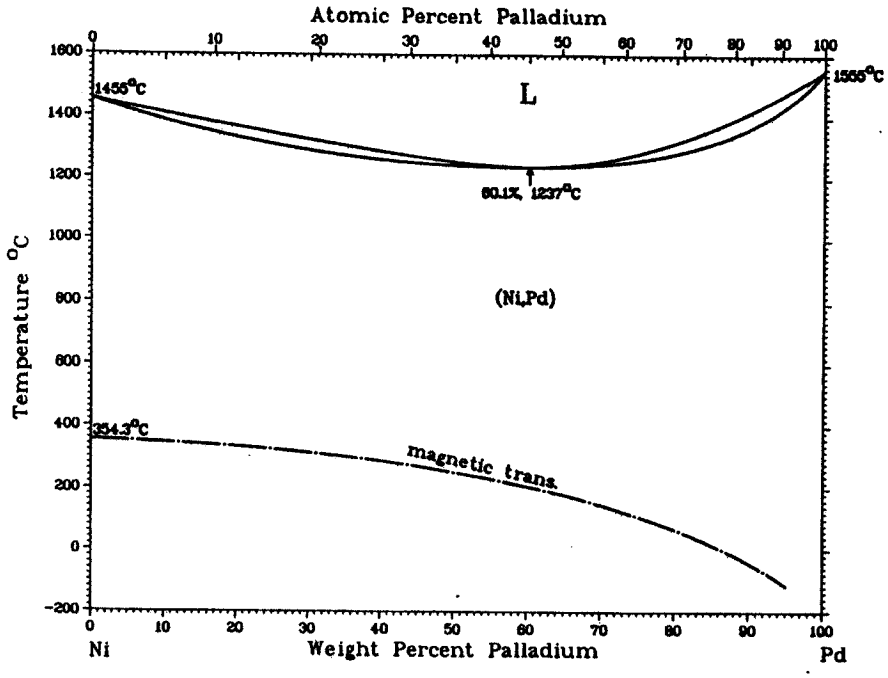


**Figure 4.16** Phase diagram for the nickel-palladium system[61].

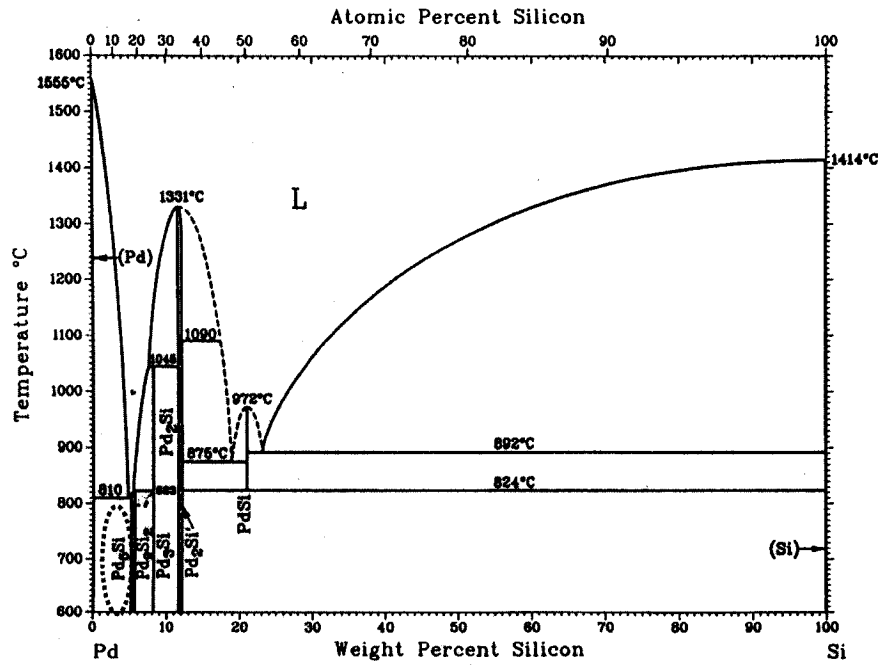


**Figure 4.17** Phase diagram for the palladium-silicon system[61].

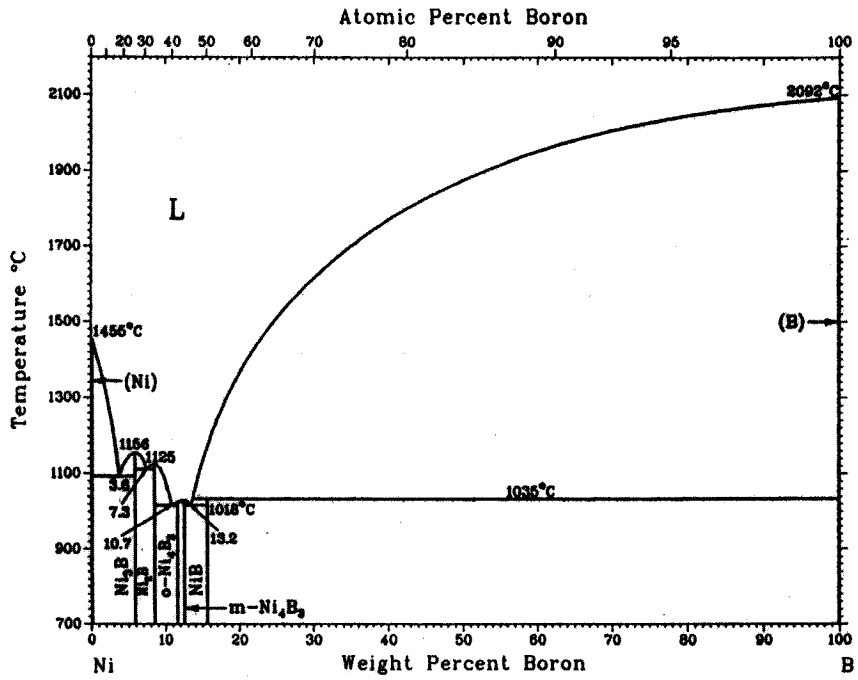


**Figure 4.18** Phase diagram for the nickel-boron system[61].

At the interface of the brazing and base metal, a reaction layer was observed as shown in Figure 4.13. A reaction layer forms as a result of the dissolution and alloying that occurs between the liquid and solid interfaces during the brazing cycle, which in effect, produces a new interface. Interdiffusion of elements from the base metal and the brazing metal occur as well as dissolution. The base metal contains a high concentration of iron compared to the brazing alloy, which has none, therefore a concentration gradient is produced where iron is allowed to diffuse inward toward the interface. In addition, carbon diffusion from the base metal also tends to accumulate at the interface. Similarly, boron from the brazing metal diffuses outward toward the interface as well. Elements such as chromium, and nickel have good mutual solubility and therefore lead to complex solid solutions. Feduska[62] has reported that relatively larger substitutional atoms (i.e. Cr, Ni, Si) have diffused across the entire interface by incipient volume diffusion. This diffusion reaction occurs by a vacancy mechanism where substitutional atoms diffuse into the grain lattice of the base metal grains. Due to the complexity and the numerous reactions occurring simultaneously, it was not possible to distinguish between solid solutions and secondary (brittle) phases. The interface between AISI 347 and the brazing

metal is illustrated in Figure 4.19, where the morphology of the complex compounds is depicted in Figure 4.19b. The rounded morphology indicates a high degree of surface energy. An accumulation of various complex compounds of the form Fe-Cr-Ni-Si has consolidated at the interface, which has the capacity to hinder diffusion into the base metal[62]. The presence of such complex compounds was confirmed by having a hardness value of approximately 600 HV compared to the base metal hardness of 166 HV.

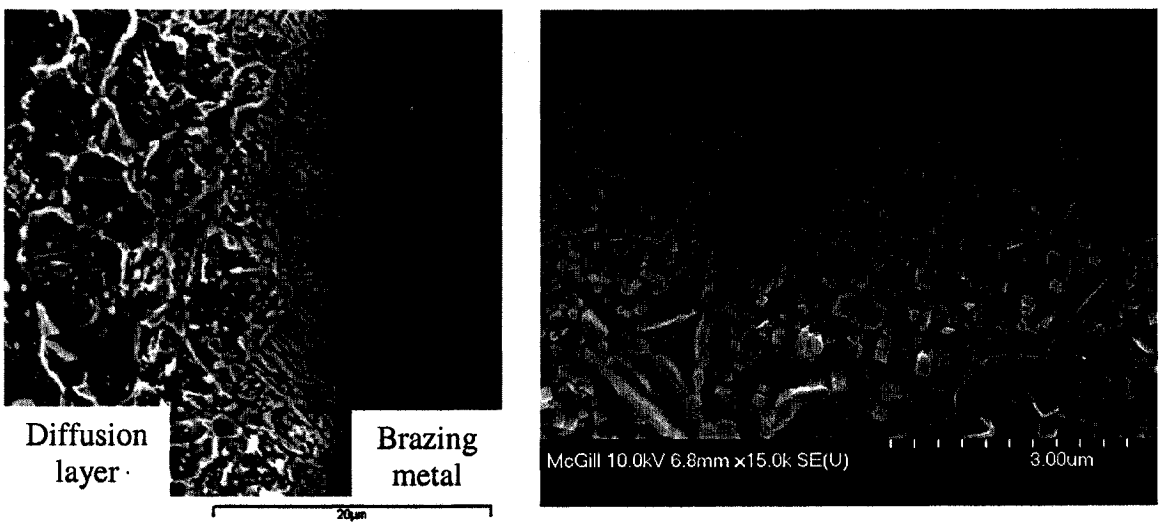


**Figure 4.19** SE image of (a) the interface between AISI 347 and the brazing metal and (b) a magnified view of the reaction layer taken within the outlined region rotated 90° CCW.

The interface between AISI 410 and the brazing metal shows a similar interdiffusion and dissolution phenomenon compared to the AISI 347 interface; however AISI 410 contains very little nickel compared to the brazing alloy. Consequently, another concentration gradient is created, where Ni diffuses into the base metal, which has a tendency to promote austenite formation at the interface upon heating and then subsequently produce martensite when cooled from the brazing temperature[63]. Figure 4.20 illustrates the AISI 410 / brazing metal interface revealing the presence of a reaction layer. The hardness of the interface measured as high as 690 HV, which confirmed the nature of Fe-Cr-Ni-Si complex compounds as being relatively hard phases. Furthermore, the hardening effect during the brazing cycle also contributed to the elevated hardness values.

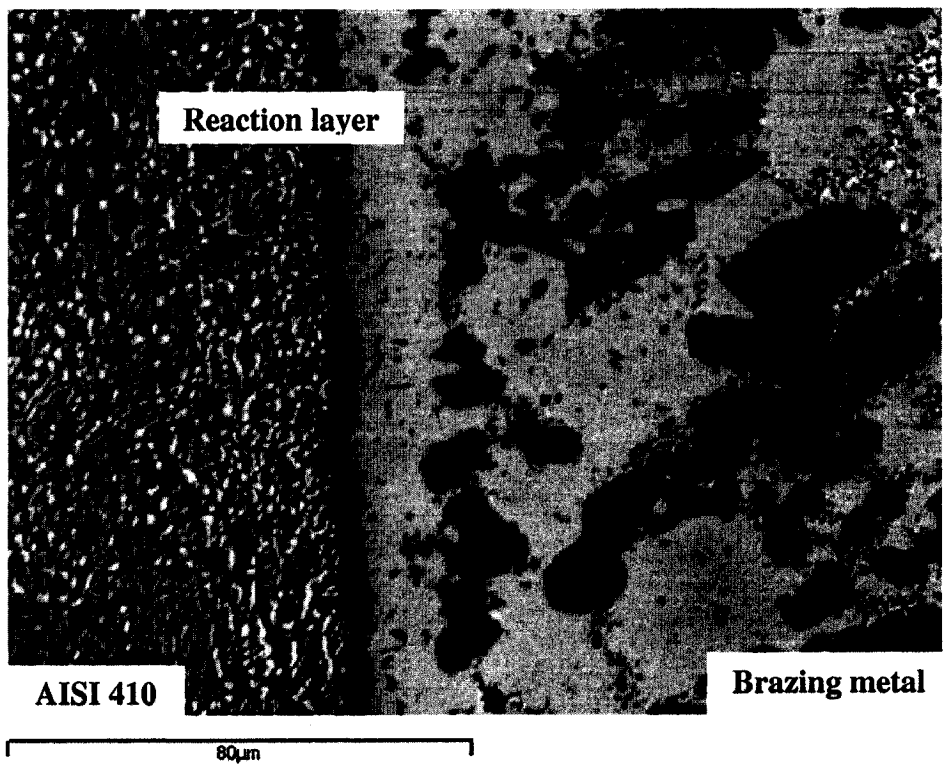


**Figure 4.20** SE image of the interface between AISI 410 and the brazing metal.

The presence of a diffusion layer confirmed that boron had successfully diffused into the grain boundaries of the base metal leading to isothermal solidification. Figure 4.21 illustrates a typical elemental mapping of boron, carbon and chromium of a single grain located within the diffusion layer. The grain boundaries reveal multiple precipitates (arrows) where boron has reacted to form a complex compound rich in boron, chromium, and carbon.

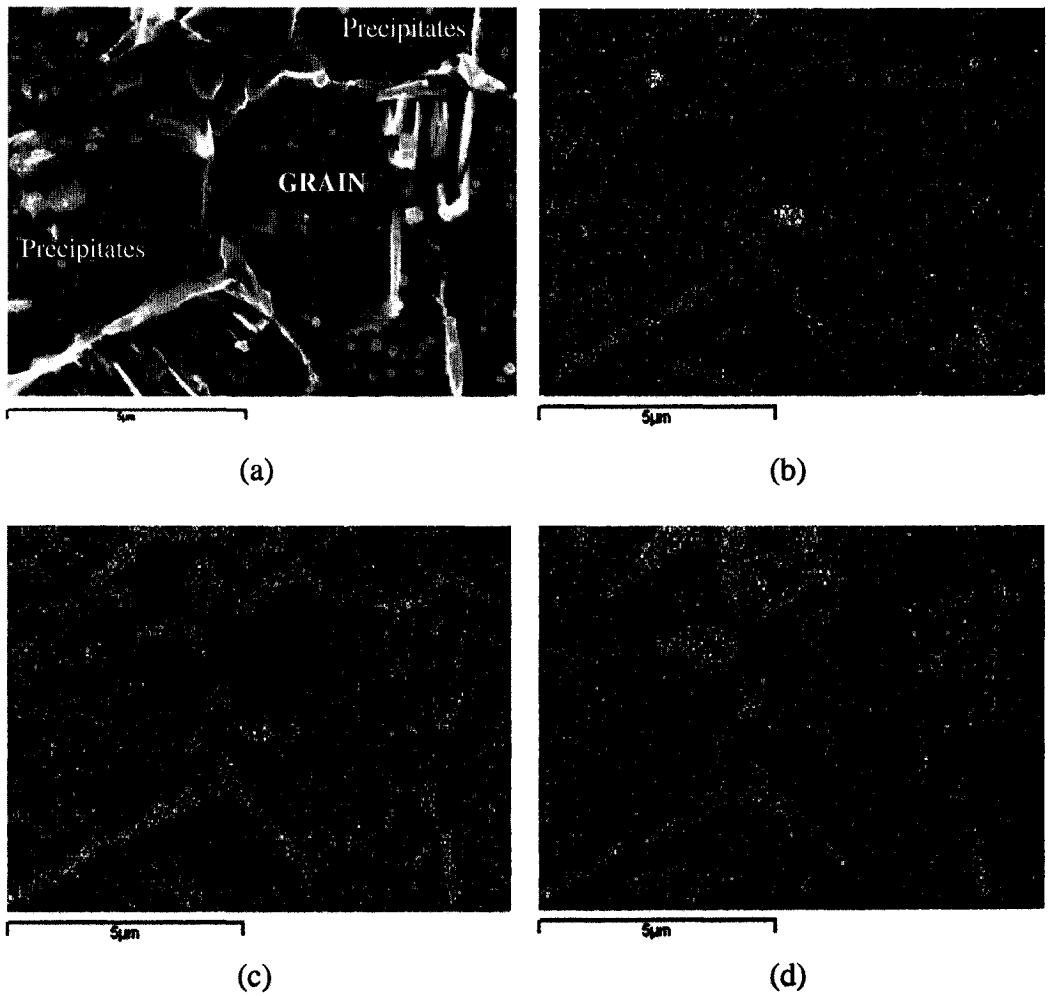


**Figure 4.21** Elemental mapping of (a) a single grain within the diffusion layer (b) boron concentration, (c) carbon concentration, and (d) chromium concentration.

The segregation of boron, carbon and chromium to the grain boundaries is characteristic of the formation of borocarbides, which has been reported for a number of steel substrates using boron-containing brazing metals[4,63,64]. The type of borocarbide observed was mostly likely of the form $M_x(C, B)_y$. Figure 4.22a shows a magnified view of a grain boundary precipitate in which a point analysis was carried. An EDS was taken to identify the constituents of the metal borocarbide ($M_x(C, B)_y$), which is depicted in Figure 4.22b. The metal borocarbide consisted of iron, chromium and traces of manganese and niobium. Similarly, the AISI 410 base metal exhibited the same metal borocarbide without the presence of niobium.

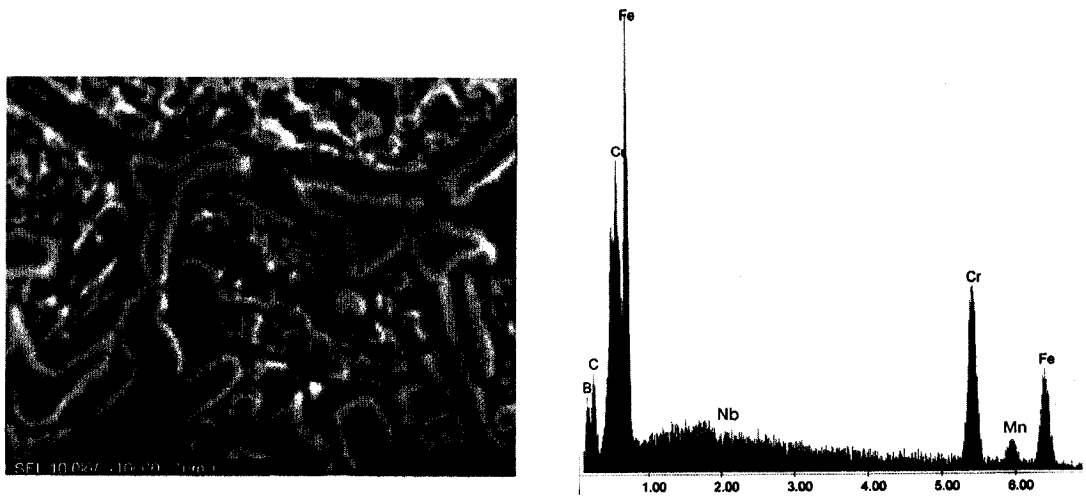


**Figure 4.22** Point analysis of (a) a grain boundary precipitate and (b) the associated EDS.

Another type of precipitate was observed along the grain boundaries illustrated in Figure 4.23. Again, from elemental mapping the micrographs show clearly that the precipitate highlighted by the arrows was rich in boron, suggesting the formation of a boride in the form of $M_xB_y$. There was no evidence of carbon content, differentiating from a borocarbide precipitate. The metal constituents of the boride were complex and had a similar composition compared to the borocarbide. Metal carbides ($M_xC_y$) that already exist in the steel base metal are known to accommodate boron through substitution of carbon into the lattice forming a borocarbide[4]. It has been shown that boron promotes the formation of borocarbides at the expense of other carbides in stainless steel[64]. Specifically, boron and carbon have very similar atomic radii, measuring 98 pm and 91 pm[65], respectively, therefore substitution of these atoms are quite common.

The presence of these secondary phases within the diffusion layer has shown to have little effect on the base metal properties. The microhardness values of both AISI 410 and 347 showed only a slight increase in the diffusion layer compared to the base metal. Rabinkin *et al.*[66] have reported that the effect of boride formation along the grain boundaries of an austenitic stainless shows no significant decrease in the mechanical strength of the base metal. Therefore, the boride and borocarbide may not have a profound effect on diminishing mechanical properties, but another concern is the potential loss of corrosion resistance. Despite the fact that one of the base metals is stabilized through the addition of niobium (AISI 347) to produce niobium carbides instead of chromium carbides, the formation of borocarbides due to grain diffusion from the brazing metal will tend to consume chromium locally. Although the corrosion resistance has not been evaluated in the present work, the corrosion aspect of the joint will not likely be compromised according to Johnson[4]. Adjacent to the interface exists a solid solution rich in nickel and palladium, which the corrosive medium must cross first before interacting with the denuded base metal[4].

The precipitates that are found within the diffusion layer are not exclusively confined to the grain boundaries, but also form at interior of the grains. Feduska[62] and Johnson[4] reported that the interstitial atoms can migrate into the lattice of the base metal also producing borides and borocarbides. Figure 4.24 illustrates the typical precipitation sites of the different compounds that can form on the grain boundaries and interior of grains, which seem to be in agreement with the findings of Feduska[62] and Johnson[4].

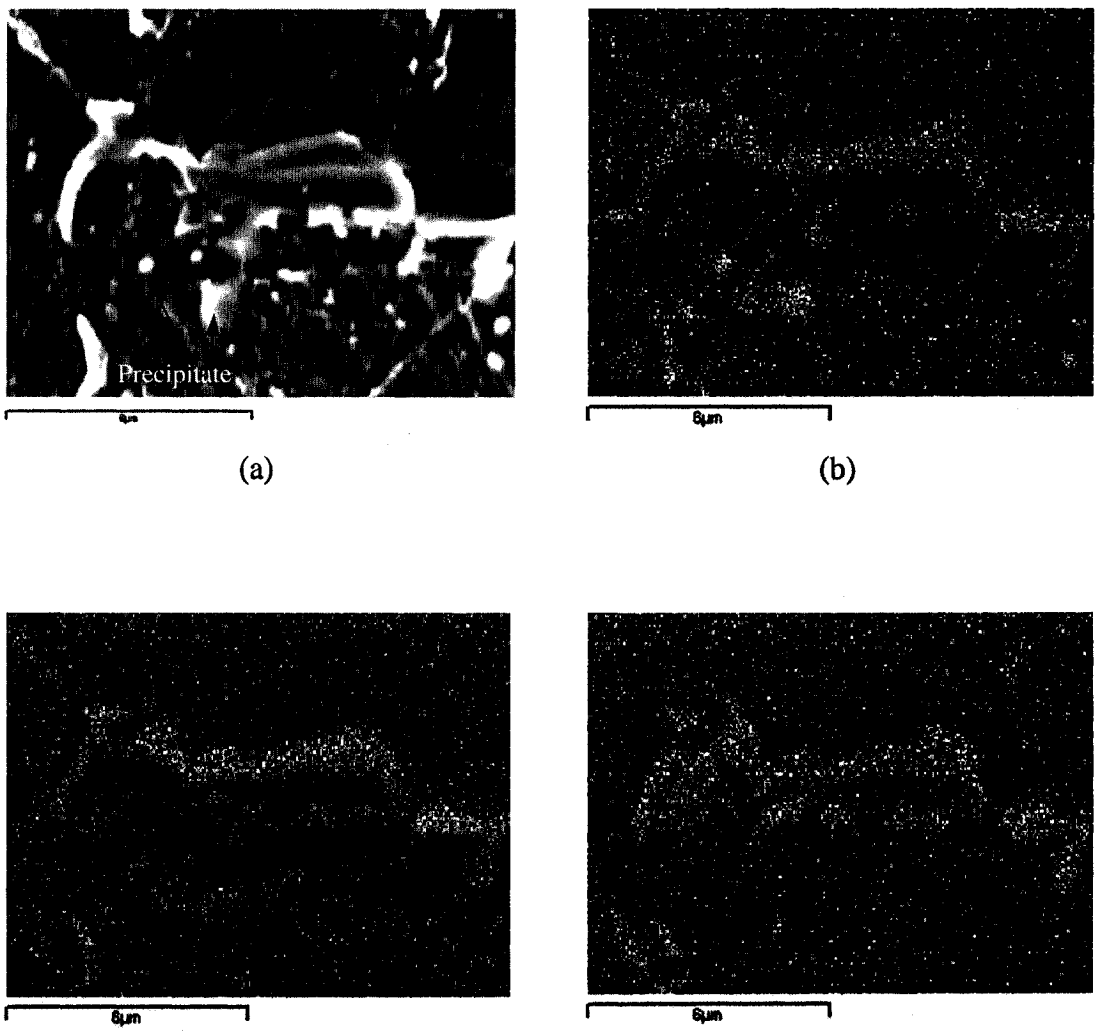


**Figure 4.23** Elemental mapping of (a) a grain boundary within the diffusion layer (b) boron concentration, (c) chromium concentration, and (d) carbon concentration.

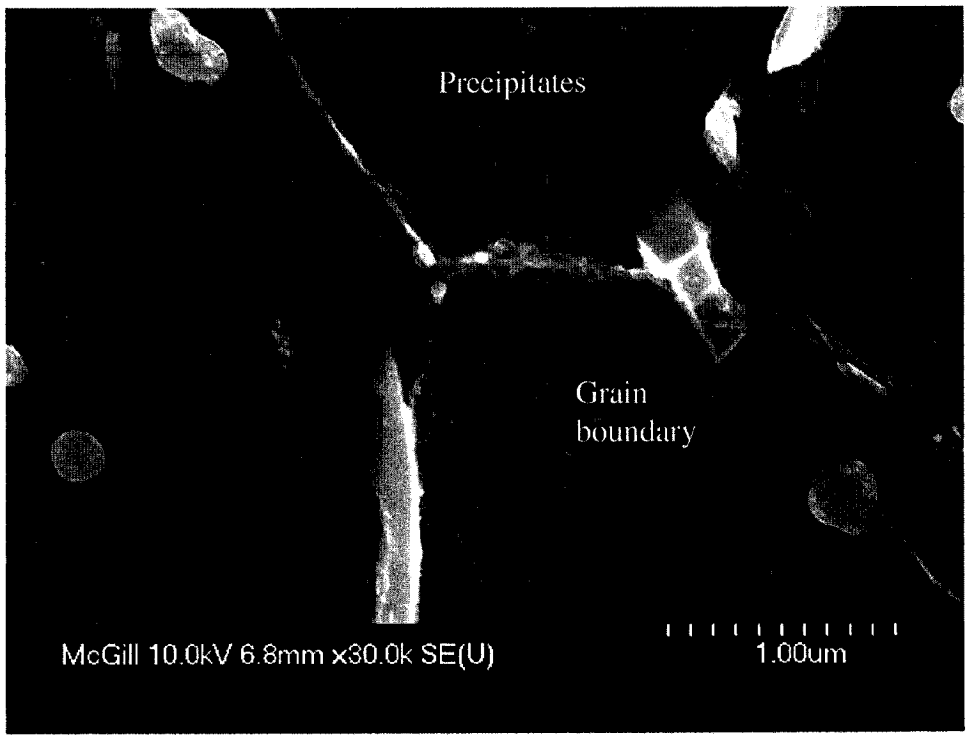


**Figure 4.24** Precipitation sites of borides and borocarbides within the diffusion layer of AISI 347.

### 4.2.1 Effect of Time

The maximum brazing clearance (MBC) defined as the maximum clearance just before the precipitation of secondary phases within the joint microstructure[43], was determined for all three brazing times. Specifically, the transition between a single phase joint and incipient secondary phase formation defines when the MBC is realized. The change in microstructure of the joint seam will also be evaluated as a function of time.

Figure 4.25 illustrates a typical micrograph taken from a portion of the wedge specimen located near the apex of the joint. The average clearance shown is approximately 35 μm using a brazing time of 30 minutes. The seam exhibits the transition between a single phase (left of the double headed arrow) and a dual phase joint (right of the double headed arrow), which is noted as the MBC. Note the discontinuous nature of the secondary phase precipitates during the onset of formation. Clearances just below the MBC exhibit a single phase solid solution free of brittle secondary phases. Exceeding the

MBC will result in the formation of secondary phases in the form of islands as shown in Figure 4.25, however the dependence of joint clearance will be examined in detail in the following section.

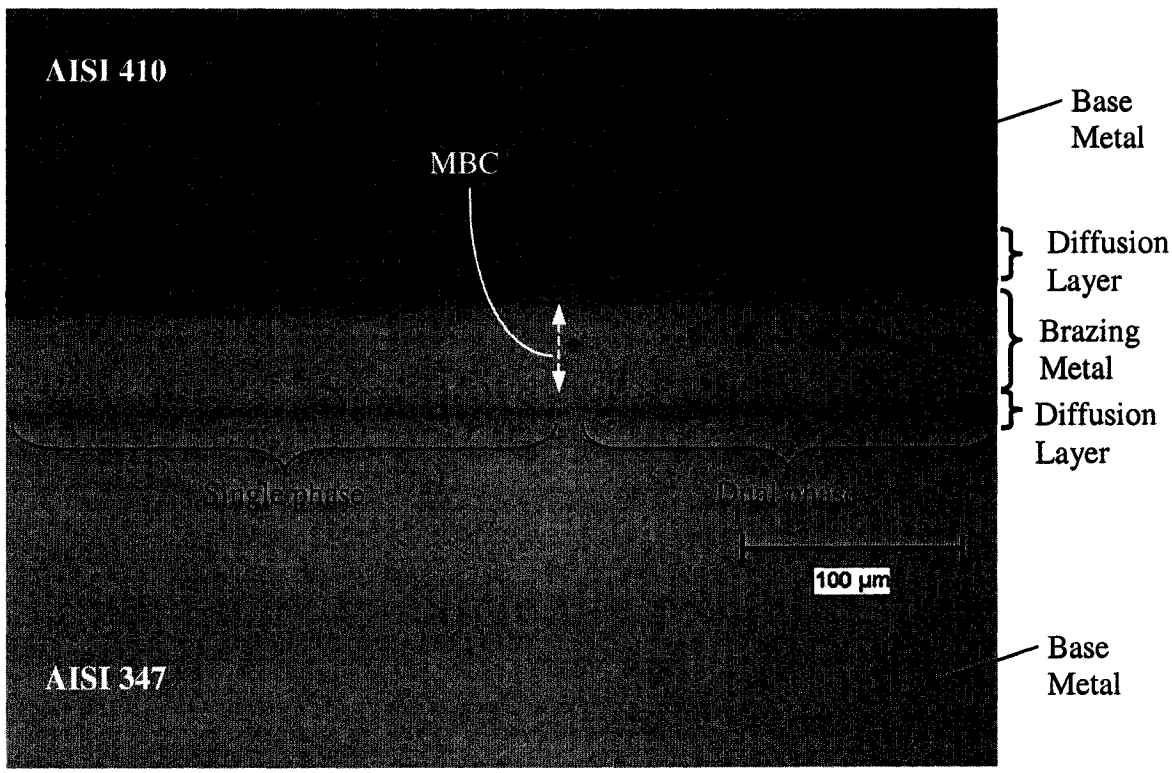


**Figure 4.25** Typical micrograph defining the MBC. Brazing time: 30 minutes; Clearance: ~35µm

The effect of time on the MBC is shown in Figure 4.26, which shows that increasing time will tend to increase the MBC. For a brazing time of 15 minutes, the MBC was determined as 30 µm. By doubling the time, the MBC increased by nearly 40% (41.4 µm), and then increasing the time a further two-fold, results in approximately in a 20% increase (50 µm). Ultimately, as the time exceeds 60 minutes, the curve begins to plateau showing only a marginal increase in MBC. This trend can be attributed to the fact that the diffusion of boron/silicon out of the seam is limited or hindered by the formation of a reaction layer at the interface. In addition, it has been reported by Knotek and Lugscheider[47] that the carbon content in the base metal tends to reduce the activity of

boron diffusion. From a practical standpoint such brazing cycles would not be cost effective in industry, and would not show a significant improvement of the overall brazement. The work of Lugscheider and Partz[38] showed that the MBC for a AISI 316 joint using a Ni-7Cr-4.5Si-2.9B-3Fe-0.1C (BNi-2) brazing metal was 35 μm for 10 minutes and 50 μm for 60 minutes. The results presented in this current work seemed to be in agreement with this previous work, however the values tend show a slight discrepancy. The difference observed in the MBC values can be attributed to the different brazing temperatures employed. The minimum brazing temperature used for BNi-2 was 1010°C, as compared to 980°C used in the current work, therefore a higher brazing temperature would suggest enhanced diffusion of boron/silicon out of the joint resulting in larger MBC values.

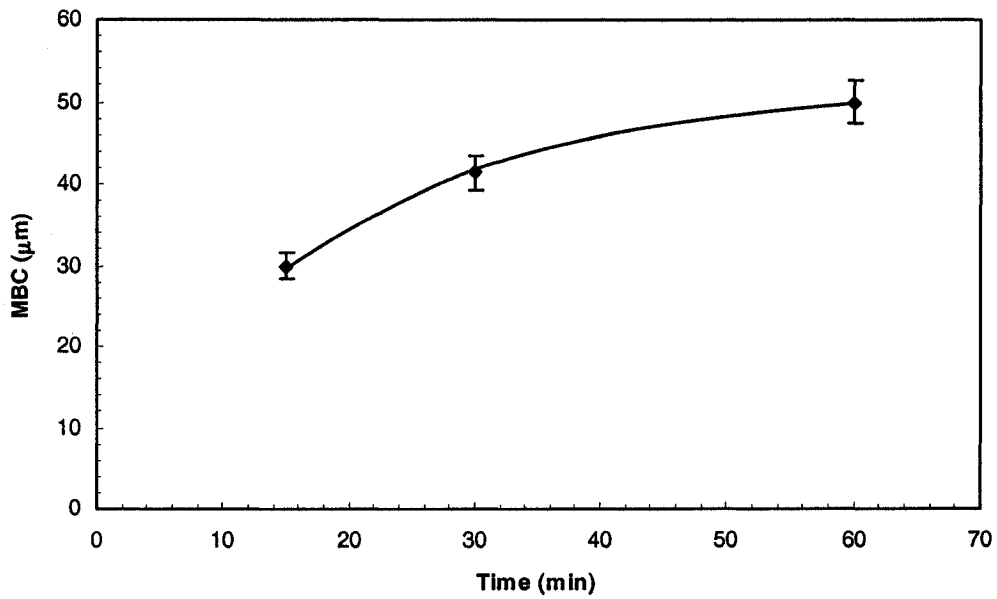


**Figure 4.26** MBC as a function of time.

The brazing time also had a significant effect on the evolution of the joint microstructure. Figure 4.27 depicts the microstructure of the joint seam for brazing times of 15, 30 and 60 minutes. A brazing clearance of approximately 100 μm was chosen arbitrarily in order to compare the joint seam microstructure. The general tendency was increasing the time will decrease the width of the secondary phases. For a brazing time of 15, 30 and 60 minutes, the width of the secondary phase within the joint seam was

66.6 μm, 54.4 μm, and 43.1 μm, respectively. The width of the secondary phase was taken as an average near the extremities of the solid solution dendrites due to the non-uniform dendritic growth, as the critical aspect is the avoidance of the brittle secondary phase. The nature of the secondary phase was continuous, and confined to the center of the joint. The precipitation of secondary phases however, is primarily governed by diffusion kinetics. Specifically, increasing the brazing time will increase the amount of boron/silicon diffusing out of the joint seam. An indirect method to evaluate the diffusion kinetics is to determine the diffusion layer within the base metal.

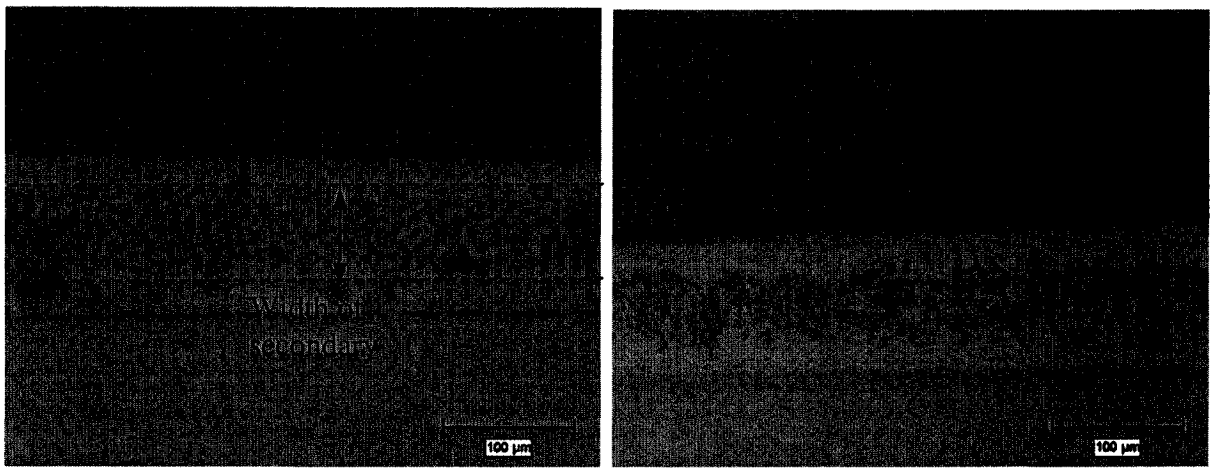

(a) (b)

(c)

**Figure 4.27** The evolution of the joint microstructure for a brazing time of (a) 15 minutes, (b) 30 minutes and (c) 60 minutes. Brazing clearance: ~100 μm.

The effect of time on the diffusion layer of both AISI 347 and AISI 410 base metals is illustrated in Figure 4.28. As expected, an increase in time will increase the diffusion layer in the case of both base metals. The diffusion behavior shows a linear behavior, which is contrary to the predicted theory. A simplified diffusion equation given by:

$$\chi^2 = k D_\tau t \Leftrightarrow \chi = k\sqrt{D_\tau t} \qquad \text{(Eq. 4.3)}$$

where $\chi$ is the depth of penetration within the base metal, t, is time, $D_\tau$ is the diffusion coefficient of boron in steel, and k, is a constant[4].

The above diffusion equation shows that the depth of penetration has the typical square root relationship with time. However, considering the ratio of the depth of penetration and time, the constants k and $D_\tau$ will cancel out to give the following expression:

$$\frac{\chi_1}{\chi_2} = \sqrt{\left(\frac{t_1}{t_2}\right)} \qquad \text{(Eq. 4.3a)}$$

The ratio of the three experimental times used was 15:30:60, or 1:2:4, wheeras from the predicted theory, the depth of penetration should have a ratio of 1:1.4:2. Therefore, the values depicted in Figure 4.28 show that the theory is an overestimate of the actual diffusion layer depths.

There are several factors that play a critical role in the discrepancy of the experimental data and the theoretical predictions. The presence of the reaction layer has proven to be a physical barrier for boron diffusion into the base metal. The complex compounds that form at the interface block inter- and trans-crystalline diffusion paths as reported by Knotek and Lugscheider[47]. The elevated microhardness values determined at the interface further support the fact that boron is also partially consumed by the formation of borides and borocarbides.

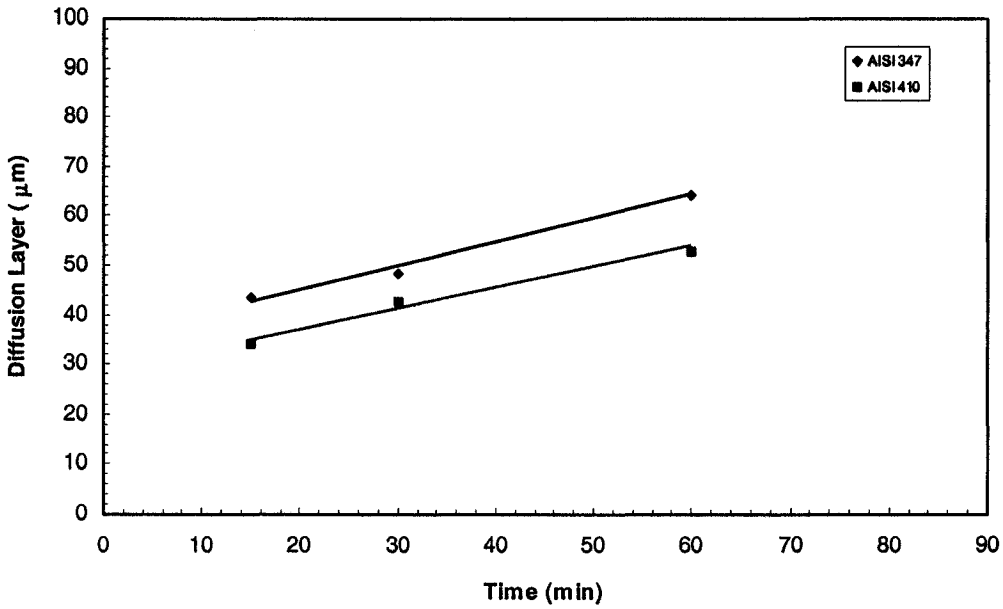


**Figure 4.28** Time dependence of the diffusion layer for AISI 347 and AISI 410 base metals.

The precipitation sites of such compounds are often found along grain boundaries and the interior of grains, which hinders available grain boundary vacancies and dislocation sites, and interstitial vacancies and dislocation regions within the grain. Hence, the flow paths would be reduced from the filler to the base metal and vise-versa[63]. The linear tendency shown in Figure 4.28 represents a portion of the diffusion process that most probably was not yet complete, hence a positive slope. It is noteworthy that the linearity shown in Figure 4.28 was based on only on three data points which represent the three brazing times that were evaluated. Therefore, there is an amount of uncertainty associated with the assumption that the diffusion layer increases linearly with increasing time. Eventually, the amount of boron would become depleted within the seam and the curve would start to plateau. Another factor that would contribute to the retarding of boron diffusion is the concentration gradient across the interface. A difference in concentration between the brazing metal and base metal acts as one of the driving forces for diffusion. At the beginning, diffusion will occur rapidly due to the large concentration gradient across the interface, in addition to diffusion through the liquid state. Dissolution of the base metal also occurs with associated interdiffusion, which dilutes the brazing metal, reducing the

effective concentration gradient. In effect, the diffusion kinetics are reduced and the rate of boron penetration within the base metal will begin to subside. The work carried out by Johnson[4] has shown that the diffusion coefficient of boron in steel is approximately 10 μm / sec., which indicates that boron penetration occurs in the first few minutes most probably corresponding to liquid state diffusion as opposed to the more sluggish, solid state diffusion.

The diffusion layer of the AISI 347 compared to the AISI 410 shows a difference of an average of 10 μm. Although, at both interfaces, similar reaction layers are formed, and the same amount of boron is present within a given clearance, the difference in compositions can indirectly affect the diffusion of boron. AISI 347 is an austenitic stainless steel with 0.05%C, whereas AISI 410 is a martensitic stainless steel with more than twice the carbon content, which will lower the activity of boron diffusion to a greater extent[47]. Furthermore, Lamb and Miller[63] have documented that boron will diffuse faster along austenitic grain boundaries at elevated temperatures. The depth of the diffusion layer for a brazing time of 60 minutes for AISI 347 and AISI 410 base metals was 64.3 μm and 52.8 μm, respectively. These results seemed to be consistent with the work of D'Silva[31] who determined a diffusion layer of 34 μm for a brazing time of 60 minutes using the same brazing metal with a superalloy base metal.

### 4.2.2 Effect of Clearance

The effect of clearance on joint characteristics was studied by sectioning the wedge joint specimen at various locations corresponding to specific clearance values. In particular, Figure 4.29 illustrates how the formation of secondary phases responds to the variation in clearance from a qualitative perspective. The clearance values shown in Figure 4.29 were approximately 35 μm, 75 μm, 150 μm, and 250 μm using a brazing time of 30 minutes. During the brazing process, dissolution effects will tend to increase the original joint clearance, therefore all clearance values reported in the current work represent the original clearance before brazing. In particular, it is the original clearance values that are of practical significance as opposed to the final clearance, which is merely a consequence of the brazing process. The final clearance value is difficult to predict and

in industry it is the original clearance that is indicated on the assembly drawings/specifications. The presence of secondary phases shows a marked increase when the clearance is increased. At a clearance of 35 μm, the joint seam is virtually free of secondary phases (Figure 4.29a) with occasional islands. It is noteworthy that the field shown in Figure 4.29 is only an approximation of a constant clearance due to the observable variable clearance wedge joint configuration. However, the clearance variation within any given metallograph represents a maximum of 10% compared to the average clearance value. Therefore, the occasional islands observed in Figure 4.29a, were most likely formed at a clearance slightly greater than 35 μm. In general, the clearance value given in this work consists of the clearance located within the center of the field for a given micrograph. As the clearance is slightly increased to 75 μm (Figure 4.29b), a continuous centerline secondary phase is observed. Further increasing the clearance to 150 μm (Figure 4.29c) and 250 μm (Figure 4.29d), a large fraction of the joint seam is occupied by secondary phases, with dendrites extending near the interface.

An increase in clearance will result in a larger diffusion distance from the joint seam to the base metal. Furthermore, a larger clearance will be capable of accommodating more brazing metal paste, and hence greater amounts of boron/silicon. Therefore, the solubility of the solid solution will be exceeded resulting in the formation of secondary phases. A local increase of boron/silicon can lead to a greater volume of borocarbides/borides within the reaction layer at the interface, which will limit diffusion into the base metal, resulting in centerline secondary phases in the joint seam. A very similar trend was observed by the work of Johnson[2] who demonstrated the effect of clearance using an AISI 321 joint brazed with a Ni-Cr-Fe-B brazing metal. At larger clearances, the joint microstructure consisted of a large continuous secondary phase occupying approximately 90% of the seam to a single phase solid solution at small clearances. It is noteworthy that the maximum clearance to obtain a sound joint, free of voids and other discontinuities, was estimated at approximately 300 μm for the AISI 347/PalNiCro/AISI 410 joint. There are no general rules that can be applied to predict this value for other systems, due to the different solubility limits, reactions, wetting properties

and diffusion kinetics. Each system must be treated separately and must be evaluated on the basis of the given brazing metal and base materials used.

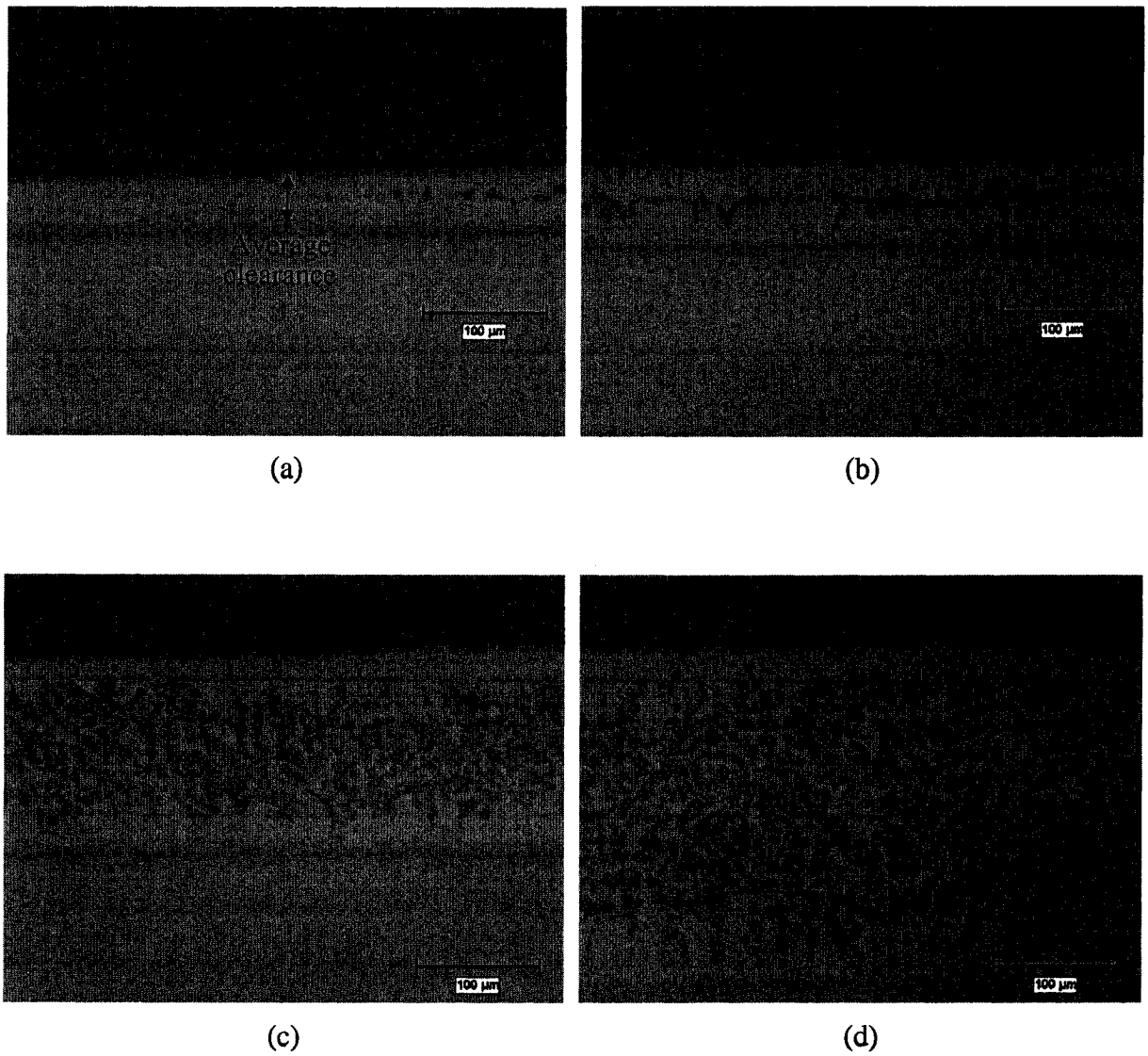


(a) (b)

(c) (d)

**Figure 4.29** The evolution of the joint microstructure for a clearance of (a) 35 µm, (b) 75 µm, (c) 150 µm and (d) 250 µm. Brazing time: 30 minutes.

A quantitative analysis of the width of the secondary phases relative to the entire joint seam was carried out and plotted as a function of time and clearance. Figure 4.30 shows that a linear relationship exists between the width of the secondary phases and the clearance. This relationship is observed for the three brazing times tested, showing little deviations from linearity. At a clearance value of only 50 µm, the width of the secondary

phases is 50% of the entire seam. Although, a joint seam occupied by 50% of secondary phases may be susceptible to centreline cracking, the much more ductile solid solution in between the center of the joint and the interface can act as a crack arrestor, minimizing or preventing failures of the joint assembly. Sound joints using clearances as large as 250 μm were successfully brazed, where the width of secondary phases was approximately 180 μm, corresponding to approximately 70% of the joint seam. Although 70% of the joint seam appears to be significant, it is only the maximum width of the secondary phases, which may reflect only on the mechanical properties and the resistance/susceptibility to crack initiation.

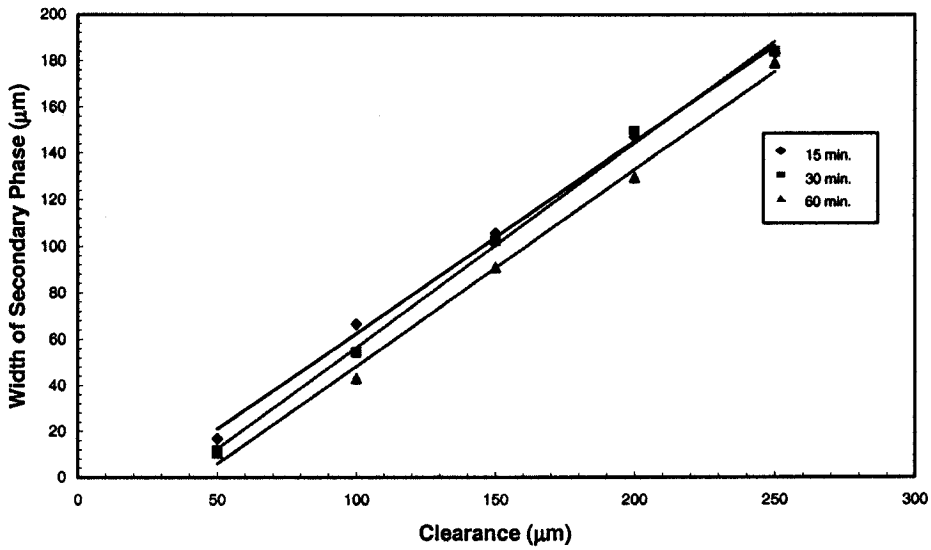


**Figure 4.30** The width of the secondary phase within the joint seam as a function of clearance and time.

The volume fraction or area percent of a given field at a defined clearance emphasizes the distribution of the secondary phases as a function of the solid solution. Figure 4.31 illustrates how the area percent was calculated with respect to the solid solution and the secondary phases for a clearance of 50 μm and a brazing time of 15 minutes. The original micrograph is depicted in Figure 4.31a showing the brazed joint, outlining the seam. The seam, consisting of the solid solution and secondary phases are shown in Figure 4.31b, corresponding to the blue and red regions that have been digitized, respectively.

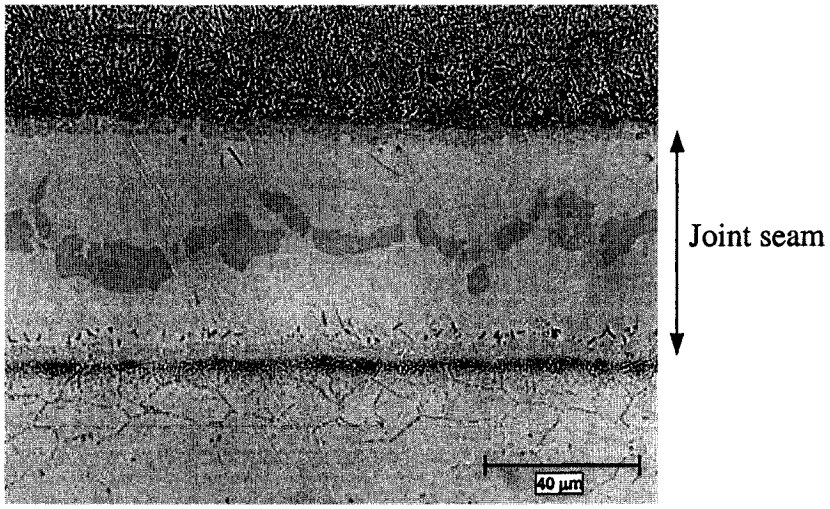


(a)

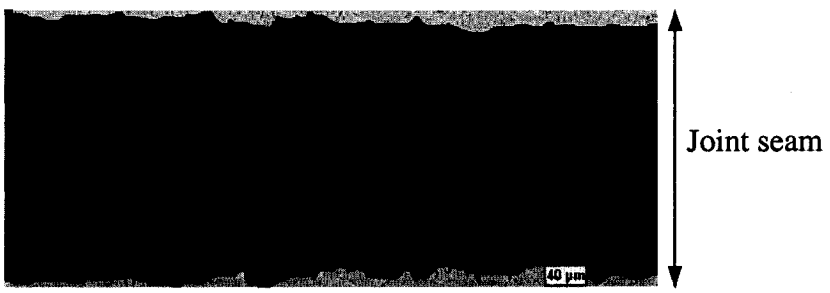


(b)

**Figure 4.31** Typical image analysis of the volume fraction of secondary phase: (a) original micrograph and (b) highlighted secondary phase and surrounding matrix. Clearance: 50µm; Time: 15 minutes.

The distribution of the secondary phases as a function of the solid solution was calculated by the ratio of blue to red and converted to a percentage, generating the plot shown in Figure 4.32. The plot was generated for the same range of clearance values and brazing times as in Figure 4.30. The area percent ranged from approximately 3% to 25% compared to the width of the secondary phases, which was much greater. The difference in the width and the area percent of the secondary phases can be attributed to the nature of the microstructure. The seam consists of islands that are partially joined by silicides, which is surrounded by a solid solution, therefore only those phases are considered. The width simply takes into account the extremities of the dendrites extending towards the

reaction layer. Increasing the clearance resulted in a gradual increase in the volume fraction of the secondary phases. The amount of secondary phases increased slightly above clearance values of 150 μm. Increasing the time decreased the amount of secondary phases by shifting the curves downwards. A significant decrease was observed only at smaller clearances, i.e. below 100 μm, in which diffusion distances are small enough for the given brazing times. At clearances of 250 μm, both a 15 minute and 30 brazing time showed little effect on the area percent of secondary phases. The diffusion distances are too large and the time was insufficient for diffusion of boron into the base metal. A brazing time of 60 minutes showed a considerable improvement at larger clearances, which confirms that a compromise between clearance and time must be realized. If a joint requires large clearances, then the operator must allow a longer brazing cycle to achieve less secondary phases within the joint seam.

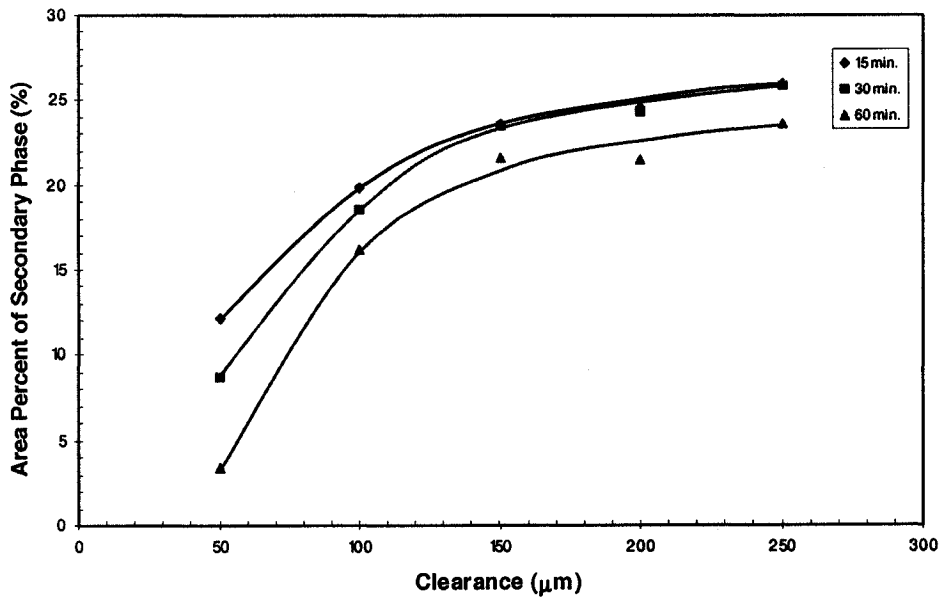


**Figure 4.32** Quantitative analysis of the amount of secondary phase as a function of clearance and time.

# *CHAPTER 5*

## *CONCLUSIONS*

The wettability of PalNiCro brazing alloy on AISI 347 and AISI 410 stainless steel substrates was evaluated as a function of time, temperature and surface roughness to determine optimal wetting conditions for brazing operations in the aerospace industry. The effect of brazing conditions on the joint microstructure characteristics was determined using the optimized parameters from the wettability studies. The following summarizes the primary conclusions from this work.

[1] A brazing temperature of 980°C using a 600 grit SiC grinding paper as surface preparation was determined as the optimal wetting conditions. AISI 347 and AISI 410 stainless steel substrates exhibited similar wetting behavior.

[2] The equilibrium contact angle for AISI 347 and AISI 410 was 10° approximately 100 seconds after melting.

[3] A surface preparation using random SiC grinding paper produced a network of waveform channels that enhanced wettability. The value of the Ra and RMS of the optimal surface preparation was 24.1 μm and 32.3 μm, respectively.

[4] The brazing thermal cycle showed no significant impact on the AISI 347 base metal, however an increase in hardness of approximately 190 HV was observed in the AISI 410 base metal due to the hardenability of martensitic stainless steels.

[5] The diffusion of boron from the brazing metal resulted in the formation of borocarbides and borides in the form of $M_x(C,B)_y$ and $M_xB_y$, respectively. The precipitation sites were primarily confined to the grain boundaries and occasionally located at the interior of grains.

[6] The microstructure of the joint seam consisted primarily of the three distinct regions: (a) a soft ductile Ni solid solution with dissolved palladium and chromium whose hardness was approximately 220 HV, (b) a palladium silicide having a hardness value of over 600 HV surrounding (c) very hard Ni-rich islands in excess of 1000 HV suggesting the presence of nickel borides. Borides are a likely candidate to form within the joint seam, due to the limited solubility of boron with nickel and the elevated hardness values that are characteristic of borides.

[7] The reaction layer observed adjacent to the diffusion layer consisted of complex Fe-Cr-Ni-Si compounds whose hardness values ranged between 600 and 700 HV. The presence of this layer acted as a barrier, hindering interdiffusion from the brazing metal to base metal and vice-versa.

[8] The influence of brazing time had a significant effect on the joint microstructure. Brazing times of 15 minutes, 30 minutes and 60 minutes resulted in a MBC value of 30 μm, 41.4 μm and 50 μm, respectively. The width of the secondary phases decreased due to the diffusion of boron/silicon into the base metal, in which time strongly influences diffusion kinetics. Furthermore, an increase in time produced a larger diffusion layer in both AISI 347 and AISI 410 base metals resulting in a value of approximately 60 μm and 50 μm, respectively. The difference between grain boundary penetration of the two base metals can be attributed by the higher carbon content of AISI 410 compared to AISI 347, which reduces the activity of boron diffusion. In addition, boron is known to diffuse faster along austenitic grain boundaries.

[9] The influence of clearance had a marked effect on the width of the secondary phases. The width ranged from approximately 15 μm for a clearance of 50 μm to as large as 180 μm for a 250 μm clearance. The distribution of the secondary phases as a function of clearance also showed a significant increase up to clearances of 150 μm, where the volume fraction was above 20%. A further increase in clearance led to a minor change in the volume fraction as the maximum allowable clearance was approached and was estimated to be below 300 μm for an AISI 347/PalNiCro/AISI 410 joint assembly.

# *RECOMMENDATIONS FOR FUTURE WORK*

While the current work has addressed wetting behavior and brazement characteristics for a given joint configuration, future work focusing on the mechanical properties and different joint configurations would shed light on the integrity of various joints. Furthermore, fatigue testing of the joint assemblies should be carried out, representing the most common mode of failure in the aerospace industry.

The current work utilized wrought stainless steels, however insight can be gained by studying the influence of initial base metal characteristics, such as cast and wrought structures with various grain sizes on the diffusion kinetics/diffusion layer.

In the aerospace industry, repair/rework of brazed assemblies are often required, such that the joint experiences multiple heating cycles. It would be beneficial to carry out studies that focus on the effect of multiple heating cycles as a function of the joint characteristics.

Another concern for brazed assemblies is the corrosion resistance of the joint. In the current work, the diffusion layer showed evidence of chromium-containing compounds, which may have an effect on the susceptibility to corrosion, due to a localized reduction in chromium content at the grain boundaries. An investigation of the effect of various corrosive media on the diffusion layer would be suggested, to evaluate whether the diffusion layer would be more prone to corrosion.

# *APPENDIX A*

## *BRAZING COOLING CYCLE*

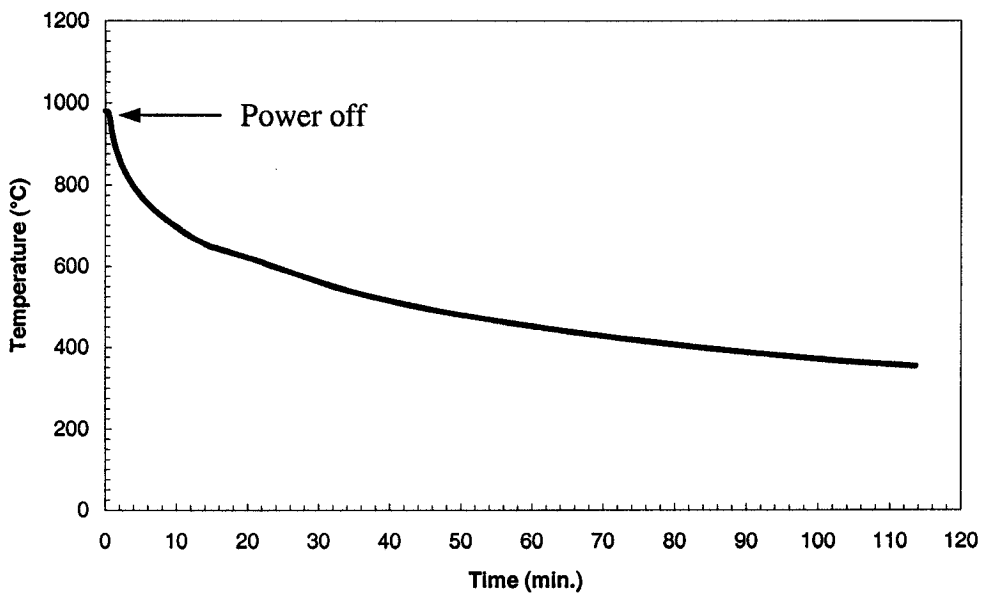

# *REFERENCES*


1. Ray, R.L., "Brazing: 1967", *West. Mach. Steel World*, Vol. 67, No. 10, Nov. 1967, 23-26

2. Johnson, R., "The Use of TETIG Diagrams in High-Temperature Brazing", *Weld. J.*, Oct. 1981, 185s-193s

3. Whalen, S.J., "Aerospace Brazing", *Weld Eng.*, Vol. 53, No. 3, Mar. 1968, 62-63

4. Johnson, R., "Microstructural Aspects of Brazing a Ferritic Steel with Two Ni-Si-B Braze Filler Metals", *Weld. J.*, Vol. 57, No. 4, 1978, 93s-102s

5. Anonymous, "Stator Element of Turbine Assembly" – Integrated Publishing, page 6-13, URL: http://www.tpub.com/content/fc/14104/css/14104_97.htm [August 7, 2004]

6. Schwartz, M.M., Brazing, 2nd edition, ASM International, Materials Park, Ohio, USA, 2003

7. Humpston, G., and Jacobson D. M., Principles of Soldering and Brazing, ASM International, Materials Park, Ohio, USA, 1993

8. Schwartz, M.M., Modern Metal Joining Techniques, John Wiley and Sons Inc., Toronto, Ontario, Canada, 1969

9. Schwartz, M.M., Brazing, ASM International, Materials Park, Ohio, USA, 1987

10. Nikitinskii, A.M., "Problem of Wetting and Surface Tension", *Weld. Int.*, Vol. 13, No. 7, 1999, 563-566

11. Nicholas, M.G., Joining Processes, Kluwer Academic Publishers, Boston, USA, 1998

12. Fletcher, M. J., Vacuum Brazing, Millsand Boon Limited, London, United Kingdom, 1971

13. ASM International Handbook Committee, ASM Handbook – Brazeability and Solderability of Engineering Materials, 10th Edition, Vol. 6, ASM International, Materials Park, Ohio, USA, 1993

14. Hiemenz, C. and Rajagopalan, R., Principles of Colloid and Surface Chemistry, Marcel Dekker, New York, USA, 1997

15. Bailey, G.L. J. and Watkins, H.C., "The Flow of Liquid Metals on Solid Metal Syrfaces and its Relation to Soldering, Brazing, and Hot-Dip Coating", *J. Inst. Of Metals*, Vol. 80, 1951, 57-76

16. ASM International Handbook Committee, Metals Handbook Desk Ed., 2nd Edition, ASM International, Materials Park, Ohio, USA, 1993

17. C.C.S. Harrison, "Vacuum Brazing", *Eng. Mater. Design*, Vol. 20, No. 12, Dec. 1976, 30-32

18. Humpston, G., and Jacobson D. M., Principles of Soldering, ASM International, Materials Park, Ohio, USA, 2004

19. Anonymous, "Brazing in a Vacuum", *Weld Des. Fabr.*, Vol. 45, No. 5, May 1972, 60-61

20. Gale, W.F., and Wallach, E.R., "Wetting Mechanism High-Temperature Brazing of Nickel-Based Alloys", *Recent Trends in Welding Science and Technology Conf. Proc., May 14-18, 1989, 529-533*

21. Arata, Y., Aohmori, and Cai, H.F., "Studies on Vacuum Brazing II – Removal of Oxide Film From Stainless Steel Surface Alloy Spreading Mechanism", *Trans. JWRI*, Vol. 12, No. 1, 1983, 27-34

22. Kopecki, E.S. , "What You Should Know About Brazing Stainless Steels Pt. 2", *Can. Mach. Metalworking*, Vol. 79, No. 3, Mar. 1968

23. Lugscheider, E., and Kruger, J., "High Temperature Brazing of High-Alloyed Steels with nickel-Base filler Metals, *Quality and Reliability in Welding Vol. 1; Conf. Proc. Sept. 6-8, 1984, 6*

24. Gubin, A.I., Novikov, V.V., "Brazing Corrosion-Resistant Steels", *Weld Prod.*, Vol. 18, No. 11, Nov. 1971

25. Lugscheider, E., Klohn, K. and Burchard W., "Structure of Low-Phosphorus Alloyed Nickel-Chromium-Silicon Brazed Stainless Steel Joints", *Weld. J.*, Vol. 59, No. 10, 1980, 283s-288s

26. Pattanaik, S., and Mizuhara, H., " Evaluation of Joints Brazed with Ni-Pd Base Filler Alloys", *Brazing and Soldering*, No. 3, Autumn, 1982, 8-10

27. Feduska, W., "New Alloys for Brazing Heat-Resistant Alloys", *Weld. J.*, Vol. 39, No. 7, 1960, 292s-300s

28. Rhys, D.W., and Berry, R.D., " The Development of Palladium Brazing Alloys", *Metallurgia*, 1962, 255-263

29. Pelster, H., and Lugscheider, E., "Development of Low-Precious-Metal High-Temperature Brazing Alloys for Joining High-Strength Components", *Schweissen und Schneiden*, Vol. 38, No. 6, 1986, E93-E96

30. McGurran, B., and Nicholas, M.G., "A Study of Factors Which Affect Wetting When Brazing Stainless Steel to Copper", *Brazing and Soldering*, No. 8 Spring 1985, 43-46

31. D'Silva, T.L., "Nickel-Palladium Base Brazing Filler Metal", *Weld. J.*, Vol. 59, No. 10, 1979, 283-286

32. Chen, R.B., and Shiue, R.K., "The Microstructural Observation and Wettability Study of Active Brazing Beryllium Copper and 304 Stainless Steel", *Journal of Materials Science Letters*, Vol. 20, No. 15, 2001, 1435-7

33. Liu, C.C., Ou, C.L., Shiue, R.K., "The Microstructural Observation and Wettability Study of Brazing Ti-6Al-4V and 304 Stainless Steel Using Three Braze Alloys", *Journal of Material Science*, Vol. 37, No. 11, 2002, 2225-35

34. Ambrose, J.C., Jenkins, S., and Nicholas M.G., "Some Effects of Composition and Surface Preparation on the Wetting Behavior of Nickel Base Brazes" *Brazing and Soldering*, No. 14, Spring 1988, 30-33

35. Izui, H. and Suezawa, Y., "Development of Pd-Ni Brazing Filler Metals for SUS 316L Stainless Steel", *Trans. Jpn. Weld Soc.*, Vol. 24, No. 2, Oct. 1993, 35-40

36. Rymar, V.I., Lotsmanov and Radzievskii, V.N., "Characteristic Features of the Wetting of Steels by Brazing Alloys with Heating in a Vacuum", *Weld Prod.*, Vol. 22, No. 5, May 1975, 45-47

37. Bell, G.R., "Gaps in High Temperature Brazing", *Brazing and Soldering*, No. 10, Spring, 1986, 24-27

38. Lugscheider, E., and Partz, K.D., "High-Temperature Brazing of Stainless Steel with Nickel;-Base Filler Metals BNi-2, BNi-5, and BNi-7", *Weld. J.*, Vol. 62, No. 6, June 1983, 160s-165s

39. Lugscheider, E., and Cosack, T., "High-Temperature Brazing of Stainless Steel with Low-Phosphorus Nickel-Based Filler Metal", *Weld. J.*, Vol. 67, No. 10, Oct 1988, 215s-221s

40. Paul, J.F., " Soldering and Brazing Stainless Steels", *Metals Eng. Quart,* Vol. 7, No. 40, Nov. 1967, 50-54

41. Lugscheider, E., Klohn, K., and Lison, R., "Strength of High Temperature Brazed Joints – Influence of Brazing Parameters", *Weld. J.*, Vol. 58, No. 10, Oct. 1979, 296s-300s

42. Suezawa, Y., and Izui, H., " Stress Measurements of SUS 410 Brazed Joint with Palladium Containing Filler Metals", *Residual Stresses – III: Science and Technology Vol. 1, Conf. Proc., July 23-26, 1991, 259-264*

43. Lugscheider, E., and Pelster, H., "Nickel-Base Filler Metals of Low Precious Metal Content", *Weld. J.*, Vol. 62, No. 10, 1983, 261s-266s

44. D'Silva, T.L., "Nickel Palladium Base Brazing Alloy", *U.S. Patent # 4,149,881*, Apr. 17, 1979

45. Smith, M.S. Jr., Hilbolt, M. S., and Mathur, P.S., "Cobalt-Palladium-Silicon-Boron Brazing Alloy", *U.S. Patent # 4,396,577*, Aug. 2, 1983

46. Smith, M.S. Jr., Hilbolt, M. S., and Mathur, P.S., "Nickel-Palladium-Chromium-Boron Brazing Alloy", *U.S. Patent # 4,414,178*, Nov. 8, 1983

47. Knotek, O., and Lugscheider, E., "Brazing Filler Metals based on reacting Ni-Cr-B-Si Alloys", *Weld. J.*, Vol. 55, No. 10, 1976, 314s-318s

48. D'Silva, T.L., "Nickel Palladium Base Brazing Alloy", *U.S. Patent # 4,149,881*, Apr. 17, 1979

49. ASM International Handbook Committee, ASM Handbook – Metallography and Microstructures, Vol. 9, ASM International, Materials Park, Ohio, USA, 1985

50. Callister, W.D. Jr., Materials Science and Engineering: An Introduction, 4th Edition, John Wiley and Sons Inc., Toronto, Canada, 1997

51. Bennett, W.S., R.F. Hillyer, Keller, D.L. and Riefenberg, D.H., "Vacuum Brazing Studies on High Manganese Stainless Steel", *Weld. J.*, Vol. 53, No. 11, 1974, 122s-131s

52. Feduska, W., "High-Temperature Brazing Alloy – Base Metal Wetting Reactions", *Weld. J.*, Vol. 38, 1959, 122s-131s

53. Milner, D.R., "A Survey of the Scientific Principles Related to Wetting and Spreading", *Br. Weld. J.*, Vol. 5, Mar. 1958, 90-105

54. ASME B46.1-2002, "Surface Texture (Surface Roughness, Waviness, and Lay)"

55. Zipperian, D., "Silicon Carbide Abrasive Grinding" Vol. 1, Iss. 2, Nov. 2002, 1-3, Quality Matters Newsletter, URL: http://www.metallographic.com [July 13, 2003]

56. ASM International Handbook Committee, Engineering Properties of Steel, ASM International, Materials Park, Ohio, USA, 2002

57. Brossa, M., and Guerreschi, U., "Effects Induced by the Brazing Thermal Cycle on the Structural Properties of Materials in Steel Brazed Joints", *J. of Nucl. Mat.*, Vol. 11, July 1988, 626-630

58. Miyazawa, Y., and Ariga, T., "A Study of the Brazeability of Nickel-based Brazing Filler Metal Foil for Joining Nickel Base Metal to Mild Steel Base Metal", *Weld. J. Supplement*, No. 7, 1993, 294s-300s

59. Nikiforova Z.V., Nesterov, B.M. and Bogdanova, V.V., "Brazing of Heat Resisting Alloys with Palladium-Based Brazing Alloys", *Weld. Prod.*, Vol. 17, No. 5, 1970, 58-61

60. Johnson, R., Baron, M., Williamson, A.C.F., "Tetig Diagrams Help Optimize Brazed Joints", *Weld. and Met. Fab.*, Vol. 48, No. 8, 1980, 553-558

61. ASM International Handbook Committee, ASM Handbook – Alloy Phase Diagrams, 10th Edition, Vol. 3, ASM International, Materials Park, Ohio, USA, 1992

62. Feduska, W., "The Nature of High Temperature Brazing Alloy – Base Metal Interface Reactions", *Weld. J.*, Vol. 37, No. 2, 1958, 62s-73s

63. Lamb, S., and Miller F.M., "The Effect of Aggression by Nickel-Base Brazing Filler Metals", *Weld. J.*, Vol. 48, No. 7, 1969, 283s-289s

64. Williams, T.M., and Talks, M.G., "Effect of Boron on the Precipitated Phases in Aged Type 316 Austenitic Stainless Steel", *JISI*, Nov., 1972, 870-871

65. Chang, R., Chemistry, 4th Edition, McGraw-Hill Inc., Montreal, Quebec, Canada, 1991

66. Rabinkin, A., Wenski, E., and Ribaudo, A., "Brazing Stainless Steel Using a New MBF-series of Ni-Cr-B-Si Amorphous Brazing foil", *Welding in the World*, Vol. 41, No. 6, 1998, 466-478